Vanadium doped TiO_2(110) thin layers: preparation, structure, and reactivity - methanol partial oxidation

Dissertation

Zur Erlangung des akademischen Grades

Doctor rerum naturalium

eingereicht im

Fachbereich Physik der Freien Universität Berlin

Xin Song

Berlin, Dezember 2016

angefertigt am Fritz-Haber-Institut der Max-Planck-Gesellschaft

Diese Dissertation wurde von Februar 2012 bis Dezember 2016 in der Abteilung Chemische Physik am Fritz-Haber-Institut der Max-Planck-Gesellschaft unter der Anleitung von Herrn Prof. Dr. Hans-Joachim Freund angefertigt.

Gutachter:

Prof. Dr. Hans-Joachim Freund, Fritz-Haber-Institut der MPG

Prof. Dr. Martin Weinelt, Freie Universität Berlin

Datum der mündlichen Prüfung: 08.03.2017

Selbständigkeitserklärung

Hiermit erkläre ich, dass ich die vorliegende Arbeit selbständig und nur unter Verwendung der angegebenen Quellen und Hilfsmittel angefertigt habe. Die Arbeit darf nicht schon einmal in einem früheren Promotionsverfahren angenommen oder als ungenügend beurteilt worden sein.

Berlin, den 13.12.2016

Xin Song

Acknowledgements

The four and a half years' study at the Fritz Haber Institute of the Max Planck Society, where the presenting research work was conducted, has become an unforgettable and invaluable experience for me. Here I would like to express my gratitude to those who have helped and supported me to complete this thesis.

I am heartily grateful to Mr. H.-J Freund, a respectable professor, for being the supervisor of my study, guiding me to the leading edge research in surface science, and supporting me in the finish of this work. It is a great fortune for me to work in his research group with a state-of-art scientific environment. I am also very thankful to Prof M. Weinelt in Free University Berlin for being my co-supervisor and useful discussions on my research projects.

I am really indebted to Dr. H. Kuhlenbeck, my scientific advisor on a daily basis, for his constant guidance, fruitful discussions, and supports in many aspects. I not only benefited immensely from his invaluable knowledge but also learned from him the proper scientific methodology. As well I am obliged a lot to Mr. M. Naschitzki for his strong technical assistance in the maintaining of the laboratory.

I also acknowledge my colleagues for their versatile help and contributions to my work. O. Karslıoğlu was the one who introduced the equipment operation at the early stages of the project. E. Primorac taught me the sample preparation and spent lots of time in the discussion of experimental results. H. Qiu, F. Feiten, and C. Büchner also helped me a lot during the research process. I would like to thank as well all other members in Freund's group for providing help with all kinds of things I would not have managed on my own.

Financial support from International Max Planck Research School was greatly acknowledged. Besides, I benefited much from the lectures, workshops and discussion meetings organized by the school.

Last, my appreciation goes to my sincere parents, my faithful wife, and my lovely daughter. Their endless love and supports have made me achieve what I have today.

Contents

List of Abbreviations

Al	Aluminum
Ar	Argon
BESSY	Berlin electron storage ring society for synchrotron radiation
BOVs	Bridging oxygen vacancis
CH_2O	Formaldehyde
CH_3O	Methoxy group
CH_3OH	Methanol
DFT	Density functional theory
H	Hydrogen
He	Helium
IMFP	Inelastic mean free path
LEED	Low-energy electron diffraction
Mg	Magnesium
MO	Oxide supporter
NEXAFS	Near edge x-ray absorption fine structure
O	Oxygen atom
^{16}O, ^{18}O	Isotope oxygen
O_2	Oxygen molecule
O_a	Oxygen adatom
O_b	Bridging oxygen
OH	Hydroxyl group
OH_b	Hydroxyl group at bridging oxygen site
QMS	Quadrupole mass spectrometer
Pb	Lead
ROH	aliphatic alcohol
SSIMS	Static secondary-ion mass spectrometry
STM	Scanning tunneling microscopy
STS	Scanning tunneling spectroscopy
Ta	Tantalum
TaO_2	Tantalum dioxide
Ti	Titanium
TiO_2	Titanium dioxide

Ti_{5c}	Five-fold titanium site
TPD	Temperature-programmed desorption
UHV	Ultra-high vacuum
UPS	Ultraviolet photoelectron spectroscopy
V	Vanadium
VO_2	Vanadium(IV) oxide
V_2O_5	Vanadium(V) oxide
V_O	Bridging oxygen vacancy
W	Tungsten
XPS	X-ray photoelectron spectroscopy

List of Symbols

A	Sample area detected by spectrometer
a, b, c	Lattice parameters
β	Heating rate
d	Distance between two atoms in the surface
C_x	Relative atom fraction of element x
E_b	Binding energy
E_{des}	Activation energy of desorption
E_p	Pass energy
E_k	Kinetic energy referred to Fermi level
$E_{k'}$	Kinetic energy of electron leaving the sample
$E_{k,measured}$	Kinetic energy measured by spectrometer
f	X-ray flux
h	Planck constant
$h\nu$	Energy of x-rays radiation
I	Number of photoelectrons per second
k_{des}	Reaction rate constant for desorption
λ	Inelastic mean free path or wavelength of electron
m/z	Mass-to-charge ratio
m_e	Mass of the electron
n	order of diffraction or order of desorption
N	Number of atoms of the elements per cm^3
ϱ	Electrical resistivity
Φ_a	Work function of spectrometer
Φ_s	Work function of sample
Ψ	Angle between scattered electrons and surface normal
r	rate of desorption
R	Retarded potential or gas constant
σ	Photo ionization cross-section
t	time
T	Detection efficiency of photoelectron or temperature
θ	Angular efficiency factor or coverage
ν	Pre-exponential factor of desorption

V	Potential barrier
V_T	Sample bias voltage and
V_z	Voltage applied to the z piezo
y	Efficiency for the formation of photoelectrons
x_i, y_i, z_i	Coordinates of piezo

Chapter 1

Introduction

This study focuses on the characterization of the surface properties of titania-vanadia mixed oxides, which has been shown to be a versatile catalyst for partial oxidation and oxidative dehydrogenation reactions.[1,2,3] The study of catalysts is relevant since they play an important role for the production of goods by the chemical industry. Many essential commodities such as plastics, synthetic fibers, pharmaceuticals, fertilizers, dyes, resins, and pigments are produced via catalytic processes.[4] For example, iron-based catalysts make the large-scale production of ammonia possible which is essential for the production of fertilizers.[4] Without them, it would not be possible to feed today's huge world population of humans. In crude-oil processing and petrochemistry, catalysis is applied in the purification stages and for chemical transformations like hydrogenation, dehydrogenation, partial oxidation, and organic molecular rearrangements.[4] Catalysts are also applied to in the area of environment protection such as the control of automobile exhaust and the purification of off-gas from industrial plants and power stations.[4] An example is the conversion of toxic gas and pollutants in the car exhaust gas by three-way catalytic converters, which are usually made of oxides combined with Pt, Pd, and Rh.[4]

A catalyst, according to Ostwald's definition (1895), is defined as a substance that "accelerates a chemical reaction without affecting the position of the equilibrium".[5] Compared to the corresponding non-catalyzed reactions, the reactions involving catalysts have lower activation energies and higher reaction rates under the same reaction conditions.

There are two types of catalysts: homogeneous or heterogeneous ones, depending on whether the catalyst phase is identical to that of the reactants or not. Catalysts that are in the same phase as the reactants are termed "homogeneous catalysts". Typically homogeneous catalysts are well-defined chemical compounds or complexes that are molecularly dispersed together with the reactants in the reaction medium. Catalysts that are in a different phase than the reactants are termed "heterogeneous catalysts".

Most heterogeneous catalysts are solid while the reaction mixture is liquid or gaseous. Titania-vanadia mixed oxide, the object of this study, is a heterogeneous catalyst for partial oxidation or oxidative dehydrogenation reactions.

In the case of heterogeneous catalysts the size of the surface area is relevant for the catalysts throughput. A high surface area will result in a high throughput, and therefore fewer catalysts material is required which reduces the cost. In many cases, the catalyst will come as finely dispersed material on a support. The support may not just act as a carrier for the catalyst particles; it may also prevent or reduce agglomeration and sintering, and it may modify the catalytic performance. The support surface which carries the catalyst particles is usually not an extended flat surface: the support may consist of powder particles; it may even have an inner surface in the case of a porous material. However, such substrate structures make it difficult to study catalysts and catalytic processes in detail. Therefore, the characterization of catalyst systems is still a challenging task for scientists.

The study of well-defined model systems is an approach to investigate the catalytic properties of heterogeneous catalysts.[6,7,8] In this approach the catalyst support or the catalysts material itself is modeled by a single crystal surface. This reduces the complexity of the system which may permit to derive more detailed conclusions about catalytic processes and catalytic centers since the spectroscopic data will be simpler due to the limited heterogeneity of the model catalyst.

The development of the surface science of solid surfaces during the last 50 years has been intimately connected with heterogeneous catalysis.[9] For oxides that are often used as supports or active materials themselves, experimental difficulties lie in the application of electron spectroscopy since oxides are electrical insulators in most cases. A way to circumvent this problem is to use thin, well-ordered oxide films on metal substrates, which do no charge upon electron impact or electron emission. In the late 1980s Vurens et al. prepared well-ordered iron-oxide films on a Pt(111) support to model catalysts active in ammonia synthesis.[8] Nowadays many oxides can be grown as ordered thin films and a vast number of papers have been published on this topic.[7,10,11]

Such model surfaces are usually studied under ultra-high vacuum (UHV) conditions, which ensure surface cleanliness and makes the use of several surface science techniques possible. Scanning probe microscopy (SPM) allows atomic scale investigations of crystalline surfaces in real space with high lateral resolution, enabling the investigation of single adsorbates molecules and defects on the surface.

In this study, the model system approach is applied to study the structure and the surface reactivity of titania-vanadia mixed oxides with the aim of characterizing the effect of admixed vanadium on the surface structure and chemical reactions at the surface. When supported on reducible oxides, vanadia accelerates oxidative dehydrogenation reactions such as the reactions of short chain alkanes to alkenes and of alcohols to the corresponding aldehydes.[12] Alkenes and aldehydes are raw materials for many industrial processes such as the production of resins, polyethylene, and polypropylene.[12] Therefore studies of oxidative dehydrogenation reactions are relevant. Recent studies have shown that vanadium oxides supported on titania powder exhibit a higher yield of acetaldehyde from adsorbed ethanol and a lower reaction temperature than vanadia on a number of other oxide supports such as zirconia, ceria, and alumina.[1]

In this study titania-vanadia mixed oxides were prepared by doping vanadium into rutile TiO_2(110). Ideally, thin TiO_2(110) films deposited on a metal substrate would be good candidates for such a preparation. However, there is no report in the literature that a well-ordered TiO_2(110) thin film could be grown on a metallic substrate. Metal or alloy single crystals have been used as conducting substrates for the preparation of TiO_2(110) thin films, such as $Ni_{94}Ti_6$(110),[13] Mo(110),[14] Ni(110),[15] Ag(100),[16] and W(100).[17,18] However, the lattice mismatch between the substrate and the TiO_2 overlayer induced strain in the TiO_2 films and thus no rutile monocrystalline film could be obtained.

The issue could be overcome by using a recipe developed by E. Primorac[19]: the film was grown on a native TiO_2(110) rutile single crystal substrate with a buffer layer between the substrate and the thin film. Details of the preparation procedure are described in Chapter 3. The interface strain is small in such a structure and therefore well-ordered Ti + V mixed oxide films could be successfully prepared. The surface properties of reduced and oxidized layers, as well as the reactivity of these layers with respect to the partial oxidation of methanol, were investigated with surface science techniques like XPS, STM, LEED, and TPD.

This thesis is arranged in the following way: In the second chapter, the scientific background is reviewed, including a brief overview of the properties of rutile TiO_2(110) and supported vanadia systems. In the third chapter, the preparation of the sample and the experimental methods are described. The experimental results and their discussion are presented in chapter 4, 5, and 6. Chapter 4 discusses the preparation and the characterization of TiO_2 thin films. Reduced and oxidized Ti + V mixed oxides show different surface structures and different activities for the partial oxidation of methanol. The results are discussed in detail in chapter 5 and

chapter 6. In the final chapter, conclusions are summarized, and an outlook on possible future studies is given.

Chapter 2

Research background

As a versatile material, titanium dioxide (TiO_2), has been used in gas-sensing technology[20], as a white pigment,[21] in the coating industry,[22] in electric devices,[23] in solar cells,[24] in heterogeneous catalysis/photocatalysis,[25,26] and many others.[27] Motivated by the various applications, many fundamental studies have been conducted to learn about the physical and chemical properties of TiO_2. In this chapter, an introduction to the surface properties of rutile TiO_2(110) is given. Such background knowledge is important since rutile single crystals with (110) termination were used as substrates for the preparation of mixed oxide thin film layers in the experiments. Following that, previous studies on titania supported oxides are reviewed with a focus on titania-vanadia mixed oxides. The influence of other oxides admixed to the titania on the catalytic properties is checked by inspecting the literature, which may shed light on the analysis of the experiment results. Finally, supported vanadia systems from the view of powder and model catalysts are discussed.

2.1 Properties of rutile TiO_2(110)

TiO_2 comes mainly in three modifications: rutile, anatase, and brookite. Being the most stable surface of rutile, TiO_2(110) has been widely investigated. The surface structure of TiO_2(110) has been well characterized,[27,28] and many surface chemistry studies have been conducted with surface science techniques.[28,29,30]

2.1.1 Surface structure of rutile TiO_2(110)

(1 × 1) surface

The structure of rutile TiO_2 belongs to the tetragonal crystal system with lattice parameters a = b = 4.59 Å, and c = 2.95 Å. The unit cell of its bulk structure is shown in Figure 2.1(a) with a ball-and-stick model. The basic building unit consists of a titanium atom surrounded by six oxygen atoms in an octahedral block.

According to the calculations of the total energy of TiO_2 slabs, the (110) surface has the lowest surface energy and is thus the most stable crystal face. Figure 2.1(b) shows the bulk truncation of the (110)-(1 × 1) surface, which is formed by splitting the bulk structure along the dashed line A where the same numbers of oxygen-to-titanium and titanium-to-oxygen bonds are broken. The (110) surface is auto-compensated, which means that there is no net charge of the surface layer, which is part of the reasons why this surface is the most stable one.

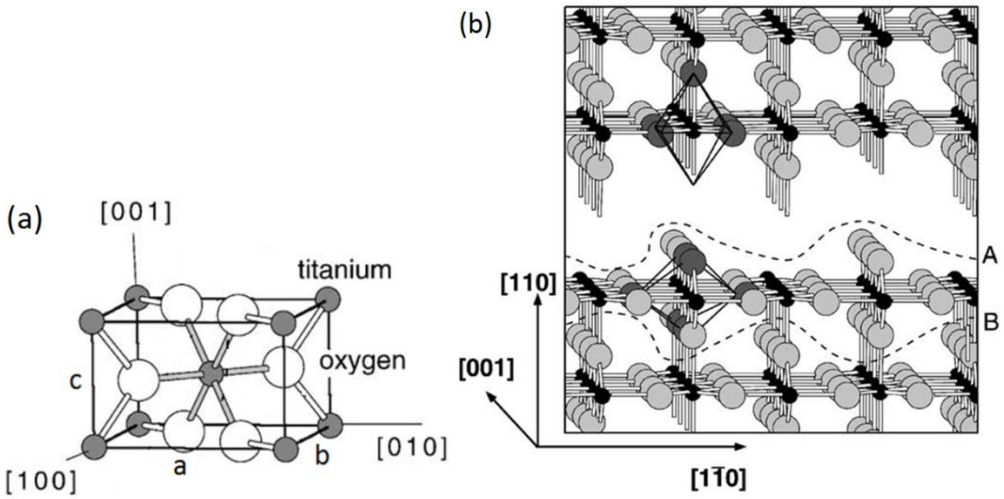

Figure 2.1 (a) Tetragonal bulk unit cell of rutile with lattice parameters a = b = 4.59 Å, c = 2.95 Å. (b) (110) surface formed by splitting the bulk structure along the dash line A. The dashed lines A and B enclose a charge neutral unit without a dipole moment. Two octahedral blocks are marked. (Adapted with permission from ref 27. Copyright 2003 Elsevier.)

There are two different kinds of Ti atoms and O atoms at the surface. Within the first layer, six-fold coordinated Ti atoms along the [001] direction behave as in the bulk, while five-fold coordinated Ti atoms have one dangling bond perpendicular to the surface. For oxygen atoms, there are three-fold coordinated atoms as in the bulk, and the so-called bridging oxygen atoms which are two-fold coordinated. The TiO_2(110)-(1 × 1) surface lattice parameters are 2.95 Å along [001] and 6.50 Å along [1$\bar{1}$0].

To enable the use of techniques employing charged particles, TiO_2(110) crystals are usually reduced by thermal treatment and/or sputtering in a vacuum so that they get electrically conductive.[31] During the treatment, the bridging oxygen atoms are partially removed because of their undersaturated coordination. Associated with each

oxygen vacancy, two Ti^{3+} sites are created.[32] The cations diffuse quickly to the bulk at elevated temperature,[33] which leads to a reduction not only at the surface but also of the whole sample. With repeated cycles of sputtering and annealing, the color of the crystal changes from colorless transparent to blue for a medium degree of reduction and black for strong reduction.[31]

The atomic-scale structures of the $TiO_2(110)$-(1×1) surface are usually examined by scanning probe techniques such as STM.[34] In STM images bright and dark rows along [001] are arranged alternately with a distance of 6.5 Å between two neighboring bright (or dark) rows. Opposite to the topography of bulk truncation, the bright rows are in plane 5-fold Ti rows, while the protruding bridging oxygen rows appear as dark rows. This appearance is attributed to the distribution of the density of states in the conduction and valence bands. The conduction band states have primarily cation 3d character, while the valence band states have primarily O 2p character. With a typical STM bias of +2 V, electrons tunnel from the tip into the crystal above the conduction band minimum. Thus Ti rows are imaged as the bright features in STM topography.

In addition, many short bright features with different brightness are usually observed on the dark O rows.[34] One type of spots with a height of ~0.5 Å is assigned to bridging oxygen vacancies that are produced during the sputtering and annealing treatment. The density of such spots is usually in the range of 5% to 7% for a slightly reduced crystal. These defects always appear as isolated spots with no apparent short-range ordering. Another type of spots with a height of 0.8 Å is called hydroxyl groups at the surface. They originate from the adsorption of water in the residual gas in the chamber.[34] Water molecules are usually likely to dissociate at the bridging oxygen vacancy sites, which then results in the filling of the vacancy with a hydroxyl group and the remaining proton binds to a neighboring oxygen atom.

(1 × 2) surface reconstruction

Repeated cycles of sputtering and annealing can result in a heavily reduced crystal as can be identified optically from the darker color of the crystal.[31] For a high degree of reduction, the surface may reconstruct: a (1×2) superstructure usually appears at the surface of a heavily reduced crystal as confirmed both from STM images and LEED patterns.[35] In STM the (1×2) reconstruction is observed as a series of bright strings along [001] with a doubling of the periodicity along $[1\bar{1}0]$. Figure 2.2 shows a STM image obtained from a heavily reduced crystal. The distance between the two rows along [001] is about 13 Å which is twice that of the (1×1) surface. The surface

reconstruction is also dependent on the extent of the reduction state of the crystal. A simple (1 × 2) reconstruction appears at crystals with dark blue color (medium reduction), while a cross-linked (1 × 2) structure can be found at crystals with blue-black color (strong reduction). In Figure 2.2 cross-links along $[1\bar{1}0]$ connecting neighboring (1 × 2) rows are seen, and the inset shows a detailed image of a cross-link.

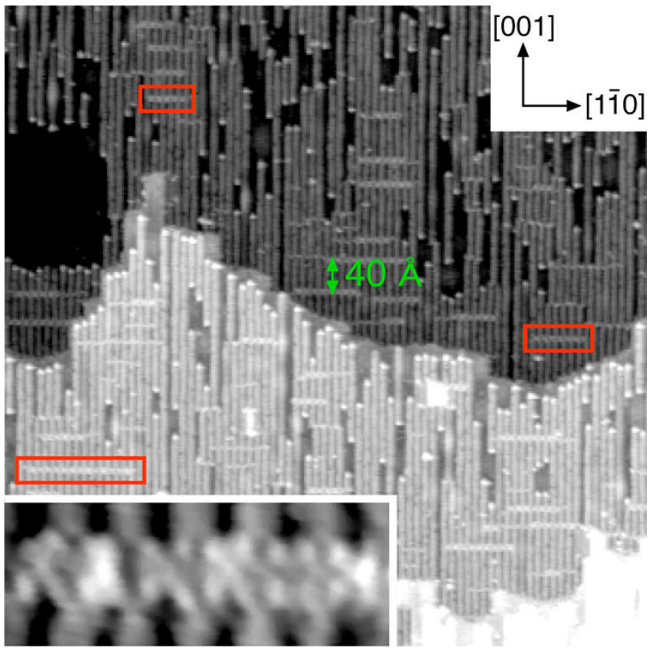

Figure 2.2 STM image of a cross-linked (1 × 2) structure of TiO_2(110). Several cross-links are marked by rectangles. The inset shows a detailed image of a cross-link. (Reproduced with permission from ref 36. Copyright 1999 American Physical Society.)

For this (1 × 2) reconstruction various models have been suggested such as the 'missing row' model, 'added Ti_2O_3 row' model, and 'added Ti_3O_5 row' model.[37,35,38] After discussion over years, the 'added Ti_2O_3 row' model suggested by Onishi and Iwasawa was commonly accepted.[35] The so-called 'added Ti_2O_3 row' model consists of double rows of Ti cations in a distorted tetrahedral configuration. The Ti cations reside in positions similar to interstitial sites in the rutile lattice. Even though the structure has Ti_2O_3 stoichiometry, it does not resemble the one found in the corundum Ti_2O_3 structure. This model has been supported by experiments such as electron stimulated desorption ion angular distribution, high-resolution STM, ion scattering measurements, and IV-LEED experiments.[39,35,40] Theoretical calculations

of the electronic structure of the (1 × 2) surface also favor this model over the others.[41] It was found that this 'added Ti_2O_3 row' structure has a lower surface free energy than the other structures and that the simulated surface is consistent with the contrast in STM. [41]

Oxidized surface

The reduced crystal can be recovered to a less reduced state to some extent by exposing the crystal to an oxygen ambient. The morphology of the oxidized surface depends on sample temperature, annealing time, gas pressure, and reduction state of the crystal. Figure 2.3 shows the dependence of the morphology on the annealing temperature.[42] Before each gas exposure a flat (1 × 1)-terminated surface was prepared by sputtering and annealing in UHV at 880 K for 30 min.

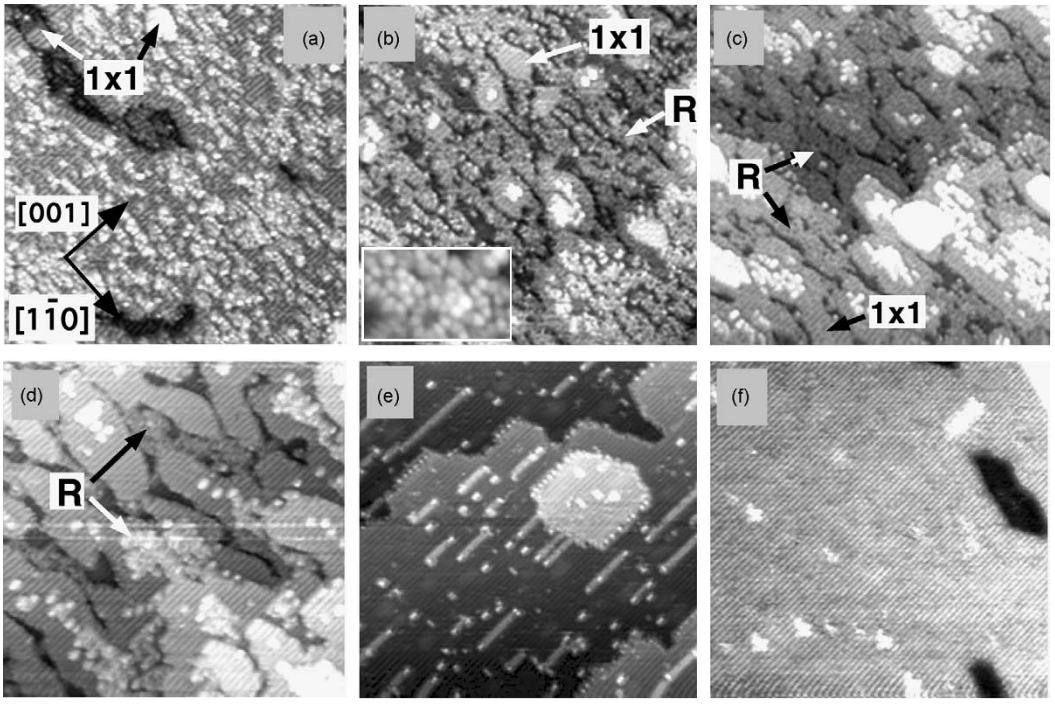

Figure 2.3 STM images (50 nm × 50 nm) of oxidized TiO_2(110) surfaces. Oxygen (1×10^{-6} mbar) was dosed to a reduced surface at (a) 500 K, (b) 520 K, (c) 550 K, (d) 660 K for 10 min, (e) 710 K for 15 min, and (f) 830 K for 20 min. 'R' stands for the rosette-like structure. An atomically resolved image of this structure is shown in the inset in (b). (Adapted with permission from ref 42. Copyright 1999 Royal Society of Chemistry.)

For medium temperatures (520–660 K) the surfaces are relatively rough. Many small-scale features are observed such as irregular networks of connected 'rosettes', small strands, and small (1 × 1)-terminated islands. The inset in Figure 2.3(b) shows an atomically resolved image of a rosette-like feature, which consists of six bright spots in a pseudo-hexagonal arrangement.

The surface becomes flat when the applied annealing temperature is higher i.e. 710 K and 830 K as seen in the STM images in Figure 2.3(e) and (f). On the (1 × 1)-terminated surfaces, 'hill-like features' and (1 × 2) strands are observed. The structure of the strands is the same as the Ti_2O_3 structure. Onishi and Iwasawa have reported the dynamic processes of the oxidation at 800 K. They acquired in-situ STM images while the reduced TiO_2 crystals sample was kept at a temperature of 800 K and exposed to oxygen with a background pressure of ~10^{-7} mbar. The atomic-level investigation shows that the 'hills' and 'strands' are from the reaction between the gaseous oxygen and the Ti interstitials which diffuse quickly at elevated temperatures.[43,44]

Both the rosette-like structure and the 'added Ti_2O_3 row' are just precursor structure that forms during the growth of additional TiO_2(1 1 0)-(1 × 1) layers. When a reduced (1 × 1) surface is heated at an elevated temperature and exposed to an oxygen ambient, rosette-like or hill-like structures nucleate randomly on the terraces. They are then transformed into new terraces, with added rows comprising double strands. The kinetics of the growth determines the relative concentration of the incomplete structures (the rosettes and strands) and the (1 × 1) islands on the surface. A flat and (1 × 1)-terminated surface can be achieved, when the growth of the new terraces is slow in comparison with surface diffusion processes. This can be achieved by applying higher temperatures (> 700 K) where the surface diffusion is much faster. The growth rate of the new terraces can be decreased by controlling the flux of the constituents i.e. using weakly reduced samples with a small concentration of interstitials, or applying lower O_2 background pressures.

Different to the effect of oxygen annealing at high temperature, the surface morphology does not reconstruct when oxygen is dosed to the TiO_2(110) surface at room temperature. Oxygen molecules are easily dissociated at the bridging oxygen vacancies present at the reduced surface. Experimental results show that bridging oxygen vacancies are healed upon oxygen adsorption at temperatures above 150 K.[45] It is suggested that each O_2 dissociation event causes filling of a single oxygen vacancy V_O and the deposition of an O adatom O_a at the nearby 5-fold Ti site:

$O_2 + V_O \rightarrow O_b + O_a$.

There exists another channel of oxygen dissociation.[46] This channel leads to the formation of O adatom pairs on Ti_{5c} rows at 300 K.[46] In each pair, two O adatoms are separated by a single unoccupied Ti_{5c} site. The combined coverage of oxygen vacancies and adatoms is higher than the original coverage of oxygen vacancies, which would not be the case if bridging oxygen vacancies were the only dissociation sites. The excess is approximately the coverage of the paired oxygen adatoms. Even though the origin of the charge transfer is still under discussion, the dissociation of O_2 on Ti_{5c} sites is either mediated by V_O-related charge or charge provided by interstitial Ti defects in the bulk. [46,47]

2.1.2 Alcohol adsorption on rutile TiO_2(110)

The reactivity of TiO_2 with alcohols is an important issue which is related to a number of technological applications. The decomposition of alcohols upon adsorption is often used to identify the catalytically active sites on metal oxide surfaces. Moreover, the catalytic and photocatalytic oxidation of organic compounds on TiO_2 is an interesting topic for researchers. Alcohols are often considered as prototype molecules for such studies. For those reasons, the chemical reaction of alcohols on TiO_2(110) has been extensively studied both experimentally and theoretically. TPD experiments have been conducted to analyze the products after the reaction of alcohols at the surface. Structural information comes primarily from STM images of the alcohol-covered surface and ab initio calculations.

Adsorption on reduced surfaces

The adsorption of simplest alcohol, methanol, has been investigated in great detail by Henderson et al.[48] Molecular and dissociative adsorption of methanol was observed. Figure 2.4(a) shows a series of CH_3OH (m/z=31) TPD spectra for different methanol exposures to reduced TiO_2(110) prepared by sputtering and annealing at 850 K in UHV. Several peaks at different temperatures are present. The peaks at ~145 K and ~165 K are assigned to methanol multilayers and methanol adsorbed at bridging oxygen sites, respectively. The assignment of the ~145 K peak was based on comparison to TPD spectra of methanol on metals, and the ~165 K peak was assigned by analogy with the behavior of water on TiO_2(110). The intense peak at ~295 K is due to molecular desorption of methanol adsorbed on 5-fold Ti sites, while the ~350 K peak is (tentatively by Henderson *et al.*) assigned to methanol

dissociation on 5-fold Ti sites. The surface methanol coverage related to the shoulder peak at ~480 K was consistent with the density of the BOVs in this experiment. Therefore this peak was assigned to a methoxy-hydroxyl recombination of methanol dissociated at bridging oxygen vacancies. SSIMS experiments have provided additional evidence on this assignment. The SSIMS results in Figure 2.4(b) show that the $TiO(CH_3OH)^+$ signal vanishes at ~295 K and the $TiO(CH_3O)^+$ signal essentially vanishes above ~500 K.

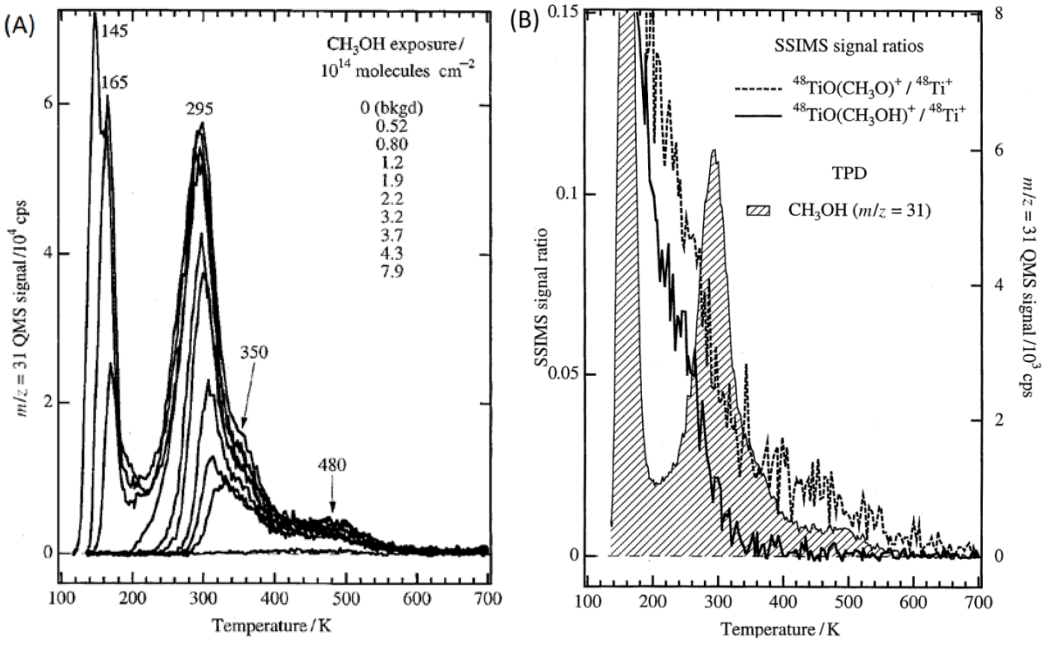

Figure 2.4 (a) CH_3OH (m/z=31) TPD spectra from various exposure on reduced TiO_2(110) surfaces at 135 K. (b) Temperature programmed SSIMS data along with CH_3OH TPD from multilayer exposure. (Adapted with permission from ref 48. Copyright 1999 Royal Society of Chemistry.)

Direct evidence for the dissociation of methanol on BOVs:

$$CH_3OH_{(g)} + V_O + O_b \rightarrow CH_3O_{(ads)} + OH_b$$

has been obtained from STM experiments.[49] Theoretical studies have shown that methanol dissociation on BOVs is energetically preferred by 0.42 eV over molecular adsorption. [50]

For larger alcohols ROH (C_2-C_8 aliphatic), BOVs are also sites for dissociative adsorption:

$$ROH_{(g)} + V_O + O_b \rightarrow RO_{(ads)} + OH_b$$

with the lowest adsorption energy, which has also been confirmed from STM experiments, for example, the dissociation of 2-butanol on BOVs.[51]

Upon annealing layers of larger alcohols on TiO_2(110), significant differences relative to methanol are observed. While a small fraction of the alkoxy species recombines with hydroxyl groups, the majority of alkoxy species undergoes a dehydration reaction leading to alkenes and water. Using isotopically labeled ethanol, CD_3CH_2OH, Gamble *et al.* have shown that this reaction proceeds via a b-hydride elimination mechanism at 640 K. [52] Systematic investigations of primary, secondary, and tertiary alcohols by Kim *et al.* have shown that the dehydration barrier decreases dramatically as the chain length and chain number increases (dehydration of 1-, 2-, and t-butanol occurs at 628, 554, and 480 K, respectively).[53]

Adsorption on oxidized surfaces

The adsorption behavior of alcohol on oxidized TiO_2(110) is different from that on the reduced surface. When methanol is dosed to an oxidized TiO_2(110) surface, formaldehyde evolved at a higher temperature (higher than 480 K on a reduced surface) together with methanol. [54] Henderson *et al.* conducted TPD experiments of methanol on TiO_2(110) that was prepared by O_2 exposure at various temperature (150 ~ 715 K) before adsorption. [48] The obtained results presented in Figure 2.5 show clearly the desorption of formaldehyde (m/z=29).

As the mass 29 signal can have contributions from formaldehyde and methanol cracking, the mass 29 traces are scaled to the mass 31 (methanol) traces at low temperature, where formaldehyde is not expected to form. Any formaldehyde desorption then shows up as the difference between the two curves. For all O_2 exposures, the ratio of formaldehyde to methanol in the ~625 K peaks is almost the same. It is assumed that a disproportionation reaction happens between two methoxy groups. When O_2 is pre-dosed to the surface at ~150 K, an additional formaldehyde shoulder evolves at low temperature (~250 K) which was attributed to a molecular O_2^- species at the surface.

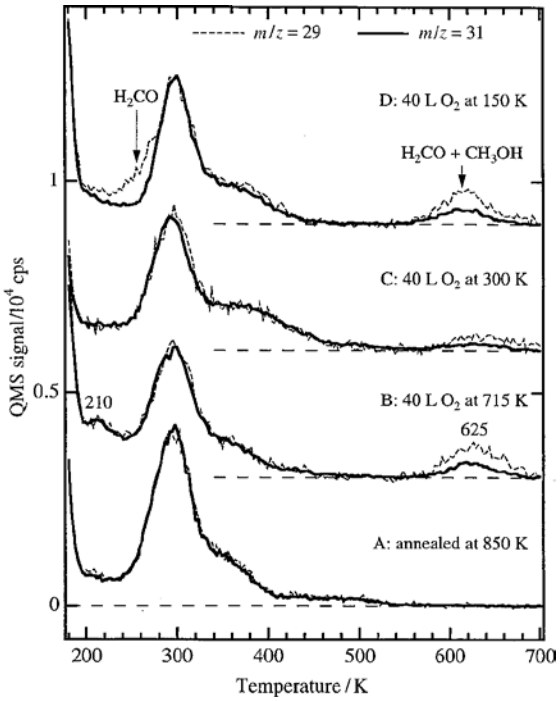

Figure 2.5 The effect of O_2 pre-adsorption temperature on the TPD properties of CH_3OH from the TiO_2(110) surface. TPD spectra for mass 29 (dashed lines) and mass 31 (solid lines) from a multilayer CH_3OH exposure at 135 K from: (a) the clean surface, (b) the clean surface exposed to 40 L O_2 at 715 K, (c) the clean surface exposed to 40 L O_2 at 300 K, and (d) the clean surface exposed to 40 L O_2 at 150 K. (Reproduced with permission from ref 48. Copyright 1999 Royal Society of Chemistry.)

For the oxidized surface, calculations of the methanol-surface interaction were conducted with different adsorption conformations of methanol (both molecular and dissociative). For the cases of full and half surface coverages, it was found that dissociative adsorption is slightly favored over molecular. [55]

2.2 Titania-vanadia oxide system

2.2.1 Doped titania oxides

Almost all the heterogeneous catalysts contain some kind of modifier that increases their activity, selectivity, and/or stability. The ability to fine tune a catalyst provides great potential for controlling these properties. Modifying oxide catalysts by doping is one of the ways to achieve fine tuning. In order to enhance the catalytic/photocatalytic properties of TiO_2, various dopant materials have been checked for their suitability.[26,27,56] For example, TiO_2 powder with cation dopants of

alkaline metal (Li, Na, K, and Cs) were found to catalyze acetone oligomerization.[57] Anion dopants such as N and F are claimed to enhance the photo-catalytic efficiency of TiO_2.[26]

While TiO_2 single crystals are applied mostly as the supporters of model catalysts in which evaporated materials usually aggregate at the surface,[58,59,60,61] the properties of TiO_2 itself have also been investigated with dopants in the subsurface or bulk of the single crystal. Researchers on doped TiO_2 single crystals have been conducting to reveal the mechanisms of the catalytic processes.[27,56] For instance N atoms replacing lattice O were doped into rutile and anatase single crystal with ion implantation method.[62] Cr-doped rutile TiO_2(110) was prepared by the calcination of the crystal with Cr_2O_3 powder in the air with following surface characterization in UHV chamber.[63] However, in most experiments, the dopants deposited by physical vapor evaporation are found to aggregate and form clusters on the single crystal surface easily. On the other hand, many DFT calculations on doping with a metal such as Au, Ni, V, Cr, W, and Mn are based on the slab model with dopants substitutionally replace lattice Ti atoms.[64,65]

2.2.2 Supported vanadia systems

Powder catalysts

Supported vanadium oxide catalysts contain a vanadium oxide phase deposited on a high surface area oxide support (e.g., Al_2O_3, SiO_2, TiO_2, etc.) and have found extensive applications as oxidation catalysts in the chemical, petroleum, and environmental industries.[12] The discovery that supported V_2O_5/TiO_2 catalysts have excellent oxidation characteristics for o-xylene oxidation to phthalic anhydride lead to the application of such catalysts, e.g., supported V_2O_5/Al_2O_3 and V_2O_5/TiO_2.[66] Vanadia-based catalysts have been intensively studied for partial oxidation or oxidative dehydrogenation (ODH) reactions.[2,3] They represent a worthwhile alternative for the production of short alkenes like ethene and propene because these reactions are exothermic and not thermodynamically limited. The peculiar properties of such VO_x/MO (oxide supporter) systems have been on the basis of the introduction of the term monolayer catalyst, first proposed by Hanke et al. in the late 1973 and subsequently revived by Wachs and Weckhuysen, i.e. catalysts consisting of isolated and/or polymeric nanostructures that wet the supporting MO.[67]

Nowadays, the development of various in operando techniques (typically InfraRed, Raman, UV–VIS spectroscopies and recently Near Ambient Pressure X-

Ray Photoelectron Spectroscopy), which are capable of investigating real catalysts (powders) close to real catalytic conditions, is helping scientists to track the catalyst action during the catalytic process, allowing a precise description of the reaction mechanisms.[68,69] From the study of the VO_x/MO systems by in operando techniques, it was found that under ambient conditions, hydrated vanadia clusters are present on oxide supports and decompose upon dehydration.[12,68,69] Under dehydrated conditions, the supported vanadia phases consist of isolated and polymeric surface VO_4 species in the sub-monolayer region and crystalline V_2O_5 nanoparticles are also present in monolayer coverage.[12,68,69] The surface VO_4 sites are the catalytic active sites for oxidation reactions by supported vanadia catalysts.[12,68,69] Both isolated and polymeric surface VO_4 sites exhibit the same specific catalytic activity and larger crystalline V_2O_5 nanoparticles above monolayer coverage tend to be less active.[12,68,69] The specific activity of the surface VO_4 sites is tunable by the oxide support cation that controls the redox properties of the surface VO_4 site. [12,68,69]

Model catalysts

Researchers on model catalysts have provided a wealth of structural and reactivity information on the VO_x/MO systems. These systems are usually prepared in ultra-high-vacuum by depositing the VO_x catalysts on planar supports that mimic the oxide supports used in real catalysts. The model catalysts are then characterized by a range of spectroscopic/microscopic tools capable of relating the structure and reactivity of the active sites.

The nature of the supporting MO, the coverage of VO_x, and the nature of the VO_x/MO interface are three major discriminating factor.[2,70,71] Catalysts based on reducible MO supports perform better than ones on non-reducible ones in selective oxidation reactions, showing higher turnover frequencies.[70] When the VO_x coverage is in the monolayer range or below, the catalysts displays a higher activity than bulk VO_x surfaces.[2] Moreover the actual interaction between the VO_x catalyst and the support can stabilize exotic VO_x nanostructures displaying a different reactivity than their bulk counterpart.[71,72]

For the VO_x/TiO_2 system, structural and chemical studies have been conducted using the TiO_2 (110) rutile single crystal as the substrate, on top of which vanadium[73,74] or vanadia[75–84] clusters/layers were prepared. STM experiments have shown that vanadium atoms, evaporated without oxidation procedure, are preferentially located on the 'upper threefold hollow' sites where they are bonded to two bridging oxygen atoms and one threefold coordinated basal oxygen atom.[74]

Vanadia clusters, prepared by evaporating vanadium in oxygen, absorb on top of the fivefold-coordinated Ti rows of the substrate at low coverage, while for coverage larger than 2 ML (monolayer) it is suggested that vanadia epitaxially grows on the TiO_2(110) (1×1) surface.[80] On the vanadia covered titania surface production of formaldehyde at different temperature has been observed through the oxidation of methanol.[78,82,83]

In those studies the vanadia-titania model system is prepared with the substrate maintained at a mild temperature (300~500 K), while powder catalysts are prepared at much higher temperature such as 773 K.[1] It was difficult to prepare the model system at high temperature since vanadium easily diffuses into the bulk of the substrate due to its high diffusion rate above 600 K. To better mimic the powder sample with the high treatment temperature, we have developed a Ti + V mixed oxide thin film that can endure annealing treatments at 800 K for several hours.

Chapter 3

Experimental

In this chapter the method of the sample preparation is described in detail after an introduction to the experimental setup. The characterization techniques applied in this work and their basic principles are discussed.

3.1 Experimental setup

The experiments were carried out in three different stainless steel UHV chambers. Ultrahigh vacuum conditions in the chambers are essential, because they minimize the influence of undesirable adsorbate species and keep the sample surface clean during the experiments. A chamber pressure in the rage of $\sim 1\times10^{-10}$ mbar leads to a coverage of 1 monolayer of contaminants within 1 to 3 hours, assuming a sticking coefficient of 1 for the adsorbate on the surface. In addition, many surface science techniques require ultrahigh vacuum for a number of reasons.

The vacuum of the chambers is maintained by several pumps. With rotary pumps a pressure in the range of 10^{-3} mbar can be reached. Turbomolecular pumps in sequence with rotary pumps reduce the pressure into the 1×10^{-8} mbar range. The pressure can be further reduced to 10^{-10} mbar by a proper bake-out procedure during which the chambers were usually maintained at 140 °C for some ten hours. At these pressures ion pumps which are oil and noise free are used to support the turbo pumps. Chamber pressure of 1×10^{-11} mbar range can even be achieved with titanium sublimation pumps. However, the base pressure in the chambers was typically in the rage of $\sim 1\times10^{-10}$ mbar, since oxygen gas was frequently used during the preparation of oxidized samples.

One of the chambers, called STM chamber in the following was equipped with the following parts: (1) A sample manipulator with xyz translation, axial rotation, a tungsten filament for electron-beam heating of the sample, and a copper block (that can be cooled with flowing gaseous or liquid nitrogen) as a thermal reservoir. (2) A

sputter gun, which is used for cleaning the sample surface (and occasionally STM tips) with a high-energy argon-ion beam. (3) A quartz-crystal microbalance that is integrated into the copper thermal reservoir of the manipulator, which is used for calibration of the metal deposition rates. (4) Commercial electron-beam evaporators (Focus) for for the deposition of Ti, Ta, and V, which are used for preparation of the oxide films that are to be investigated. (5) A leak valve, which is used for back-filling the chamber with a gas, keeping precise control on the pressure within several orders of magnitude. (6) A low-energy electron diffraction (LEED) apparatus, which is used for identifying the degree of surface crystallinity and the periodicity of ordered surface structures. (7) A quadrupole mass spectrometer (QMS) with a pumped Feulner cup,[85] which is used for monitoring concentrations of residual gases and for temperature-programmed desorption (TPD) experiments. (8) A tubular gas doser with 10 mm inner diameter and a 20 μm pinhole. The end opening is positioned at a distance of ~1 mm in front of the sample surface, which reduces the degree of chamber contamination by the dosed gas. The pin-hole acts as a pressure reduction stage, so that pressures in the gas-inlet system in the mbar range can be employed to dose under UHV compatible conditions. (9) An X-ray gun with Al-Kα and Mg-Kα radiation and an Omicron EA125 electron energy analyzer for X-ray photoelectron spectroscopy (XPS), which is used for chemical analysis of the surface. (10) A room temperature scanning tunneling microscope (Omicron STM), which is used for imaging surface structures. Parts (2)-(5) are for the sample preparation, while parts (6)-(10) are for the sample characterization.

Two other chambers, a system mainly used for UPS ("UPS chamber") and a chamber for XPS and NEXAFS ("BESSY-XPS chamber"), have components similar to parts (1)-(7) of the STM-chamber, so that samples of the same quality can be prepared. The UPS-chamber was additionally equipped with a rotatable electron energy analyzer for ARUPS (angular resolved ultra-violet photoelectron spectroscopy) using UV radiation from a He discharge lamp (21.22 eV). The BESSY-XPS chamber was operated at the UE52–PGM-PES beamline of the BESSY II electron storage ring in Berlin, at which photon energies in the range from 100 eV to 1500 eV are available. Synchrotron radiation sources extend the application range of photoelectron spectroscopy, beyond what is possible with standard laboratory point sources.

3.2 Sample preparation

The substrate used in this study is rutile single crystal of TiO_2(110) with dimension of 7 mm × 8 mm × 2 mm, purchased from Crystal GmbH in Germany. Before transfer into the UHV chambers, the crystal was fixed on a sample holder as shown in Figure 3.1. It was mounted on a heating plate by holding plates and screws. The heating plate was supported on another plate with sapphire spacers in-between. Two different materials, Ta or Pt, were used for the plates and screws. K-type thermocouple wires for the measurement of sample temperature were fixed at one side of the crystal by ceramic glue, with the other end spot welded to the thermocouple leads.

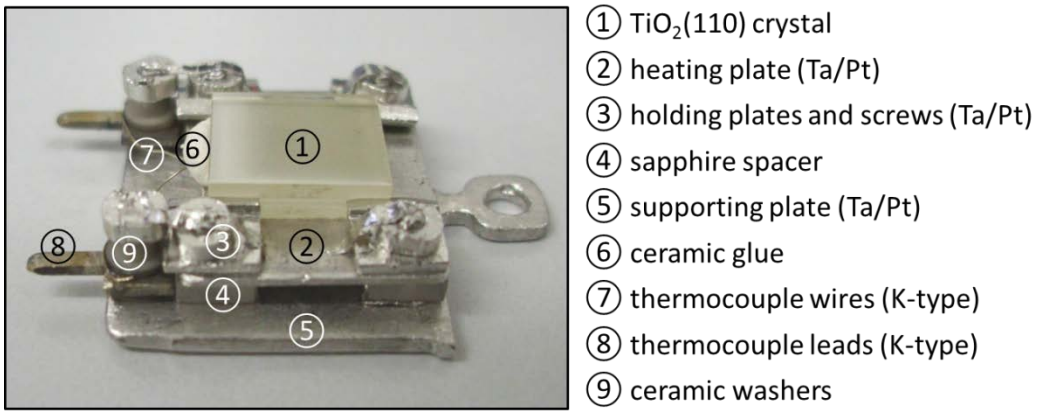

Figure 3.1 A Rutile TiO_2 sample supported on a holder. Its components are listed at the right.

Before the preparation of the thin film layers, TiO_2(110) single crystal substrates were cleaned by cycles of sputtering and annealing. Each cycle consisted of sputtering with Ar^+ ions (1 keV, 5 μA) for 30 min at room temperature followed by annealing at 970 K in vacuum for 30 min. These cycles were repeated until LEED images exhibited sharp (1×1) spots with low background intensity and XPS spectra did not show recognizable peaks other than those of TiO_2. This procedure did not only clean the substrate but also reduced it. The latter is required since conductive substrates are needed for the application of relevant techniques such as LEED, XPS and STM. While stoichiometric TiO_2 is electrically insulating (ϱ = 2000 Ωcm), a reduced crystal is conductive (ϱ = 10-100 Ωcm) after introducing Ti^{3+} defects into the bulk by sputtering and annealing. After the initial preparation, the conductive crystals had a light blue color which grew darker in the course of the experiments due

to the annealing cycles required in further preparation steps. Figure 3.2 shows examples of crystals with different colors: initial white-yellowish for the purchased crystal without cycles of sputtering and annealing, light blue for the crystal after several cycles of treatments, and dark blue for the crystal after tens of cycles of treatments. However, the heating up rate should not be too high to avoid the cracks such as in Figure 3.2(c). Because the thermal conductivity of TiO_2 (10 W/(m·K)) is lower than that of metals (10–400 W/(m·K)), high heating rates produce large temperature gradients within the crystal and create thermal stress. Cracks in the crystal may form from the growth of small scratches in the presence of thermal stress. In this study heating rates smaller than 2.0 K/s were used to avoid excessive thermal stress.

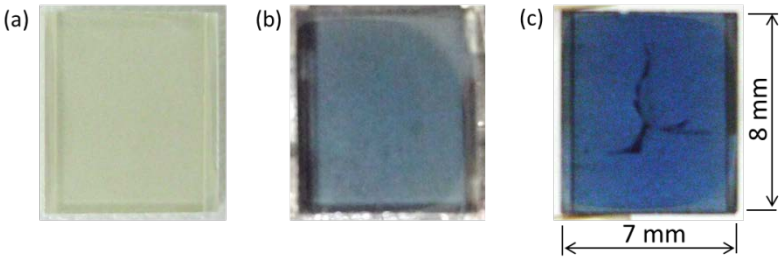

Figure 3.2 Rutile TiO_2 samples with different appearance: (a) a purchased crystal shows white-yellowish color. (b) A reduced crystal after several cycles of sputtering and annealing shows light-blue color. (c) After tens of cycles of sputtering and annealing the crystal turns blue and cracks appear within the crystal.

In order to prevent the crystal for being over-reduced (black-blue color), two procedures of oxidation-reduction of the substrate were usually conducted before the preparation of a new thin film layer. Once the old layer on the substrate was removed by sputtering, the crystal was positioned in front of the gas doser and annealed at 970 K in oxygen for 10–20 minutes (pressure of the doser backline is 1 mbar, corresponding to ~1×10^{-6} mbar at the sample surface). After annealing in oxygen, the sample was annealed at 850 K for 10–15 minutes in UHV before cooling down to room temperature. This oxidation-reduction procedure also induces the formation of large terraces at the surface that are preferred for STM imaging and for the growth of overlayers.

As mentioned in the introduction, thin film layers of Ti + V mixed oxide were used for the investigation and prepared according to a recipe developed by E.

Primorac.[19] The TiO_2(110) thin film was prepared on the rutile substrate with a Ti + Ta mixed oxide interlayer between the film and the substrate, as shown in Figure 3.3.

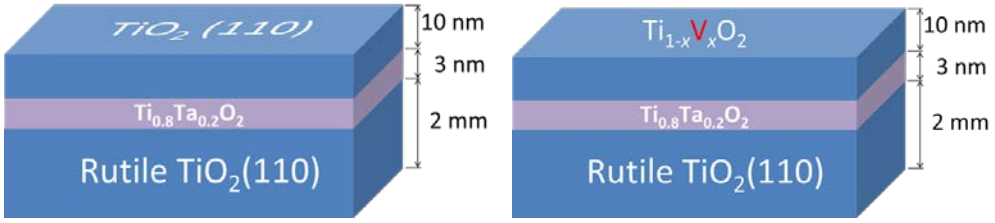

Figure 3.3 Schematic models of TiO_2(110) thin film (left) and TiO_2(110) films with admixed V (right) grown on a rutile (110) substrate with Ti + Ta mixed oxide interlayer. The Ti + V mixed oxide layer was prepared by doping V into the TiO_2 thin film. The diffusion of V into the substrate was prevented by the Ti + Ta mixed oxide interlayer.

The TiO_2(110) thin film was grown on the rutile substrate with a Ti + Ta mixed oxide interlayer between the substrate and the overlayer. The Ti + Ta mixed oxide layer ($Ti_{0.8}Ta_{0.2}O_2$, ~30 Å thick) was prepared on the substrate by co-deposition of Ta and Ti in an oxygen ambient atmosphere (1×10^{-6} mbar). Subsequently, the TiO_2(110) thin film (~100 Å thick) was epitaxially grown on the Ti+Ta mixed oxide layer by deposition of Ti at the same oxygen pressure followed by annealing in vacuum. During the deposition and annealing steps, the temperature of the substrate was maintained at 800 K. Details of the Ti + Ta mixed oxide interlayer and its impact on the TiO_2(110) thin film overlayer are discussed in section 4.1.

To prepare the Ti + V mixed oxide layers, Vanadium was added to the TiO_2(110) layer either by vanadium co-deposition during the growth of the TiO_2(110) layer or by deposition of vanadium onto the TiO_2(110) in O_2 (1×10^{-6} mbar). The final step was to anneal the sample in ultrahigh vacuum (2×10^{-10} mbar) at 800 K for 10 min. Both ways of vanadium doping lead to essentially identical Ti + V mixed oxide layers since during annealing in vacuum vanadium dilutes into the layer due to its high diffusion speed at 800 K. The doping concentration of V was tuned by adjusting the evaporation time. Before V disposition the deposition rate was calibrated with a quartz microbalance. With this recipe a Ti + V mixed oxide layer can be prepared and V diffusion into the rutile substrate was hindered by the Ti + Ta mixed oxide interlayer due to the tantalum ions (Ta^{4+}) having a larger ionic diameter than the Ti^{4+} ions. Vanadium concentrations are given as cross-section weighted V 2p XPS intensities divided by the sum of the cross-section weighted V 2p and Ti 2p XPS

intensities in scans. XPS spectra were recorded at normal and grazing electron exit angles (0° or 60° with respect to the surface normal of the sample) for different surface sensitivity.

Two different states of the Ti + V mixed oxide were investigated: reduced states and oxidized states. Reduced states of the sample were prepared by annealing the mixed oxide layer in vacuum, while oxidized states were prepared by annealing the layers in oxygen (i.e. 10^{-6} mbar O_2 at 800 K for 10 min). The surface properties of the samples in the different states are discussed in chapter 5 and chapter 6.

3.3 Characterization techniques

3.3.1 X-ray photoelectron spectroscopy

Introduction

X-ray photoelectron spectroscopy (XPS) is a chemical analysis technique based on the photoelectric effect. In XPS experiments, the sample is irradiated with X-rays, which interact with atoms in the sample causing emission of electrons, the kinetic energies of which are then analyzed. The inelastic mean free paths (IMFP) of the electrons are in the order of nanometers in solids, which makes XPS a surface sensitive technique. Because different elements have significantly different sets of core level electron energies, XPS is used to analyze the chemical compositions of surfaces. With a high energy resolution of the technique, information about the chemical environment of an element can be obtained since the core level electron energies depend slightly on the chemical environment.

Theoretical aspects

The standard laboratory X-ray sources are based on Mg Kα (1253.56 eV) and Al Kα (1486.58 eV) radiation (originating from electronic transition in Mg or Al atoms). A specialized source of X-rays which is becoming widely used in research is synchrotron radiation. Synchrotron radiation is generated by the acceleration of ultrarelativistic charged particles through magnetic fields. The radiation produced in this way has a characteristic polarization and the frequencies generated can range a broad electromagnetic spectrum.

A schematic representation of photoemission process is shown in Figure 3.4. X-rays radiation of wavelength hν ejects electrons from electronic states with different binding energies in the sample leading to a range of ejected electron kinetic energies. If the sample is at ground potential, electrons ejected from a state with binding energy E_b are emitted from the sample with a kinetic energy $E_{k'}$ given by:

$$E_{k'} = E_k - \Phi_s = h\nu - E_b - \Phi_s$$

where E_k is the kinetic energy referred to Fermi level, Φ_s is the work function of the sample. However the kinetic energy at the sample surface cannot be measured directly because Φ_s is usually not known. The energy of photoelectrons in the experiment as measured by the spectrometer is $(h\nu - E_b - \Phi_a)$, where Φ_a is the work function of the spectrometer. The ejected electrons pass through the first lens element and are then retarded by an amount R, determined by the lens voltages, before entering the analyzer. The analyzer is a band pass filter only transmitting electrons with energy very near to the pass energy E_p which are then stopped in the detector. Therefore the electrons have a measured kinetic energy of $(R + E_p)$:

$$E_{k,measured} = R + E_P = E_k - \Phi_a = h\nu - E_b - \Phi_a$$

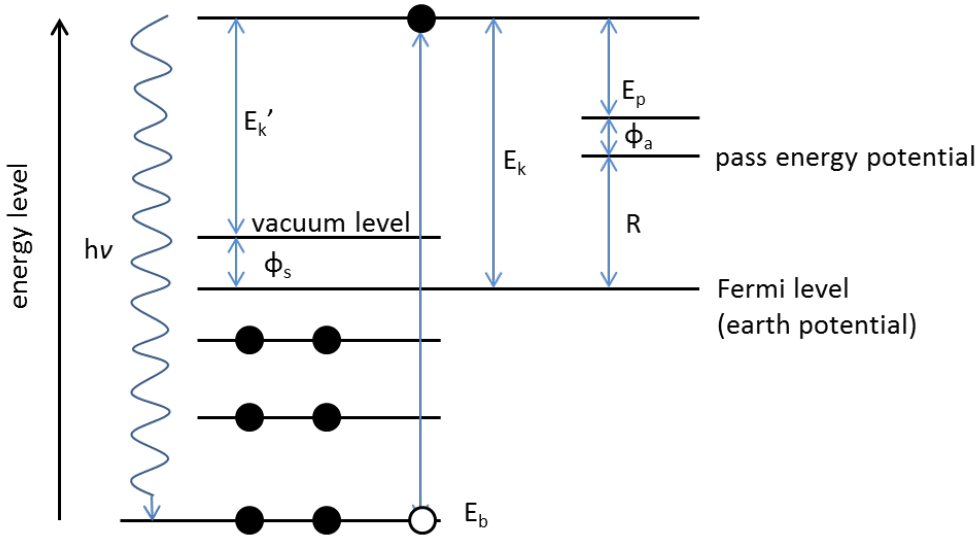

Figure 3.4 A schematic representation of the photoemission process. The kinetic energy of the electron leaving the sample ($E_{k'}$), the kinetic energy referred to Fermi level (E_k), the work function of the sample (Φ_s), retarded potential (R), pass energy (E_p), and the work function of the analyser (Φ_a) are marked separately.

The standard electron energy analyzer for XPS systems is the hemispherical electrostatic analyzer equipped with an electrostatic lens system at the entrance. Incoming electrons are firstly retarded/accelerated to certain energy in the lens system before entering the hemispherical analyzer. The electrons are then deflected into elliptical trajectories by the radial electrical field between the inner and the outer hemisphere of the analyzer. For a fixed electrical field gradient, only electrons with kinetic energies in a certain energy interval can pass from the entrance slit through the exit opening. Electrons with higher kinetic energy approach the outer hemisphere, while electrons with lower kinetic energy are deflected toward the inner hemisphere. At the exit plane a detector, usually a channeltron or a channeltron array or a multichannelplate, detect the number of electrons for a given detection time, and then this data is stored and displayed as a function of the kinetic or binding energy as a spectrum.

Experimental details

Determining the relative concentrations of elements in the sample is one of the main functions of XPS. In the case of a homogeneous concentration through the sample, the number of atoms of the elements per cm^3 of the sample **N** is determined by:

$$\mathbf{N = I / S = I / (f \sigma \theta y \lambda A T)}$$

where I is the number of photoelectrons per second (peak area), f is the x-ray flux, σ is the photo ionization cross-section for the atomic orbital of interest, θ is an angular efficiency factor for the instrumental arrangement, y is the efficiency in the photoelectric process for the formation of photoelectrons of the normal photoelectron energy, λ is the inelastic mean free path of the photoelectrons in the sample, A is the area of the sample from which photoelectrons are detected, and T is the detection efficiency for electrons emitted from the sample. In one measurement, values of f, θ, y, and A are the same for different elements; $\boldsymbol{\sigma}$ are adopted from the tabulated values by J.H. Scofield;[86] λ is obtained from the software "QUASES-IMFP-TPP2M" by S. Tougaard based on the Tanuma, Powell, and Penn TPP2M formula;[87] T is determined by normalizing an Ag/Au foil survey spectrum; I is calculated from the fitting of XPS peak intensities. Then the relative atom fractions of each element can be calculated according to the relative number of atoms:

$$C_x = \frac{N_x}{\sum N_i} = \frac{I_x/S_x}{\sum I_i/S_i} = \frac{I_x/(\mathrm{f}\sigma_x\theta\mathrm{y}\lambda_x\mathrm{A}T_x)}{\sum I_i/(\mathrm{f}\sigma_i\theta\mathrm{y}\lambda_i\mathrm{A}T_i)} = \frac{I_x/(\sigma_x\lambda_xT_x)}{\sum I_i/(\sigma_i\lambda_iT_i)}$$

where values of f, θ, y, and A are canceled out.

The surface sensitivity can be increased by using x-rays with lower photon energy, which is practical with synchrotron radiation. Another way to increase the sensitivity is to adjust the sample position relative to the x-ray source and the analyzer. The usual positioning of a sample in an XPS experiment is such that the angle between the surface normal of the sample and the axis of the analyzer is 0° (normal). If this angle is increased to θ (grazing) then the electrons also have to travel parallel to the surface in order to leave the solid in the direction of the analyzer. By comparing the relative atom fractions of different elements for different exit angles, the depth distribution of elements can be obtained to determine if the sample is a vertically homogenous mixture or not.

3.3.2 Low-energy electron diffraction

Introduction

Low-energy electron diffraction (LEED), based on elastic backscattering of low energy electrons, is commonly used to determine the symmetry of the surface structure with long rang order. The energy of the incident electron beam is in the range from 20 eV to 150 eV, which corresponds to a wavelength of around 1 Å. The mean free path of the electron with such energy lies in the range of several Angstroms, making this technique very surface sensitive. In model catalysis where single crystals are employed, LEED is useful in the analysis of the quality of the single crystal surfaces, the reconstruction of the surfaces, and the structure of ordered adsorbates. LEED is routinely used in many surface science laboratories to check the cleanliness and order of the surfaces. The appearance of a LEED pattern with bright and sharp spots is widely regarded as an evidence for a clean and ordered surface.

Theoretical aspects

When electrons of low energy (50–200 eV) are employed for the measurements, it is reasonable to suppose that only diffraction from the several top layers of ordered atoms is observed. Figure 3.5(a) shows a schematic diagram of a diffraction process occurring at a surface in real space, where electrons are scattered elastically in all directions. In LEED experiments the angle of the incident electrons with respect to

the normal of the surface is usually zero. Scattered electrons will exhibit an interference pattern with constructive interference in directions with

$$\sin\Psi = \frac{n\lambda}{d} = \frac{\mathrm{n}h}{d\sqrt{2m_eE_{kin}}}, \qquad n = 0, 1, 2, \ldots$$

Ψ is the angle between scattered electrons and the surface normal; n is the order of the diffraction; d is the distance between two atoms in the surface; λ is the wavelength of the electrons with

$$\lambda = \frac{h}{\sqrt{2m_eE_{kin}}}$$

h is Planck constant; m_e is the mass of the electron; E_{kin} is the kinetic energy of the electron.

If the scattered electrons are collected with a fluorescent screen, one observes a pattern of spots, each of which corresponds to a direction in which constructive interference takes place. Because of the inverse relationship between interatomic distances and the angles in which constructive interference between the scattered electrons occurs, the separation between LEED spots is large when interatomic distances are small, and vice versa. The LEED pattern is essentially an image of the so-called "reciprocal lattice", and it is convenient to consider the diffraction process in the reciprocal space. Figure 3.5(b) shows the corresponding reciprocal space with an Ewald sphere. The Ewald sphere construction is a geometrical construction used to determine the condition for constructive interference in the reciprocal lattice by applying the law of the conservation of momentum. In the reciprocal space the distance between adjacent lattice rods is 2π/d. The wavevector $\boldsymbol{k}_0$ (2π/λ) of the incident electron is drawn to scale on this diagram, with its tip pointing towards the origin (000). A circle, the Ewald sphere, is then drawn with radius $|\boldsymbol{k}_0|$, centered at the origin of the vector (point P). The condition for constructive interference is satisfied with the scattered beam having a wavevector $\boldsymbol{k}'$, if any of the reciprocal lattice rods are intersected by the Ewald sphere. By conservation of momentum $\boldsymbol{k}_0 = \boldsymbol{k}' + \boldsymbol{g}$ where the change in momentum on scattering is represented by the vector $\boldsymbol{g}$. In LEED the incident electron beam is normal to the surface and the Ewald sphere is constructed as shown in Figure 3.5(c). The incident wavevector $\boldsymbol{k}_0$ increases with increasing electron beam energy, so that the size of the Ewald sphere increases, cutting more and more rods. This means that, as the beam energy increases, more and more spots will appear on the LEED screen and the spacing between spots will progressively decrease. Note that in the figure the Miller Index (h k) is marked as (0 k)

with h kept constant and k varied. This is because only part of reciprocal space can be drawn with the diffraction conditions satisfied in one azimuth.

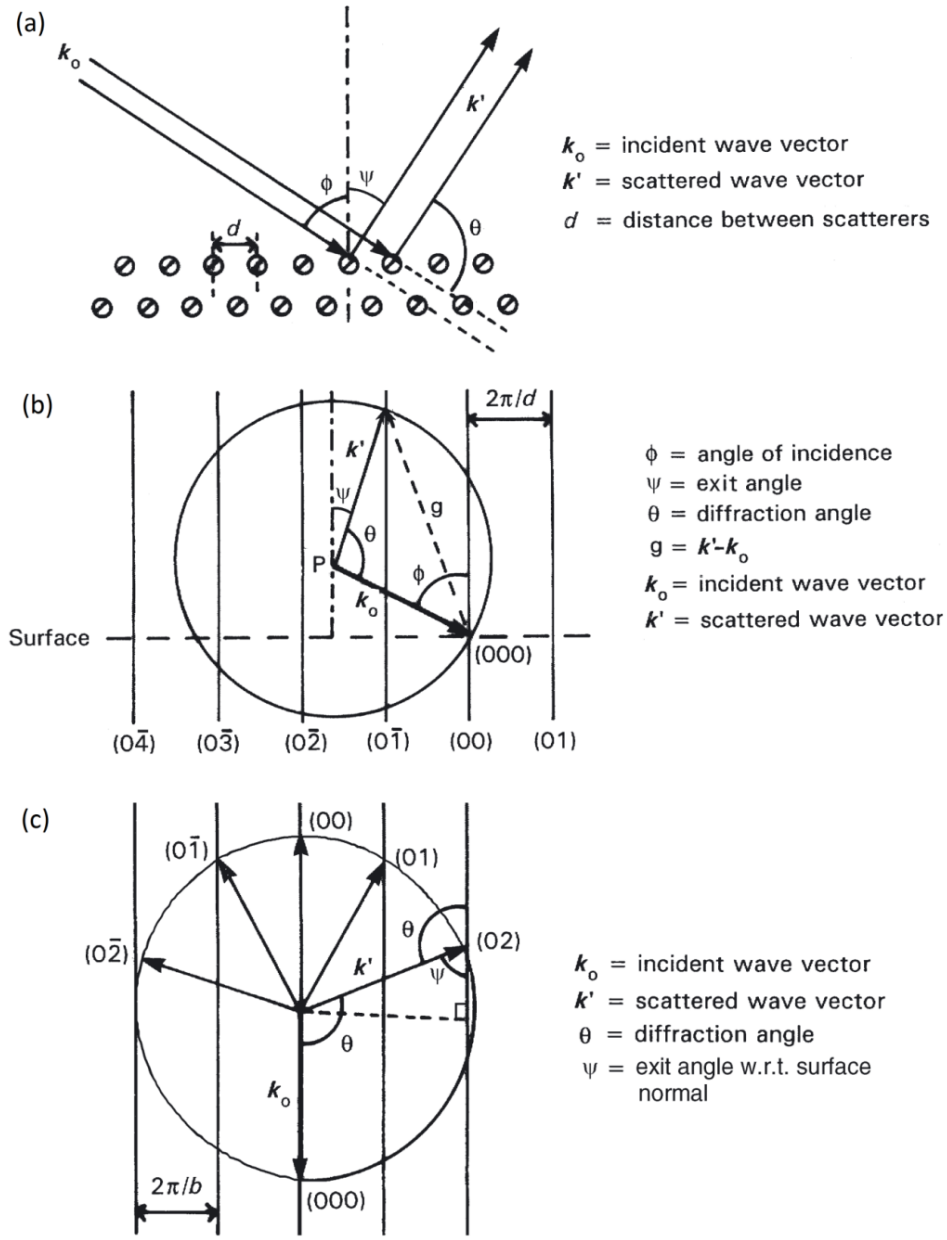

Figure 3.5 (a) A schematic diagram of a diffraction process occurring at a surface in real space. (b) Ewald sphere construction in the corresponding reciprocal space. Only diffracted beams where the Miller index h=0 are shown. (c) The Ewald sphere construction for an electron beam incident normal to the surface. (Reproduced with permission from ref 88. Copyright 2009 John Wiley & Sons Ltd.)

Experimental details

A typical experimental arrangement used in a LEED experiment is illustrated schematically in Figure 3.6, which comprises a fluorescent screen and an electron gun aligned along the central axis of the screen.

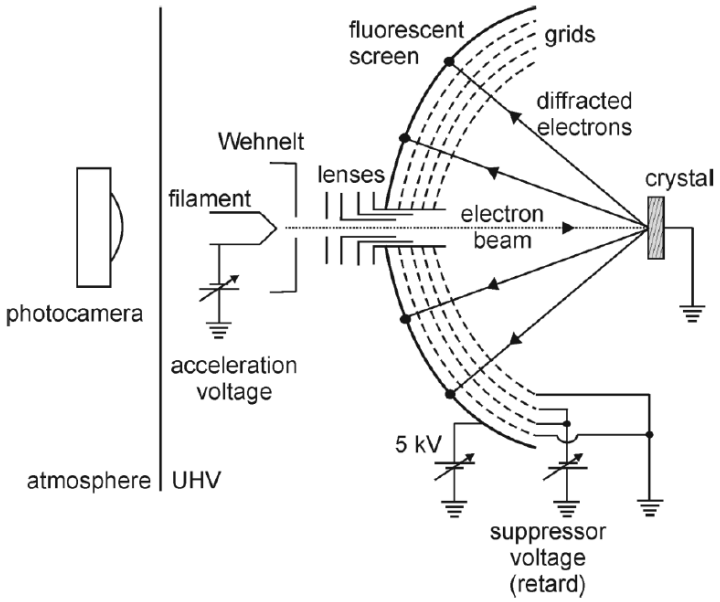

Figure 3.6 A schematic diagram of a standard 4-grid LEED optics apparatus.

Electrons are emitted from the electron gun filament (LaB6, W or Ir coated filament), which then follow paths along the central axis with the aid of Wehnelt cap and electrostatic lenses, and finally hit the sample at ground potential in order to prevent charging. The electrons are then backscattered from the sample surface onto a system of grids surrounding the electron gun. The backscattered electrons are of two types; elastically scattered electrons forming a set of diffracted beams which create the LEED pattern, and inelastically scattered electrons, which may make up 99% of the total flux, but which don't contribute to the pattern. The backscattered electrons are then accelerated towards the screen biased to 3-6 kV. The first and the last grid are kept at ground potential. The grounded grids function as shielding to the electric field generated by the grids and screen with high voltages so that linear beam trajectories are possible. The two grids (called retard, suppressor or gate) in the middle are at a potential of several volts below the incident electron beam. Therefore the inelastically scattered electrons which have lost more than a few volts cannot

reach the screen – they are repelled. The function of the negatively biased grid is to repel the inelastically scattered slow electrons ("secondaries") which actually constitute a significant part of the total back-scattered electrons. The fluorescent screen is biased positively at a few kilovolts for accelerating the electrons before strike, in order to create a visible fluorescence. The pattern that forms on the screen can be viewed through the viewport and recorded by a camera.

In a quantitative way, LEED can also be performed in the LEED–IV or SPA–LEED (Spot Profile Analysis) modes, where the instrumentation is more advanced. In LEED–IV, the intensities (I) of some diffraction spots are measured as a function of electron beam energy (V). The resulting curves have to be reproduced by theoretical calculations to a certain degree of accuracy. Calculations take multiple scattering of electrons from the first few layers of the surface into account. The calculation process requires an initial guess for the structure and proceeds iteratively to find the correct structure. In SPA–LEED, shapes of diffraction spots are measured. From the broadening and sharpening of the spots, information regarding the density of defects and processes like surface phase transitions can be extracted.

3.3.3 Scanning tunneling microscopy

Introduction

Imaging directly the surface, preferably in atomic detail, is required in the research of a catalyst. While optical microscopy is of no use to this end due to its rather long wavelength of visible light, electron microscopy was developed and achieved magnifications on the order of one million times. However not all catalysts can be imaged atomically with electron microscopy when diffraction effects take place during imaging. The developments since 1980' in determining the surface structure are the scanning tunneling microscope (STM) and the scanning or atomic force microscope (SFM or AFM). The general concept behind scanning probe microscopy is that a sharp tip is rastered across a surface by piezoelectric translators, while a certain property reflecting the interaction between the tip and the surface is monitored. As a result, scanning probe microscopy yields local information. In this work STM was applied to reveal the surface structure. In this section principles and experimental details of STM are introduced.

Theoretical aspects

STM is based on the quantum tunneling of electrons between the surface and a very sharp tip. The cloud of electrons at the surface is not entirely confined to the surface atoms but rather extends into the vacuum. When an extremely fine tip approaches the surface to within a few Angstroms, the electron clouds of the two begin to overlap. A small bias potential on the tip is sufficient to cause a measurable tunneling current over the tunneling gap between the tip and the surface. Although it is not easy to fully describe the tunneling process of STM, the phenomenon of quantum tunneling can be understood with a simple one-dimensional model. In a simple system where an electron is incident upon an infinitely thick potential barrier of height V, the Schrödinger equation has two components:

$\mathrm{H} = -\left(\frac{\hbar^2}{2\mathrm{m}}\right)\left(\frac{\mathrm{d}^2}{\mathrm{dx}^2}\right)$ for x < 0 inside the well

$\mathrm{H} = -\left(\frac{\hbar^2}{2\mathrm{m}}\right)\left(\frac{\mathrm{d}^2}{\mathrm{dx}^2}\right) + \mathrm{V}$ for x > 0 inside the barrier

The solutions of these equations are:

$\psi = Ae^{ikx} + Be^{-ikx},\ k = (2mE/\hbar^2)^{1/2}$ inside the well

$\psi = Ce^{ik'x} + De^{-ik'x},\ k = (2m(E-V)/\hbar^2)^{1/2}$ inside the barrier

The wave function inside the barrier has an imaginary part and a real part. The real part decays exponentially with distance inside the barrier, which means that there is a finite probability to find electron inside the barrier. Consider two nearby metallic electrodes with a work function φ, separated by a large distance. The effective overlap of the Fermi level wavefunctions is negligible, because of the exponential decay of the two separate wavefunctions. If these electrodes are brought close together, with some separation, then the overlap of the wavefunctions may be sufficiently great to facilitate quantum mechanical tunnelling and, under the influence of an applied potential difference, the passage of a measurable current. The tunneling current is in the range of pico- to nanoamperes, and varies exponentially with the distance between tip and surface.

Experimental details

It is the steep variation of the tunneling current with distance that enables one to obtain an image of the atoms in the surface when the tip is rastered over the surface.

The most common method of measuring STM images is to record the height of the tip over the surface while keeping the tunneling current constant. If the tunneling current is from the surface to the tip, the STM images the density of occupied states. However, if the potential is reversed the current flows in the other direction, and one images the unoccupied density of states. It is important to realize that STM does not necessarily image atoms, but rather a section of the density of states near the Fermi level. One must be careful in translating STM pictures directly into ball models of the surface. Figure 3.7 illustrates the operation of an STM in a very schematic fashion. The key components are the tip, some means of achieving very delicate movements in the x-, y- and z-directions and a computer system to control the whole operation. Fine control of the tip position (both laterally and vertically) is achieved by the use of piezoelectric crystals, on which either the STM tip or the sample is mounted. The piezoelectric crystals move in a well-defined fashion in each of the three spatial directions as the applied potential difference in each direction is varied.

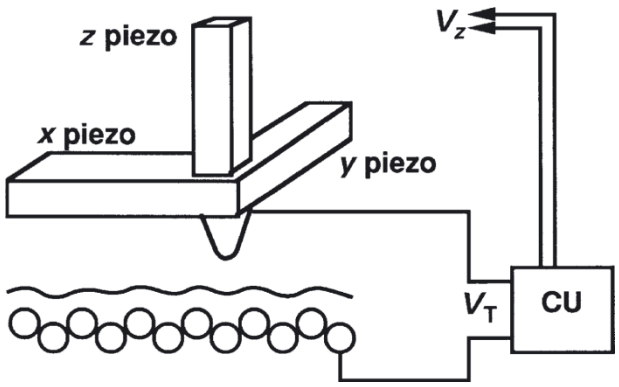

Figure 3.7 Schematic diagram of the operation of the STM, where CU is the control unit, V_T is the sample bias voltage and V_z is the voltage applied to the z piezo to maintain constant tunneling current. (Reproduced with permission from ref 88. Copyright 2009 John Wiley & Sons Ltd.)

In both modes, the tip is brought close to the surface (a few Angstroms) and a potential difference is applied, with the consequence that a current begins to flow. This current is the tunneling current, and it is monitored as the tip begins to scan across the surface. In constant voltage mode, the potential between the tip and the surface (the bias voltage) is maintained at a constant value, and the image represents the variation in the measured tunneling current with position. The more commonly employed mode is constant current mode, however. In this mode, the instantaneous tunneling current is measured at each position and the bias voltage is adjusted via a

computer-controlled feedback loop such that the tunneling current re-assumes some pre-set value. The STM image thus represents the variation in the z-voltage with coordinate (x_i, y_i). Adjustments to the bias voltage cause the piezoelectric crystal to move up and down, and if the displacement of the crystal is known for a given change δV in the bias voltage, then the image may be plotted as tip displacement (height), z_i against surface coordinate (x_i, y_i).

It is possible to obtain chemical information from STM when it is used in the spectroscopic mode, for example by measuring at a fixed distance the tunneling current I as a function of the voltage over the gap (I/V spectroscopy). This method of measurement is termed "scanning tunneling spectroscopy" (STS).

3.3.4 Temperature-programmed desorption

Introduction

Temperature-programmed desorption (TPD) is a technique for studying surface-adsorbate interactions. In TPD, a sample with adsorbed molecules on its surface is heated up with a constant heating rate. Meanwhile, the desorption products are monitored by a mass spectrometer. The outcome of the experiment is a plot of mass signals of gas partial pressures versus temperature.

Theoretical aspects

Figure 3.8 shows a schematic set-up for TPD. The signal from the thermocouple is fed to a temperature control unit, which controls the power of heating through a feedback loop. This arrangement increases the crystal temperature linearly as a function of time. The crystal is placed at the entrance of the mass spectrometer housing, which is commonly referred to as "Feulner cup".[85] There is a small opening for the Feulner cup, which allows desorption products to come almost exclusively from the sample and not from the surrounding surfaces. The spectrometer is usually pumped differentially by a separate pump. The differential pumping is important for getting high-quality spectra; otherwise, inefficient pumping leads to noise signals and broadening of the peaks. The temperature and mass signals from the mass spectrometer are then collected and plotted into a spectrum. Signals of different masses are usually recorded simultaneously so that information of desorbed species is collected to analyze the surface-adsorbate reaction.[89]

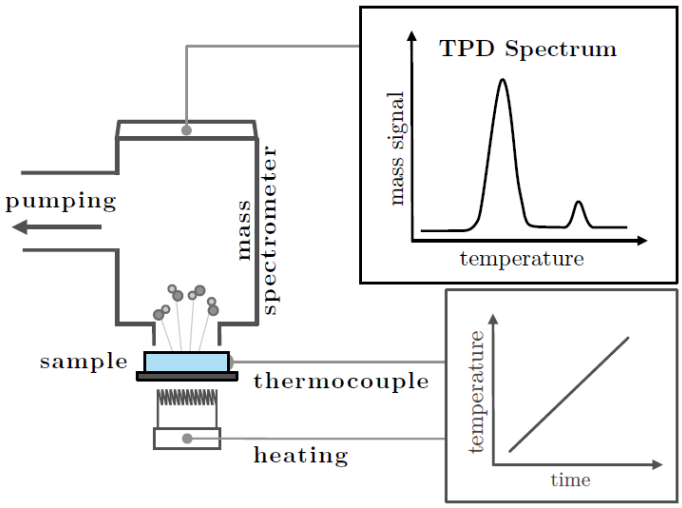

Figure 3.8 Scheme of a temperature programmed desorption experiment. (Reproduced with permission from ref 90. Copyright 2013 HU Berlin)

Analysis of TPD spectra can be conducted in a quantitative fashion to obtain values for kinetic parameters related to desorption like activation energy, the pre-exponential factor for desorption and the order of desorption. The fundamental equation in TPD is the Polanyi-Wigner equation, which gives the relationship between the rate of desorption and the kinetic parameters of desorption.[89] If the pumping speed is infinitely high to prevent readsorption of the desorbed species back onto the surface, readsorption may be ignored, and the relative rate of desorption – defined as the change in adsorbate coverage per unit of time – is given by:

$$r = -\frac{d\theta}{dt} = k_{des}\theta^n = v(\theta)\theta^n \exp\left(-\frac{E_{des}(\theta)}{RT}\right)$$

$$T = T_0 + \beta t$$

where r is the rate of desorption; θ is the coverage in monolayers; t is the time; k_{des} is the reaction rate constant for desorption; n is the order of desorption; v is the pre-exponential factor of desorption; E_{des} is the activation energy of desorption; R is the gas constant; T is the temperature; T_o is the temperature at which the experiment starts; β is the heating rate.

Complete analysis of TPD data applying the Polanyi-Wigner equation is rather complex because both E_{des} and v (and sometimes n) depend on coverage θ. Simplified methods are developed, which make use of spectral features that are easily accessible.

The most popular relationship that is derived from Polanyi-Wigner equation is the Redhead formula,[91] which gives the activation energy as a function of the peak maximum temperature:

$$E_{des} = RT_{max}\left[\ln\left(\frac{vT_{max}}{\beta}\right) - 3.46\right]$$

In deriving this relation, the order of desorption is taken as 1 and the pre-exponential factor and activation energy are assumed to be independent of coverage. This equation is very often applied to determine E_{des} from a single TPD spectrum, with an assumption of the value of v being 10^{13} s^{-1}.

Another popular method has been developed by Chan, Aris and Weinberg,[92] in which E_{des} and v are expressed in terms of the peak maximum temperature (T_{max}) and the peak width at half the maximum intensity (W):

$$E_{des} = RT_{max}\left[-1 + \sqrt{\left(\frac{W}{T_{max}}\right)^2 + 5.832\,\frac{T_{max}}{W}}\right] \qquad \text{for n=1 (first-order desorption)}$$

$$v = \frac{E_{des}\,\beta}{RT_{max}^{\,2}}\exp\left(\frac{E_{des}}{RT_{max}}\right)$$

The obtained E_{des} and v values are extrapolated to zero coverage, in order to obtain the desorption parameters of a single molecule adsorbed onto an otherwise empty surface.

"Leading edge analysis" is another approximate method which is worth mentioning because it operates quite well at high coverage with a minimum number of assumptions.[93] In this case, only the "leading edge" part of the spectrum is utilized, where the coverage is high but decreasing very slowly, which allows for the "constant coverage assumption". In order to fix both T and θ, a relatively small temperature interval is selected at the low-temperature, high-coverage side of a TPD spectrum. An Arrhenius plot of this short interval can be obtained from

$$\ln(r) = \ln(v) + n\ln(\theta) - \frac{E_{des}}{RT}$$

in which slope and intercept give the kinetic parameters.

Chapter 4

Surface properties of TiO_2 thin film layer

This chapter introduces the surface properties, including structure and reactivity, of the TiO_2 thin films under reducing and oxidizing conditions. The characterization of the surface properties of the TiO_2 thin films is helpful for the study of Ti + V mixed oxides that are discussed in chapter 5 and chapter 6. In addition, an analysis of the Ti + Ta mixed oxide interlayer, which is the substrate for the Ti + V mixed oxide thin film, was conducted and is discussed with respect to its diffusion blocking effect and its influence on the TiO_2 overlayer.

4.1 Function of the interlayer

Ti + V mixed oxide layers are usually prepared by reactive deposition of vanadium in an oxygen environment on TiO_2 single crystal substrates (usually ~2 mm thick), which results in TiO_2 supported vanadia systems. Several experiments have shown that at temperatures higher than 600 K deposited vanadium diffuses quickly into the bulk of the substrate, leaving no vanadium at the surface. In order to produce a Ti + V mixed oxide that can endure high temperature annealing, TiO_2 thin films with a thickness in the range of several nanometers as a host oxide are a way out provided that the vanadium can be stabilized in the layer.

For not too thick layers, deposited vanadium on TiO_2 should be still detectable with surface science techniques even after high temperature annealing. Using thin films also enables the study of non-conducting oxides (Ti + V mixed oxide in our case), which are usually prepared on a conducting substrate. Not only for TiO_2 but also for other oxides it has been shown that electrically insulating thin layers can be

studied with methods employing charged particles.[8,9] Therefore, it is reasonable to use thin TiO_2(110) layers instead of massive single crystals.

Metal or alloy single crystals have been applied as conducting substrates for the preparation of TiO_2(110) thin films, such as $Ni_{94}Ti_6$(110),[13] Mo(110),[14] Ni(110),[15] Ag(100),[16] and W(100).[17,18] The TiO_2(110) thin films were either grown by oxidation of the substrate (i.e. a Ti-containing $Ni_{94}Ti_6$ alloy),[13] or by Ti deposition on the substrates with post-oxidation.[14,15,16,17,18] However, lattice mismatch between the substrate and the TiO_2 overlayer was a commonly unavoidable problem, which induces strain in the TiO_2 films. To compensate the strain, most TiO_2 films were thus reduced with a low level of non-stoichiometry.[15,17,18] Discrete islands of TiO_2 rather than a continuous film were found at the substrate surface in many cases.[13,14,15,16,17,18] The domain boundaries of the discrete islands form a complex surface structure and affect the chemical activity of the TiO_2(110) overlayers. Also crystallographic shear planes may exist in the TiO_2(110) thin film.[15]

There is no report in the literature that a well ordered TiO_2(110) thin film could be grown on a metallic substrate. Due to the different lattice parameters of TiO_2(110) (see part 2.1.1), lattice mismatch was always observed between the substrate and thin film. A lattice mismatch can be avoided if a rutile single crystal with (110) surface is employed as substrate for the growth of Ti + V mixed oxide layers. However, vanadium diffusion at high temperature must be prevented.

An interlayer between the mixed oxide overlayer and the rutile substrate, acting as a diffusion barrier, would be a way to solve this problem.[19] The diffusion barrier can be achieved by introducing ions with a larger ionic diameter than that of the Ti^{4+} cations into TiO_2 forming a stressed interlayer of mixed oxide. Cations of oxides with rutile structure were preferred, since in this case one may expect that the introduction of alien cations into the host lattice does not change the structure significantly. A rutile type matrix of the interlayer is proficient for the growth of a well-ordered TiO_2 layer and a Ti + V mixed oxide. Table 4.1 lists lattice parameters of some oxides with rutile type structure.

Table 4.1 Structural parameters of oxides with rutile type structure.[19]

	TiO_2	**β-PbO_2**	**TaO_2**	**WO_2**
Cation radius	0.75 Å	0.92 Å	0.82 Å	0.80 Å
Structure	Tetragonal	Tetragonal	Tetragonal	Monoclinic
Lattice constant	a = 4.59 Å	a = 4.91 Å	a = 4.96 Å	a = 5.56 Å, b = 4.90 Å
	c = 2.95 Å	c = 3.39 Å	c = 3.39 Å	c = 5.66 Å, β = 120.5°

The suitabilities of Ta, W, and Pb as alien cations in such a diffusion blocking interlayer were tested by E. Primorac during the development of the recipe.[19] They were first co-evaporated with Ti in an oxygen environment (1×10^{-6} mbar) at 800 K, so that a mixed oxide layer was produced on a rutile substrate with (110) surface. LEED and XPS were employed to test the structure and the oxidation state of the ions in the as-prepared mixed oxide layer. If the mixed oxide layer exhibited a rutile type surface, a thin film layer of pure TiO_2 was prepared on it. The film was then annealed at high temperature in vacuum to examine the thermal stability of the interlayer. When the interlayer fulfilled the two conditions (having rutile structure and being thermally stable), vanadium was mixed into the pure TiO_2 thin film to form a Ti + V mixed oxide layer, which was then annealed in vacuum at high temperature to check if the interlayer blocks the diffusion of vanadium.

No LEED pattern similar to that of TiO_2(110) was observed for the Ti + Pb mixed oxide, and the concentration of lead at the surface was higher than in the bulk as inferred from angle-resolved XPS measurements. This indicates that a lead containing component aggregates at the surface, which rendered the layer useless for the given purpose. On the other hand, tungsten cations appeared to be well mixed into the TiO_2, forming an oxide layer of rutile type. However tungsten ions were found to diffuse to the top TiO_2 layer upon annealing at 800 K for about 30 min. In view of this short stability time at elevated temperature, this type of blocking layer was also not considered for further application.

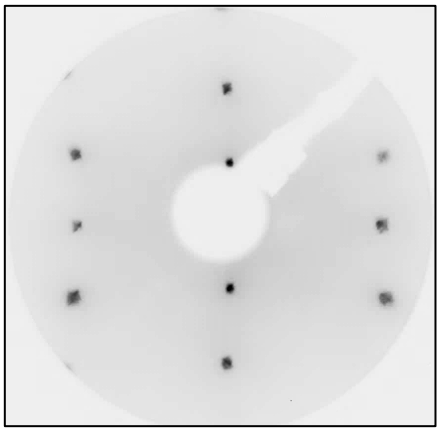

Figure 4.1 (1 × 1) LEED pattern of the Ti + Ta mixed oxide interlayer (with 20% Ta) grown on a TiO_2(110) substrate.

After several systematic tests, Ta ions were selected as the alien component of the interlayer, since a mixture of TaO_2 and TiO_2 forms a rutile structure and was found to be more stable with respect to high-temperature treatment. Tantalum with concentrations (relative to titanium) of 10% to 30% was introduced into the lattice of TiO_2, and there was no significant impact observed onto the crystal structure, although a slight lattice expansion in this layer relative to regular TiO_2 is conceivable. The LEED pattern of the Ti + Ta mixed oxide interlayer shown in Figure 4.1 is identical to that of TiO_2(110), which means that TiO_2(110) thin films of high-quality can successfully be grown on this layer due to the absence of a notable interface strain. Moreover, as deduced from XPS data, the Ta 4d spectrum of the interlayer (spectrum (c) in Figure 4.2) shows that the oxidation state of Ta is probably 4+, which is another indication for the solubility of Ta cations in the rutile lattice.

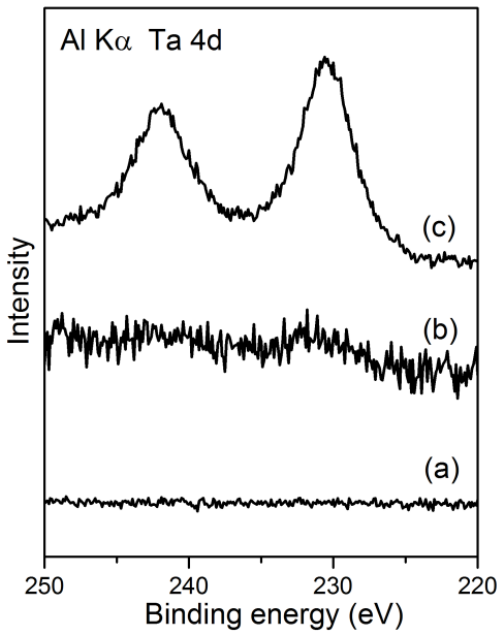

Figure 4.2: XPS spectra (Al-K*α*: 1486.6 eV, normal emission) of the Ta 4d core level measured of (a) a freshly prepared TiO_2(110) thin film, (b) the TiO_2(110) thin film after annealing in vacuum at 900 K for more than 2 hours and (c) the as-prepared Ti + Ta mixed oxide interlayer with 20% Ta.

The thermal stability of the Ti + Ta mixed oxide interlayer was examined by checking the diffusion of Ta into the TiO_2(110) top layer upon thermal treatment. The Ta 4d level has a reasonable photoionization cross section for Al-kα radiation so that even rather small contaminations can be seen. Spectrum (a) in Figure 4.2

displays a XPS spectrum of the Ta 4d energy range from the freshly prepared TiO_2 layer. As expected, there was no indication of Ta 4d emission. Spectrum (b) in Figure 4.2 shows up a weak Ta signal (corresponding to a Ta concentration of less than 2%) after annealing the sample for more than 2 hours at 900 K. The sample may be annealed at 800 K for 10 h before a Ta 3d signal gets visible. During the investigation of Ti + V mixed oxide overlayer, the XPS spectrum of Ta 4d range was measured from time to time to check for a Ta contamination. In case of even just a weak sign of such a contamination the film was sputtered off and a new film was prepared.

The blocking property of the Ti + Ta mixed oxide layer with respect to the diffusion of vanadium was tested by checking the change of the vanadium concentration in the Ti + V mixed oxide overlayer upon annealing. V 2p spectra were measured before and after annealing the sample at 800 K for a certain time i.e. 30 min. The concentration of vanadium in the mixed oxide was the same in both measurements, which means that the interlayer indeed blocks the vanadium diffusion. Details related to the Ti + V mixed oxide are introduced in chapter 4 and chapter 5.

It was found that the Ti + Ta mixed oxide interlayer does not just block the diffusion of vanadium, but also hinders the diffusion of the Ti ions between the overlayer and the substrate. This was tested with valence band photoelectron spectroscopy of TiO_2(110) overlayers without vanadium. Figure 4.3 displays highly surface-sensitive spectra of the TiO_2(110) band gap regime, where the reduction-induced band gap state is located. The band gap state at 0.8 eV below the Fermi level results from the reduction of the TiO_2(110) surface, and can be eliminated by oxidation of the sample. The exact nature of the band gap state is still an actively discussed issue[94], but there is some kind of agreement that it is induced by reduced cations.[94,95,96]

Spectra (a) and (c) in Figure 4.3 are for the oxidized TiO_2(110) substrate and the oxidized TiO_2(110) thin film. Both samples were prepared by annealing in oxygen (1×10^{-6} mbar) at 800 K for 10 min. No peak was observed indicating no band gap states for both samples. After the former oxidation procedure, the substrate and thin film samples were reduced by sputtering at room temperature and annealing in vacuum at 800 K for 10 min. As a result, the band gap state at 0.8 eV is observed in the spectra of the reduced surfaces as shown in spectra (b) and (d). However, the intensity of the band gap state in the spectrum of the reduced thin film is much higher than that in the spectrum of the reduced substrate, although both samples were prepared with the same annealing condition. This indicates that the diffusion of the reduced Ti cations between the substrate and the top layer is blocked by the Ti + Ta mixed oxide interlayer. Otherwise, the peak intensities of the band gap state for

the thin layer and the single crystal surface would be identical. This suggestion is further confirmed from the extended annealing procedure of the thin film. As shown in spectrum (e) the intensity of the 0.8 eV state does not decrease but remains the same after annealing the thin film in vacuum at 800 K for 10 more minutes. If the interlayer would not hinder the diffusion and there is ion exchange between the overlayer and the substrate, this second annealing step would lead to a decrease of the band gap state intensity due to diffusion of the reduced cations into the substrate.

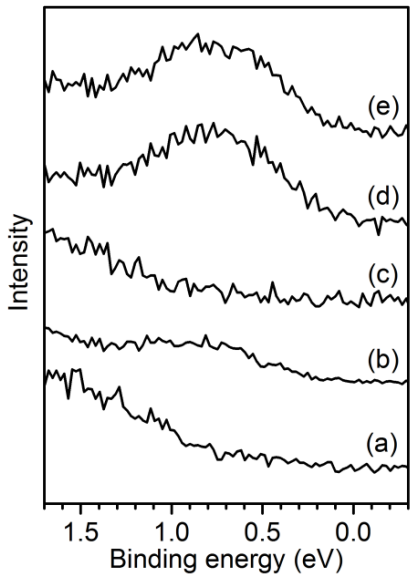

Figure 4.3 Surface sensitive HeI UPS spectra (electron detection at 70° off-normal) of the TiO_2(110) band gap region. (a) single crystal annealed at 800 K in 10^{-6} mbar O_2 for 10 min, (b) single crystal reduced by sputtering at room temperature and annealing at 800 K for 10 min, (c) TiO_2(110) thin film annealed at 800 K in 10^{-6} mbar O_2 for 10 min, (d) TiO_2(110) thin film reduced by sputtering at room temperature and annealing at 800 K for 10 min, and (e) the layer produced in step (d) annealed for 10 more min at 800 K in vacuum. (Reproduced with permission from ref 97. Copyright 2016 American Chemical Society.)

With this blocking layer the epitaxial TiO_2(110) thin film is thus decoupled from the rutile (110) substrate: the travel of Ti ions from the layer into the substrate and vice versa are strongly hindered. This does probably not just apply to reduced cations ("Ti^{3+}") but also to non-reduced cations ("Ti^{4+}") since their diffusion would also lead to a balance of the degree of reduction between substrate and overlayer. The interlayer largely prevents Ti atom exchange between the substrate and the overlayer which essentially has two profitable aspects: (1) fully oxidized TiO_2(110) layers can be grown on a reduced substrate and studied with experimental methods employing

charged particles, and (2) the TiO_2(110) overlayer can reduced and oxidized, even strongly if required, without changing the state of the substrate to a comparable extent. In the following section 4.2 and section 4.3, the surface properties of both the reduced and oxidized TiO_2(110) thin film are discussed. These layers were studied in order to establish a knowledge basis for the study of the mixed oxide layers.

4.2 Reduced TiO_2 layer

The surface structures of the TiO_2(110) thin film layer and the TiO_2(110) single crystal under reducing conditions were studied with LEED and STM. Both samples were reduced by annealing in vacuum at 900 K for 20 min. LEED images of the thin film layer show the typical (1 × 1) pattern (not shown here), the same as the pattern obtained from the reduced surface of the bulk sample (see the pattern in section 2.3). However, there are differences in the STM images shown in Figure 4.4. The spots between rows with different brightness are due to bridging oxygen vacancies which are expected for a reduced surface, and hydroxyl groups (brighter spots) which result from the dissociation of residual water at the bridging oxygen vacancies.

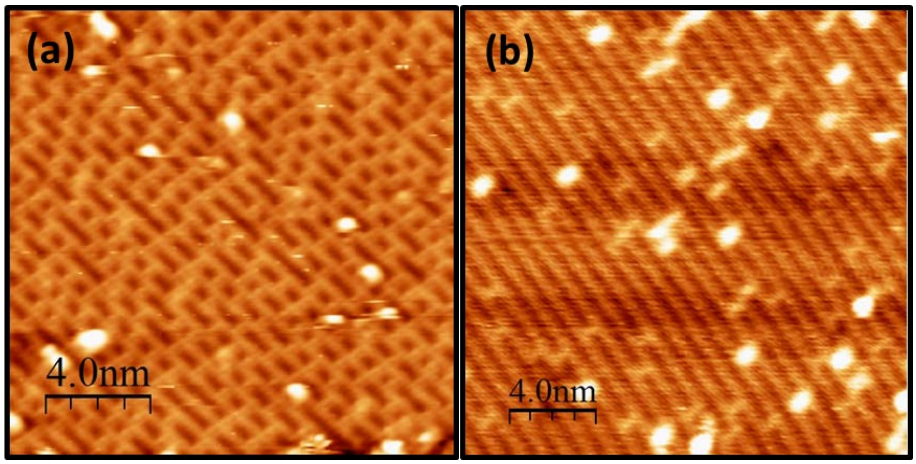

Figure 4.4 STM images of (a) the TiO_2(110) thin film (2.0 V, 0.1 nA) and (b) the TiO_2(110) bulk substrate (1.5 V, 0.1 nA) obtained after annealing in vacuum at 900 K for 20 min.

The densities of these features are significantly different in the two images. About 15% of the unit cells contain a bridging oxygen vacancy at the surface of the layer whereas the density is only 7% for the single crystal surface. The higher density of

bridging oxygen vacancies reflects a higher Ti^{3+} cation concentration in the thin film. They did not diffuse to the bulk of the substrate due to the blocking effect of the interlayer, which is in agreement with conclusion drawn from the valence band spectra pf the band gap state (see Figure 4.3). As described in the experimental part (chapter 2), the temperature of the sample during the preparation of Ti + V mixed oxide layers was mostly about 800 K. This annealing temperature is lower than the 900 K applied here and does not induce such a high density of 15% but a density of about 7% for the thin film (STM image is similar to image (b)).

Methanol TPD was used to characterize the chemical reactivity of the TiO_2(110) thin films. Figure 4.5 shows TPD spectra of methanol on a TiO_2(110) thin film, together with spectra from the bulk substrate without interlayer. Spectra from a previous methanol TPD study on a reduced single crystal by Henderson et al. are displayed for comparison.[48]

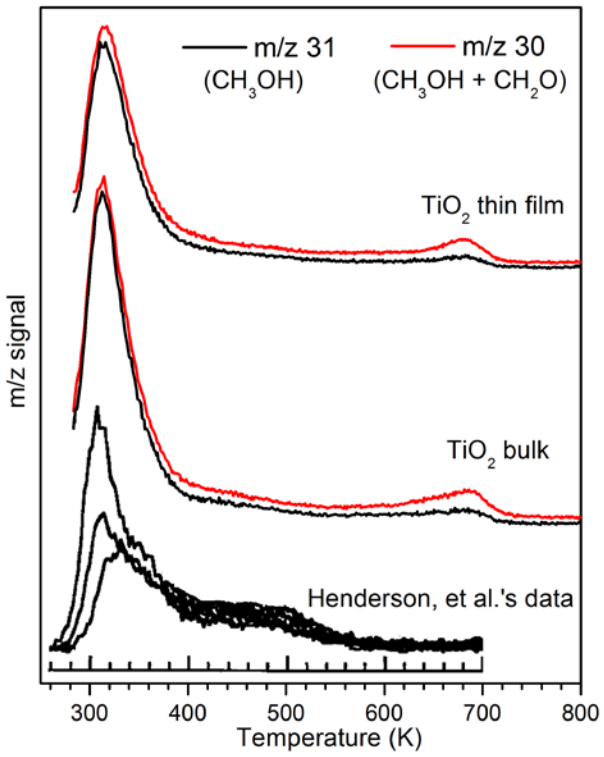

Figure 4.5 Mass 30 (red lines) and mass 31 (black lines) TPD spectra of CH_3OH on a TiO_2(110) thin film and a bulk single crystal. The TiO_2(110) thin film was annealed in vacuum at 800 K for 10 min prior to methanol adsorption, while the bulk sample was annealed in vacuum at 900 K for 10 min. Spectra from Henderson's experiments are displayed at the bottom for reference.

Prior to methanol adsorption, the TiO_2(110) thin film was reduced by annealing in vacuum at 800 K for 10 min, and the bulk sample by annealing in vacuum at 900 K for 10 min. Both annealing processes result in a similar density of the bridging oxygen vacancies. The methanol TPD spectra show mass 30 and 31 signals between 250 K and 800 K. Mass 31 is a main fragment of methanol, while mass 30 has contributions from both methanol and formaldehyde. For the TiO_2(110) thin film an intensive peak at 350 K was observed. This peak is reported to be due to methanol produced by recombination of fragments from the dissociation of methanol on 5-fold-coordinated Ti sites at the TiO_2 surface.[48,98] Beside this intensive peak, a peak at 680K for mass 31 was observed, indicating desorption of methanol around 680K. At the same temperature also a peak for mass 30 is seen. This may be assigned to CH_2O, CH_3OH, or a mixture of both. The ratio of the intensities of the mass 30 and 31 peaks at 680 K differs from the intensity ratio of the peaks at 350 K, which are assigned exclusively to methanol. This demonstrates that part of the intensity of the mass 30 peak at 680 K must be due to formaldehyde. Very similar spectra for methanol on bulk TiO_2(110) were observed, which clearly shows that the chemical properties of the thin film surface are very similar to those of the single crystal surface. Henderson and coauthors did also study methanol adsorption on reduced TiO_2(110).[48] However they did neither observe a methanol nor a formaldehyde desorption peak at 680 K.

Spectra for the mass 16, 18, 30 are compared in Figure 4.6. The contribution of methanol to the intensities was subtracted prior to plotting, so that the intensity for each mass represents methane, water, and formaldehyde produced at the surface. In the spectra, there is a prominent peak of water around 520 K, but no peak of methane was observed. Formaldehyde is produced at 680 K, as already discussed.

In Henderson's experiments, methanol was dosed at low temperature (~100 K), while it was dosed at room temperature in the present case. However, the TPD peak at 680 K was also observed when dosing was performed at low temperature. In this case, the different heating rate applied may play an important role. In Henderson et al's experiments, studies were conducted with a heating rate of 2 K/s, while in the present case the heating rate was 0.5 K/s. In TPD experiments the position of the peak maximum usually shifts to a higher temperature for a higher heating rate. This is illustrated in Figure 4.7 which shows a set of TPD experiments with heating rates of 0.5 K/s, 1.0 K/s and 2.0 K/s. Obviously the temperature of the peak maximum shifts from 680 K to 700 K and finally to 720 K with increasing heating rate. This could explain why they did not see the peak at 680 K in the spectra obtained for reduced TiO_2(110) with a heating rate of 2 K/s, since the spectra were only measured up to 700 K.

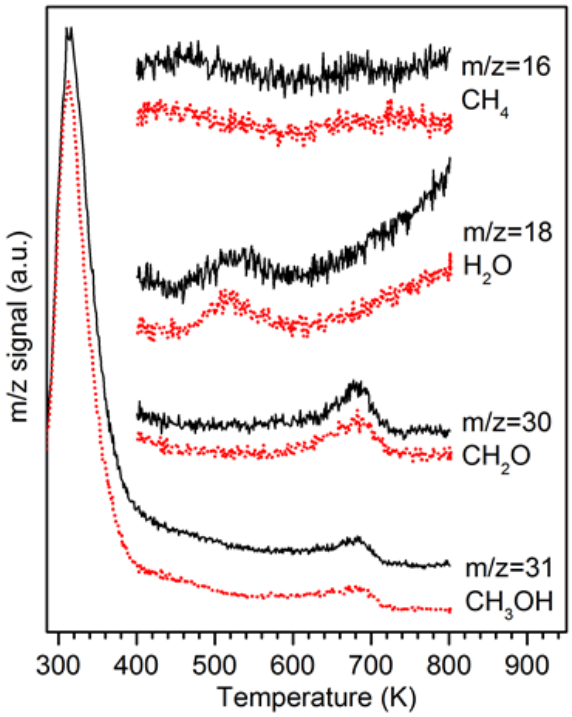

Figure 4.6 TPD spectra (masses 16, 18, 29 and 31) of methanol adsorbed at room temperature onto a TiO_2(110) thin film (solid line, black) and a TiO_2(110) single crystal (dotted line, red). The contributions of methanol were subtracted prior to plotting.

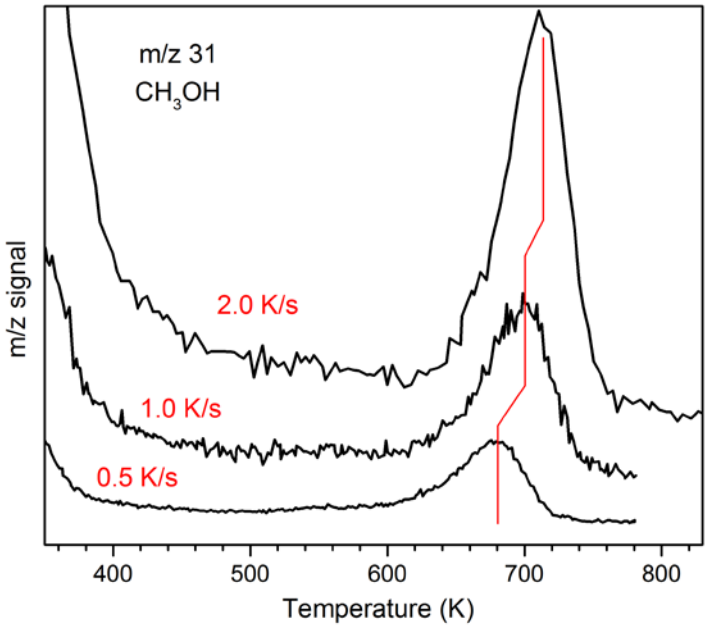

Figure 4.7 Methanol (m/z 31) TPD spectra with heating rates of 0.5 K/s, 1.0 K/s and 2.0 K/s.

While no peak at 680 K was detected by Henderson et al., other researchers found a formaldehyde desorption peak at this temperature,[78,79] but no methanol desorption. The production of formaldehyde was explained through the decomposition of methoxy groups that were stabilized at bridging oxygen vacancies:[99]

$CH_3O_{(a)} \rightarrow H_2CO_{(g)} + H_{(a)}$ Equation 1

This reaction produces H atoms as a by-product. It is proposed that the concomitant desorption of methanol may be explained by a reaction of these hydrogen atoms with methoxy groups to produce methanol:

$CH_3O_{(a)} + H_{(a)} \rightarrow CH_3OH_{(g)}$ Equation 2

Such a methanol production mechanism was also postulated by other researchers, with the reaction details being somewhat different.[48,100]

A left question is why the methoxy groups at the bridging oxygen vacancies are stabilized and do not combine with hydroxyl groups below 680 K. The stabilization of those methoxy groups is likely related to the desorption of water at 520 K. Prior to the reaction with methoxy, hydroxyl groups have recombined each other to form water, which has consumed the hydrogen at the surface, and thus no hydrogen is left. By applying the Redhead equation[91] with a pre-exponential factor of 10^{13} s^{-1} and a heating rate of 0.5 $K \cdot s^{-1}$, an activation energy of 1.96 eV for the reaction occurring at 680 K is obtained. This value is close to the energy barrier of 1.85 eV for the formation of formaldehyde on bridging oxygen vacancies obtained recently by Lang et al.[101] with DFT (density functional theory).

4.3 Oxidized TiO_2 layer

The surface structure of oxidized TiO_2(110) layers was studied for two cases: partially oxidized surfaces and fully oxidized surfaces.

A partially oxidized surface is here the surface of a thin film directly after preparation without the final vacuum annealing step (that is in 10^{-6} mbar oxygen at 800 K during Ti evaporation). In this case part of the evaporated Ti ions have not been fully oxidized. Figure 4.8a and b show STM images recorded from such a partially oxidized layer.

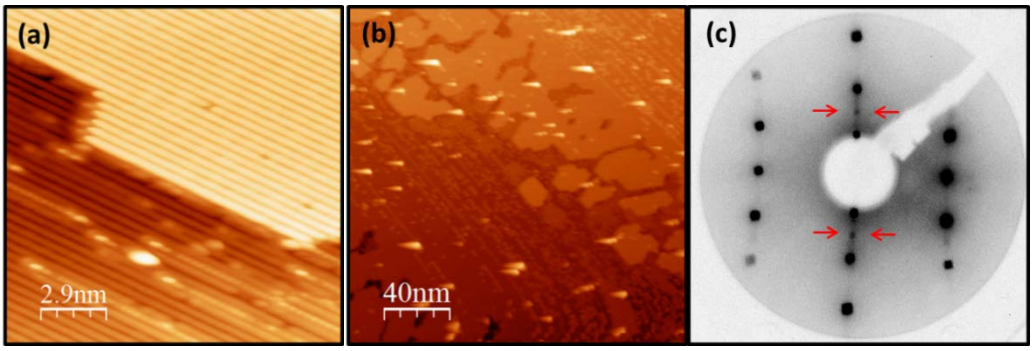

Figure 4.8 (a) and (b) STM images of an as-prepared TiO_2(110) thin film without vacuum annealing. (c) LEED pattern of this thin film

In image (a), rods parallel to [001] are observed above the bright Ti rows and having a height of about 2 Å. More rods together with several separated islands were observed in image (b) which shows a larger scanning area. The regular pattern of the rods gives extra sharp spots in the (1 × 1) LEED pattern marked by arrows in image (c). The appearance of the rods resembles the Ti_2O_3 rods found by Onishi and Iwasawa.[44] In their experiments a rutile single crystal was annealed at 800 K in oxygen of 10^{-7}, which is similar to the oxidizing condition in our case. In Onishi's and Iwasawa's experiments reduced Ti cations from the bulk were oxidized at the surface while in the case discussed here the Ti which is oxidized at the surface comes from the Ti evaporator. From the similar appearance of the rods, it is concluded that the observed rods are actually the Ti_2O_3 rods that are proposed by Onishi and Iwasawa. The rods disappeared when the thin film sample was annealed in vacuum which led to a surface similar to that shown in Figure 4.4, or when the thin film was annealed in oxygen for a longer time which resulted in a fully oxidized surface as discussed in the following.

When a reduced bulk crystal is oxidized at 600 K, rosette-like structures and/or small islands of TiO_2 are usually formed at the surface through the reaction of O_2 with reduced cations diffusing from the bulk to the surface, making the surface rough.[31] However, in the case of a TiO_2 thin film grown on a blocking layer, the diffusion of reduced cations from the bulk to the top layer is inhibited by the blocking layer, which means that the top layer may be fully oxidized.

Oxidation of the TiO_2(110) thin film was performed by annealing in O_2 (1×10^{-6} mbar) at 600 K for 10 min. A STM image of the thin film surface after oxidation is compared in Figure 4.9 to an image of a single crystal surface subjected to the same oxidation treatment. The STM image (a) is from the thin film sample and shows a

flat (1 × 1) terrace with some bright features on the bright Ti rows. Bridging oxygen vacancies are not visible. The height of the bright features on the 5-fold Ti sites is about 0.7 Å, which is the same as the height of oxygen adatoms that were found when oxygen was dosed to a TiO_2 surface at room temperature.[95,34] The oxygen adatoms are assumed to originate from the dissociation of O_2 molecules at the bridging oxygen vacancies and Ti sites.[95,34] On the other hand, a rough surface was produced for the bulk sample that was annealed in oxygen as well at 600 K, as shown in Figure 4.9(b). The application of an interlayer that blocks the cation diffusion makes it possible to fully oxidize the thin film while maintaining a reduced substrate.

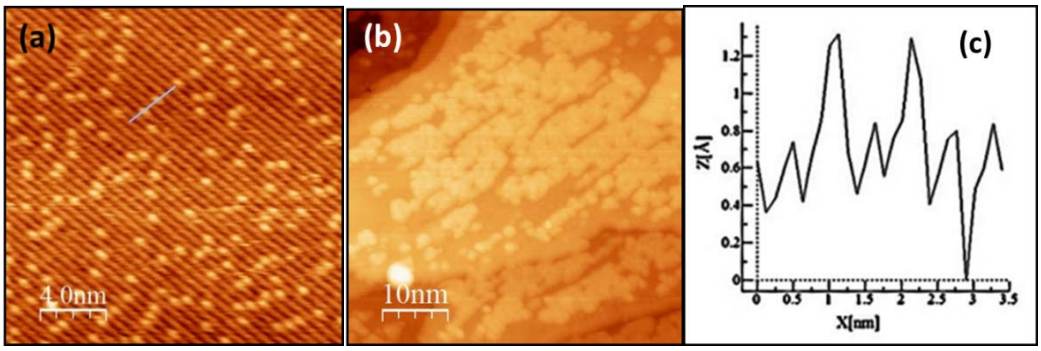

Figure 4.9 STM images (2.0 V, 0.1 nA) obtained after (a) oxidizing the TiO_2(110) thin film in 10^{-6} mbar O_2 at 600 K for 10 min, and (b) oxidizing the regular TiO_2(110) substrate in 10^{-6} mbar O_2 at 600 K for 10min. (c) A line profile along [1 $\bar{1}$ 0] as marked in image(a) is displayed.

The reactivity of the surface changes once it gets oxidized. Oxidized thin film surfaces without bridging oxygen vacancies exhibit a reactivity with respect to methanol adsorption, which is very similar to what is known for oxidized single crystal surfaces.[48,100] Figure 4.10 shows TPD spectra of methanol on a TiO_2(110) thin film that was annealed in oxygen at 600 K. The methanol peaks in the range between 300 K and 400 K are still visible, as they are due to desorption of molecular methanol from Ti sites at the surface which are present both on reduced and oxidized surfaces. However, the desorption state at 680 K that appear in Figure 4.6 are not visible anymore, since there are no bridging oxygen vacancies. But a new peak at about 600 K is observed for methanol and formaldehyde. No methane or water peaks could be detected.

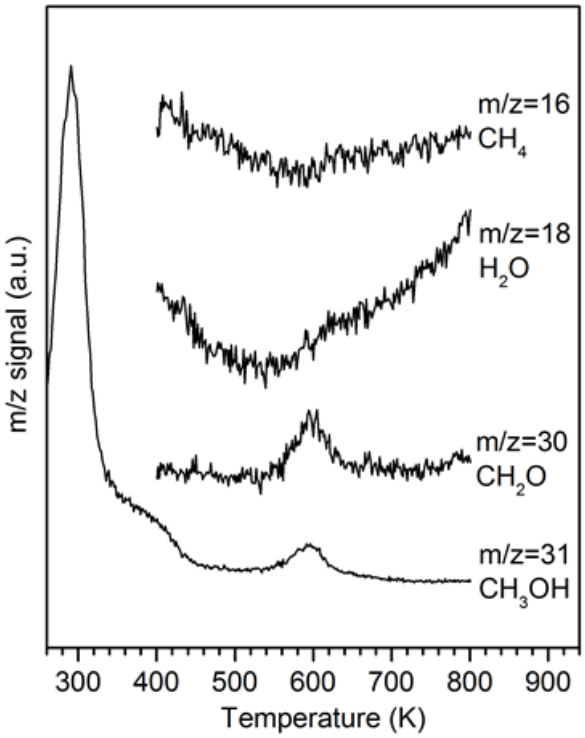

Figure 4.10 TPD spectra (masses 16, 18, 30 and 31) of CH_3OH on a TiO_2(110) thin film after annealing in O_2 at 600 K.

The desorption of methanol and formaldehyde from an oxidized TiO_2(110) single crystal surface at a similar temperature has been reported before by other researchers.[48,78,79,100,83] Henderson and coauthors have also investigated the effect of O_2 on the methanol reaction on the TiO_2(110) surface.[48] They dosed O_2 on the bulk crystal at 150 K, 300 K and 715 K to modify the surface on which the reactivity with respect to methanol was then tested. They found signals similar to our findings at a slightly higher temperature of 625 K. The 625 K TPD peak was assigned to formaldehyde formation from methoxy species bound to 5c-Ti sites in the presence of oxygen ad-atoms.[48,100,83] The hydrogen released in this reaction does probably react with methoxy groups to methanol (see equations 1 and 2). An activation energy of 1.73 eV for the reactions is estimated using the Redhead equation,[91] which again fits quite well to the computed energy barrier of 1.76 eV obtained by Lang et al with DFT.[101]

4.4 Summary of chapter 4

An interlayer, designed to prevent the diffusion of vanadium from the Ti + V oxide overlayer to the rutile substrate is introduced. The interlayer consists of a Ti + Ta mixed oxide with a rutile type structure and a good thermal stability.

TiO_2(110) thin film overlayers were prepared and studied in order to produce reference data for the comparison to the Ti + V mixed oxide. The surface structure and the reactivity were characterized for reduced and oxidized layers. It was found that the Ti + Ta mixed oxide interlayer does not only prevent the diffusion of vanadium, but also the Ti cation exchange between the overlayer and the rutile substrate. Therefore a fully oxidized TiO_2(110) layer can be grown on a reduced substrate, which is useful for certain studies that require an oxidized surface. The TiO_2(110) overlayer can also be strongly reduced if required, without changing the state of the substrate to a comparable extent. STM and LEED show that the film is well ordered with large terraces and methanol TPD experiments indicate that the chemical properties of the thin layer are essentially identical to those of a single crystal surface.

Chapter 5

Ti + V mixed oxide layers under reducing conditions

In this chapter, the surface properties of Ti + V mixed oxide layers exposed to reducing conditions are discussed. Vanadium with various concentrations from 0 to 20% was doped into the TiO_2(110) thin film layers with post-annealing in vacuum to produce Ti + V mixed oxide layers (the so-called "reduced layers"). The surface structures of Ti + V mixed oxides were examined and compared to that of the pure TiO_2(110) thin films, to characterize the effect of vanadium doping. The chemical reactivity of methanol on the surfaces of the mixed oxides was also studied to further investigate the effect of vanadium on the reactivity. To find out the origin of the doping effect, the oxidation states of vanadium and titanium in the mixed oxide layer were measured with surface sensitive XPS.

5.1 Surface structure of the reduced layers

The surface structures of the ordered reduced Ti + V mixed oxides were studied with STM and LEED and compared to the surface structure of the TiO_2(110) thin film without vanadium doping. Figure 5.1 shows STM images of the TiO_2 thin film before and after doping with 2% of vanadium. Both surfaces were annealed in vacuum at 800 K for 10 min before STM measurements. On the (1 × 1) surface of the TiO_2 thin film without vanadium, flat terraces with sizes of tens of nm were observed (image (a)). After doping 2% vanadium into the TiO_2 thin film, many rod-like structures (2 nm to 20 nm long) along [0 0 1] appear on the flat terraces, as shown in image (b). The randomly distributed rods also induce the diffused intensities between the (1 × 1) LEED pattern spots as shown in image (e).

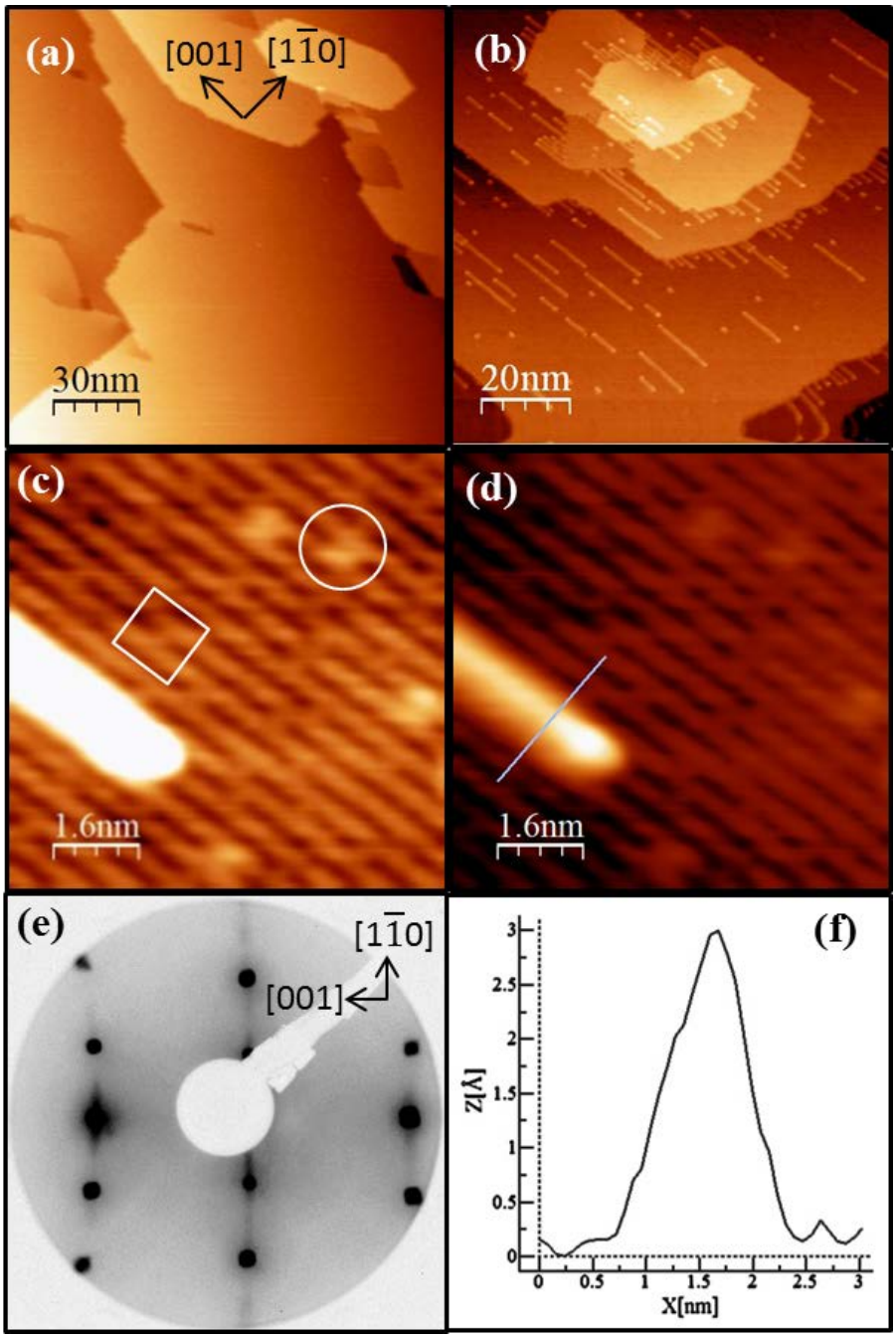

Figure 5.1 (a) STM image of a TiO_2(110) thin film annealed in vacuum at 800 K for 10 min. (b) STM image of a TiO_2(110) thin film with 2% vanadium. (c) Atomically resolved image of the same sample for (b). In the image, an oxygen vacancy is marked by a square and a hydroxyl group by a circle. (d) The same image as (c) but with different brightness and contrast in order to show the feature of the rod. (e) LEED pattern of the same sample for (b). (f) A line profile crossing the rod in image (d).

To better resolve the surface structure, atomic images with smaller scanning area were recorded from this surface. Image (c) displays one of the detailed images and shows that the surface still has a typical (1 × 1) TiO_2(110) structure with some spots of different brightness (marked by a square and a circle) on the dark O rods. Bright spots of the type marked by a square are usually assigned to bridging oxygen vacancies on the TiO_2(110) surface.[34] The density of such structures displayed in the image is about 15% per unit cell, higher than 7% found for the TiO_2(110) thin film surfaces that are treated with the same annealing procedure (see section 4.2). The brighter spot marked by a circle has large height and is attributed to a hydroxyl group resulting from the dissociation of water (from the residual gas atmosphere) at the surface. In image (c) a bright rod is also observed, which is actually the rod-like structure along [0 0 1] in image (b).

To better examine this type of rod, image (c) is shown with different brightness and contrast in image (d). The rod-like structure is centered above the bright Ti rods and occupies two unit cells of (1 × 1) matrix along [1 $\bar{1}$ 0]. From a line profile crossing the rod (image (f)), the rods are about 1.2 nm wide and 0.3 nm high. All these geometric profiles are the same as those reported for the "Ti_2O_3 rods" at the (1 × 2) reconstructed surface of a heavily reduced TiO_2(110).[35,102] Additionally, the appearance of those rods is very similar to that of the rods observed on the as-prepared TiO_2 thin film that was partially oxidized (see section 4.3). Although the appearances of the rods from STM and their effect on the LEED pattern are similar, they differ from each other: the rods on the partially oxidized TiO_2 thin film disappear after annealing the sample in vacuum, while the rods on the Ti + V mixed oxide layers cannot be removed by vacuum annealing. The character and the origin of the "Ti_2O_3 rods" on the mixed oxide layers were further examined by studying mixed oxide layers doped with more vanadium.

When more vanadium was doped into the TiO_2 thin film, more and longer rods along [0 0 1] were generated. The STM images in Figure 5.2 were recorded from a TiO_2(110) thin film with 8% vanadium. Image (a) with a size of 200 nm by 200 nm shows flat terraces with some islands. A better resolved image is shown in panel (b). The surface is fully covered by the Ti_2O_3-like rods. Different from the bright Ti rows observed from the TiO_2(110) (1 × 1) surface, the smallest distance between rods is about 1.3 nm, which is twice the (1 × 1) lattice parameter (0.65 nm) along [1 $\bar{1}$ 0]. Additionally short bright rods along [1 $\bar{1}$ 0] was observed crossing the rods along [001]. The distance between rods is mostly 1.3 nm, with 1.95 nm occasionally. The periodicity of the rods is reflected in the LEED pattern by the (1 × 2) type superstructure spots in image (d). The LEED shows a diffuse intensity between the

regular TiO_2(110) spots with the (1 × 2) type spots as maxima. The (1 × 2) type spots are from the regular distance (1.3 nm), while the diffuse intensity results from the occurrence of larger distances (1.95 nm) between the rods on the surface. These rods together with the cross-links are shown with a larger magnification in image (c). The appearance of these rods is uniform indicating that they may be composed of just one type of compound, either titanium oxide or vanadium oxide. The rods are probably not composed of vanadium oxide since a calculation of a fully covered surface would correspond to a vanadium concentration much higher than the 8% detected by XPS. Moreover vanadium tends to diffuse to deeper layers rather than to stay at the surface. Actually the STM images shown here are very similar to STM images of heavily reduced (1 × 2) reconstructed TiO_2(110) surfaces,[35,103,104] which is a good indication that the rods seen in the STM images just contain titanium.

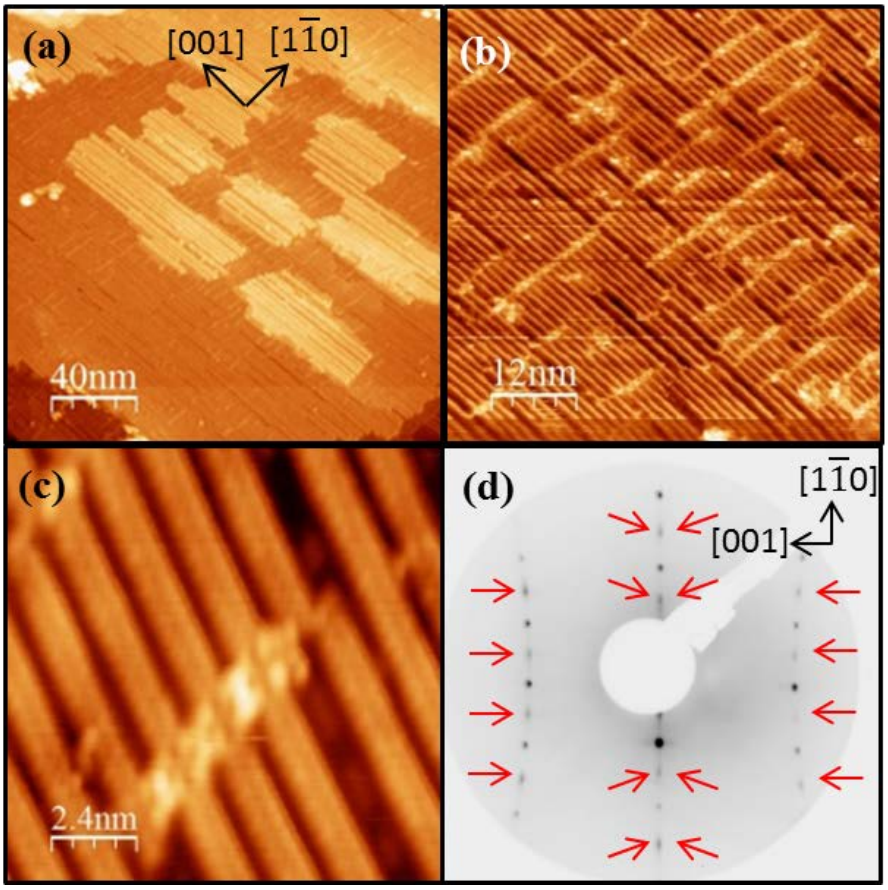

Figure 5.2 (a) STM image of a TiO_2(110) thin film with 8% vanadium. (b) An enlarged STM image of the same sample. (c) Atomically resolved image of the sample. (d) (1 × 2) LEED pattern of the sample, in which red arrows mark the spots of the (1 × 2) superstructure.

Since during STM the tip probes the electronic state of the surface, an attempt to probe the local electronic structure of the (1 × 2) surface was conducted by applying different bias voltages for imaging. Figure 5.3 shows images of the same scanning area of a TiO_2(110) thin film with 8% vanadium, which were recorded with a positive and a negative bias voltages. Image (a) with +2.0 V displays the empty state of the surface, while Image (b) with -0.8 V displays the filled state of the surface. The (1 × 2) rods are observed from both images; however, the cross-links are almost invisible from the filled state image, which indicates that less electron density of state is found within 0.8 V below the Fermi level for the cross-links. Although the atomic composition of the cross-links is unclear, it apparently differs from the (1 × 2) rods.

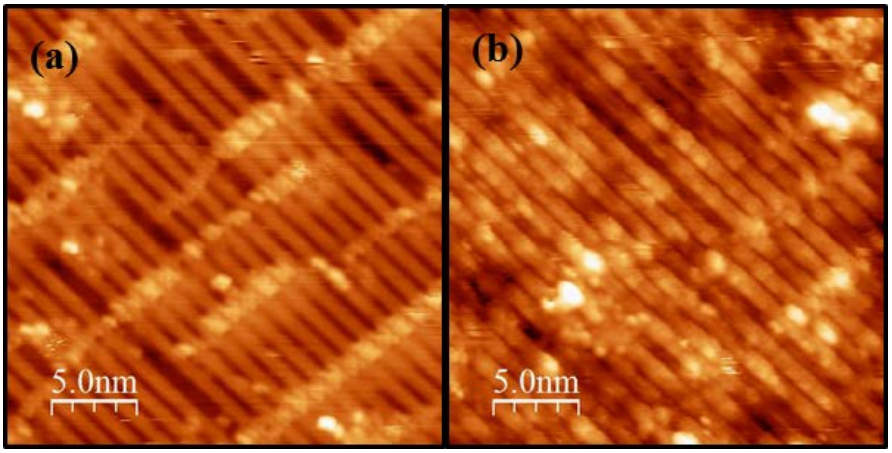

Figure 5.3 (a) Empty state STM image of a TiO_2(110) thin film with 8% vanadium, recorded with a positive bias of +2.0 V and a tunneling current of 0.1 nA. (b) Filled state STM image for the same scanning area as (a) but recorded with a negative bias of -0.8 V and a tunneling current of 0.1 nA.

The (1 × 2) reconstructed surface of regular TiO_2(110) results from a strong reduction of the sample. It may be prepared by high temperature annealing in vacuo at temperatures in the range of 1300 K.[16,103,104] It was proposed that during annealing at high temperature there is a massive O atoms loss from the TiO_2 surface as well as diffusion of Ti^{3+} ions into the bulk, leading to the reconstruction of the (1 × 1) surface to an O-deficient (1 × 2) surface.[103] In the present case of the V-doped TiO_2 layer, a mild annealing temperature of 800 K was applied and at this condition a (1 × 2) structure was not observed on pure TiO_2(110) as confirmed by Figure 5.1(a). Apparently the (1 × 2) surface of the Ti+V mixed oxide layer is a result of vanadium doping into the TiO_2 thin film.

5.2 Reactivity of the reduced layers

The chemical activity of the mixed oxide layers was examined with TPD using methanol as the probe molecule. Figure 5.4 displays TPD spectra recorded for methanol adsorbed on a layer with 2% of vanadium. Methanol (m/z=31) has major desorption peaks at 350 K and 680 K. Water (m/z=18) desorbs at 500 K, and formaldehyde (m/z=30) desorption is found at 680 K. There is also a weak methane signal (m/z=15) at about 700 K while ethylene (m/z=27) intensity higher than the noise level of the spectrometer is not observed. These results are similar to results reported for a TiO_2(110) layer without vanadium except that the intensities are somewhat different.[97]

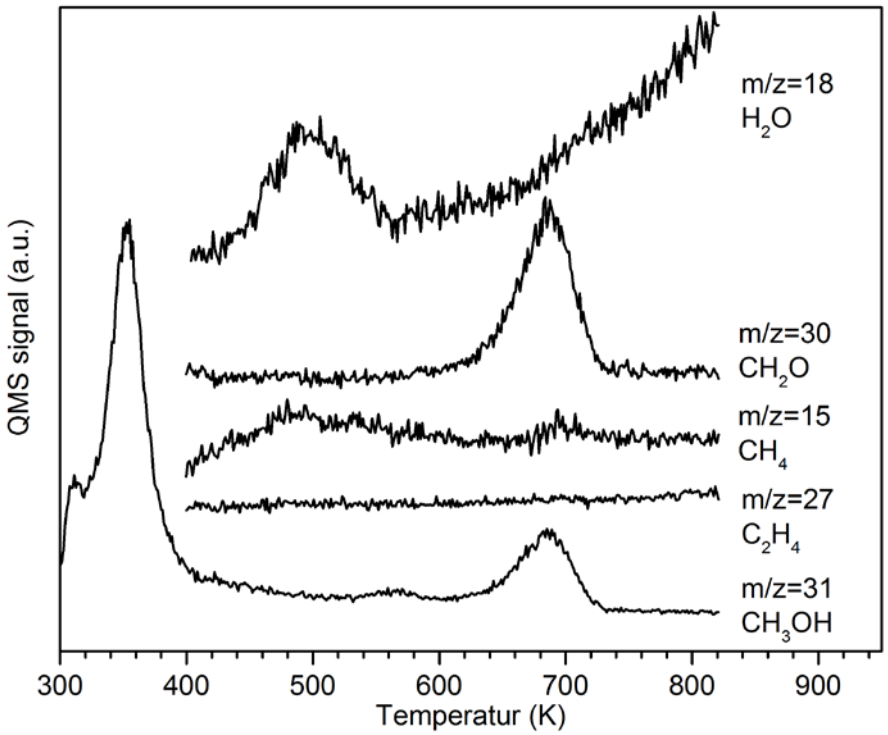

Figure 5.4 TPD spectra (masses 15, 18, 27, 30 and 31) of methanol adsorbed at room temperature onto a TiO_2 layer with 2% vanadium.

Formaldehyde TPD spectra of (m/z=30) for different vanadium concentrations are shown in Figure 5.5(a). The intensity of the peak at 680 K is highest for 2% of vanadium and decreases when the vanadium concentration is increased beyond this level or decreased below it. The amount of formaldehyde produced by a film with 7%

of vanadium is approximately the same as the amount produced by the pure TiO_2 thin film while the amount is near to zero when the layer contains 12% of vanadium.

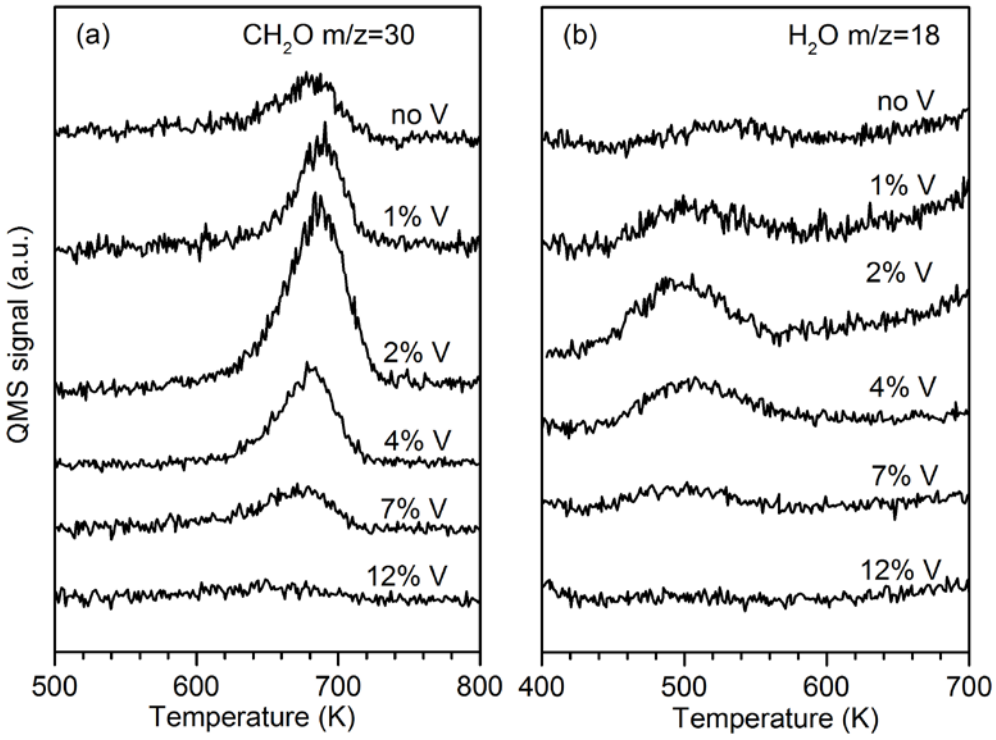

Figure 5.5 TPD spectra of m/z 30 for formaldehyde (a) and m/z 18 for water (b) of methanol on TiO_2 thin films with different vanadium concentrations (0%, 1%, 2%, 4%, 7% and 12%).

According to TPD studies of methanol on TiO_2(110), the desorption of formaldehyde at 680 K is related to methoxy groups bound to BOV sites.[97,78,79] The stabilization of those methoxy groups is linked to the desorption of water around 500 K. Therefore the dependence of water desorption on the vanadium concentration would be similar to that of formaldehyde desorption, and this trend for water is shown in Figure 5.5(b). As expected, the intensity of the water peak around 500 K is highest for 2% of vanadium. The large amount of formaldehyde and water desorbing from the film with 2% of vanadium reflects the high concentration of BOV sites at the surface of this film, which is about 15% as estimated from the STM image in Figure 5.1(b). The BOV density at the surface of the layer without vanadium is only 7% which leads to the smaller intensity of the formaldehyde

desorption peak in Figure 5.5(a). The surface of the layer with 12% of vanadium is largely covered with the (1 × 2) reconstruction. There are not many BOVs but many "Ti_2O_3" rods which are apparently inactive with respect to the partial oxidation of methanol. The TPD data do only exhibit structures which are also known for methanol on regular TiO_2(110) without vanadium, which is a strong indication that there is no direct methanol-vanadium interaction.

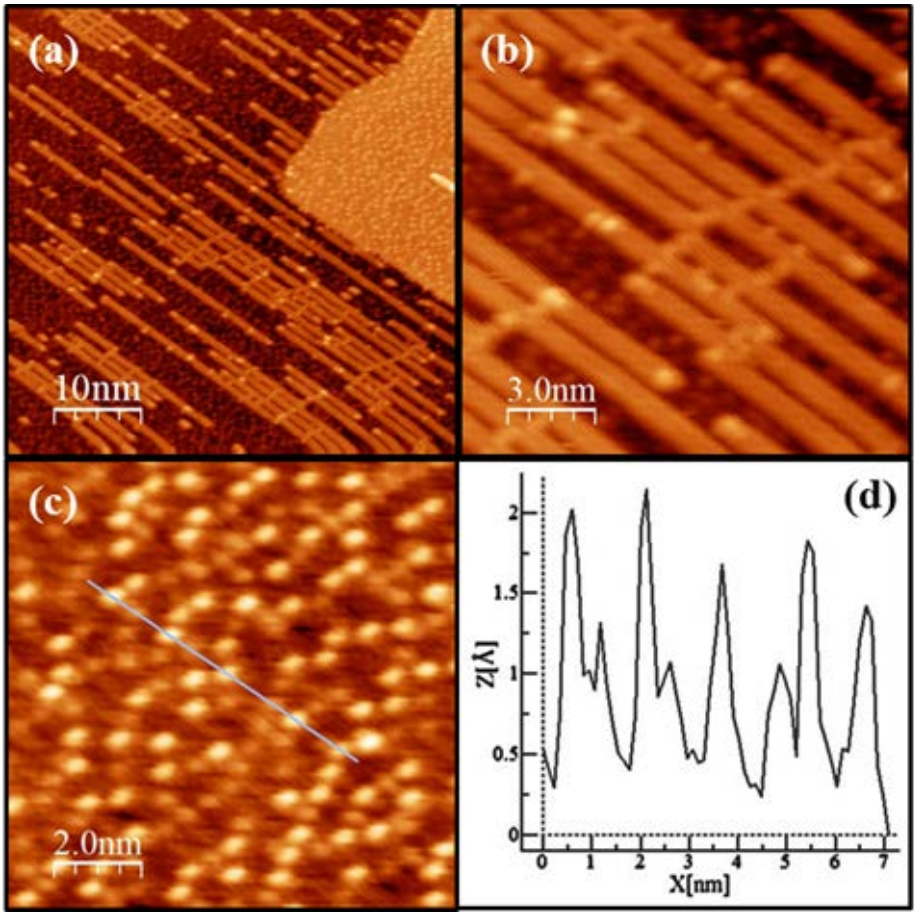

Figure 5.6 (a) STM image recorded after methanol adsorption on a TiO_2 thin film with 2% vanadium. The sample was flashed to 400 K before scanning to desorb molecularly adsorbed methanol. (b) Part of image (a) containing mainly (1 × 2) rods. (c) Part of image (a) showing an area without (1 × 2) rods. (d) Height profile measured along the line in image (c).

Directly recording STM images of the surfaces with adsorbed methanol is an alternative way to examine the chemical activity of the mixed oxide layer. This STM experiment was conducted on the mixed oxide layer with 2% vanadium, which surface exhibits both (1 × 1) terraces and (1 × 2) rod features. Firstly 50 L of

methanol at 300 was dosed K the surface of the layer and then the sample was flashed to 400 K. The only methanol-related species at the surface after flashing are methoxy groups bound to BOVs and hydroxyl groups. The recorded STM images are shown in Figure 5.6. The images exhibit only a few methanol-induced protrusions on the (1 × 2) rods [see Figure 5.6(b)], indicating that the rods are essentially inactive for methanol adsorption and formaldehyde production, which is in agreement with the conclusions drawn from the TPD experiments. Different from the (1 × 2) rods the (1 × 1) area between the rods is densely covered with methanol related species [see Figure 5.6(c)]. The height profile of those methanol related species is recorded in Figure 5.6(d). Species with two different heights (0.6 Å and 1.5 Å) are revealed. Following a comparison with literature values,[34,105,49,106] are attributed to hydroxyl and methoxy groups, respectively. Both densities of the hydroxyl/methoxy groups are about 15% relative to the density of surface unit cells. This number is the same as the density of BOVs found at this surface before adsorption.

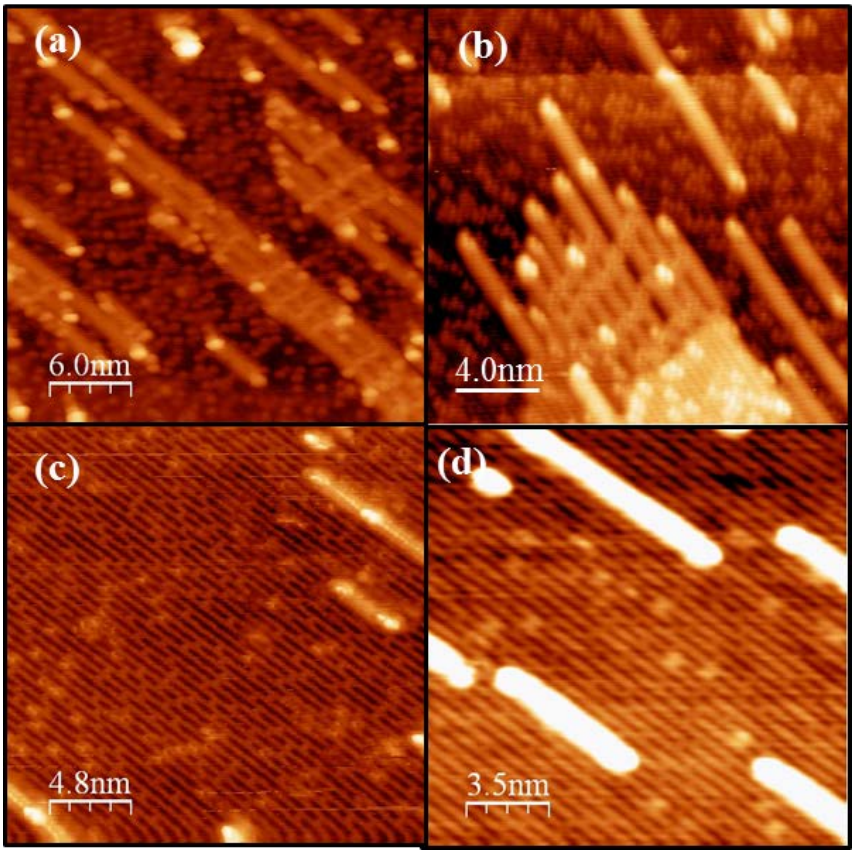

Figure 5.7 STM images of a TiO_2 thin film with 2% vanadium recorded after methanol adsorption and flashing to (a) 420 K, (b) 550 K, (c) 700 K, and (d) 800 K sequentially.

The methanol covered surface (Figure 5.6(a)) was then flashed to 420 K, 550 K, 700 K and 800 K step by step. Figure 5.7 shows the evolution of the methoxy and hydroxyl groups at the surface depending on the flashing temperature. No change was observed for the surface flashed to 420 K with respect to Figure 5.6. However the density of the bright spots decreases after sample flashing to 550 K as shown in Figure 5.7(b). In fact only spots with 1.5 Å, which are methoxy groups, were left at the surface, since hydroxyl groups have reacted to form water at about 500 K, as concluded from the methanol TPD experiments. On the sample flashed to 700 K, most methoxy groups have reacted to methanol and formaldehyde, and thus only a few are left at the surface. In Figure 5.7(c) BOVs are observed again together with several bright spots (methoxy groups). After flashing the sample to 800 K, the surface of the mixed oxide recovered to the state of the sample in the reducing condition without methanol adsorption (Figure 5.7(d)), which was expected as all methanol-related species desorb below 800 K.

5.3 Origin of the increased reducibility

In order to reveal the origin of the increased reducibility of TiO_2 films by vanadium doping, examination of the oxidation states of vanadium and titanium in the mixed oxides was conducted. This experiment was taken for a V-doped TiO_2 layer with synchrotron XPS (photon energy: 630 eV, emission angle: 0° and 80° with respect to surface normal). The Ti + V mixed oxide layer was annealed in 2×10^{-6} mbar O_2 at 850 K for 1 min and annealed in vacuum at 850 K for 5 min respectively, before recording the spectra. The results are displayed in Figure 5.8 showing the spectra of Ti 2p and V 2p core levels measured.

At a photon energy of 630 eV, the information depth of V 2p and Ti 2p spectra is 5-6 Å for 0° detection angle and only ~2 Å for a detection angle of 80°. This means that in the latter case the spectra are strongly dominated by electrons from the topmost surface layer, whereas electrons from deeper layers contribute more in the spectra recorded at 0°. In addtition, band bending which shifted all levels by 0.5 eV to lower binding energy was observed after annealing the sample in oxygen. Therefore the energy scales in the graphs showing spectra of oxidized surfaces were shifted and aligned to Ti 2p binding energies of 459.0 eV like in the spectra of reduced surfaces. The spectra were further normalized to the maximum peak intensity before plotting.

The Ti 2p and V 2p peaks were fitted with one or more mixed Gaussian-Lorentzian functions with Shirley backgrounds. Figure 5.9 shows the fit of the data

recorded at grazing angle, in which Ti 2p spectra are fitted by two separate peaks, the V 2p spectrum for the sample annealed in vacuum is fitted by two peaks, and the V 2p spectrum of the sample annealed in oxygen is fitted by three peaks with different binding energies. Binding energies close to the literature values[107,108,109,76] for Ti (Ti^{4+}, Ti^{3+}) and V (V^{5+}, V^{4+} and V^{3+}) were obtained from the fits.

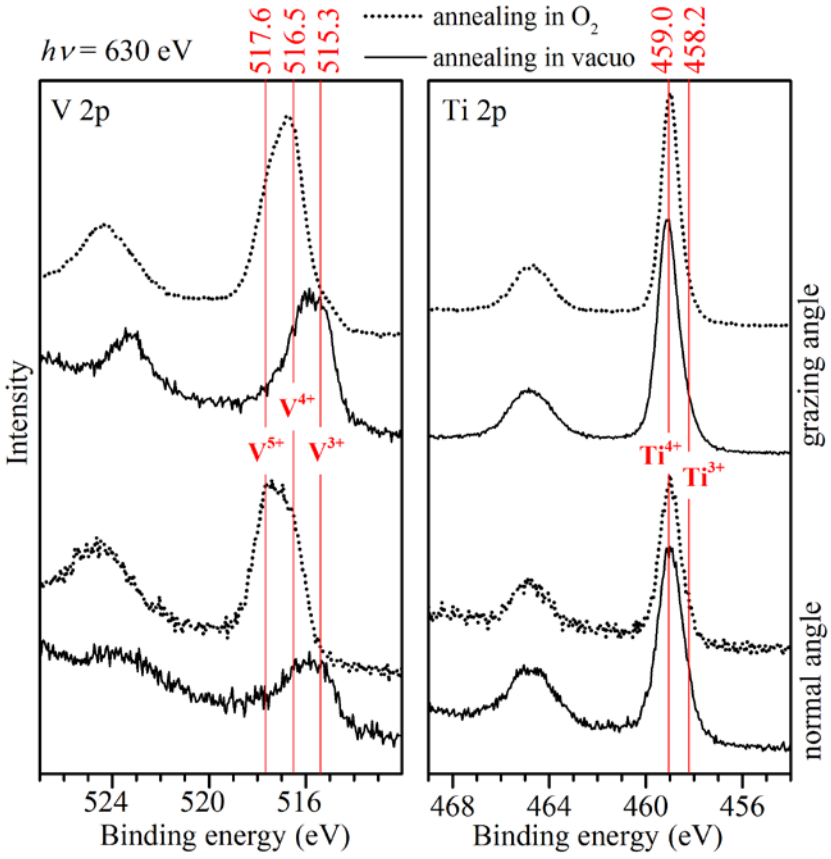

Figure 5.8 Synchrotron XPS spectra of V 2p and Ti 2p core level measured for V-doped TiO_2 layers. The spectra plotted with solid lines were recorded after annealing the layer in 2×10^{-6} mbar O_2 at 850 K for 1 min; the ones plotted with dotted lines were recorded after annealing in vacuum at 850 K for 5 min. The photon energy was 630 eV, and electron detection angles of 0° and 80° with respect to surface normal were employed. (Adapted with permission from ref 110. Copyright 2016 Elsevier.)

Results of peak fitting are listed in Table 5.1. The numbers show that the concentration of vanadium at the oxidized surface (65%, 0°) is much higher than at the reduced surface (23%, 0°). In the case of the reduced surface the concentration of vanadium at the surface is lower than below it as concluded from the

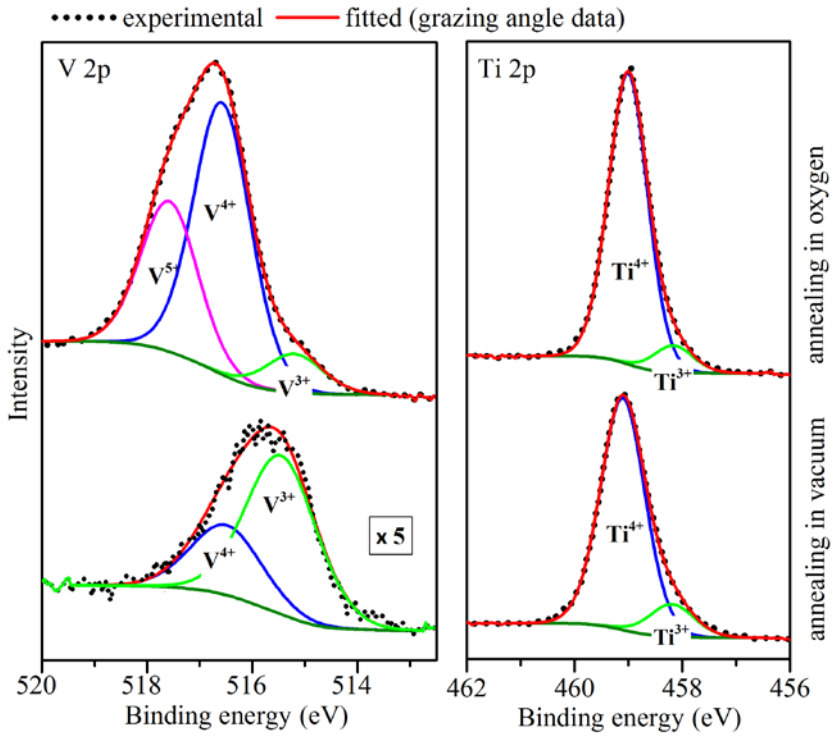

Figure 5.9 V 2p and Ti 2p spectra fitted (with Shirley backgrounds) by two or three peaks related to different oxidation states of the vanadium ions and titanium ions. Only data with grazing angle are shown here; the fit of the spectra recorded at normal angle is similar. (Adapted with permission from ref 110. Copyright 2016 Elsevier.)

Table 5.1 Relative concentrations of vanadium and titanium ions with different oxidation states as obtained from the spectra shown in Figure 5.8. The binding energies listed in this table result from peak fitting of the spectra.

oxidation state		**V^{5+}**	**V^{4+}**	**V^{3+}**	**V**	**Ti^{4+}**	**Ti^{3+}**	**Ti**
binding energy (eV)		517.6	516.5	515.3		459.0	458.2	
annealing in O_2	% (80°)	22	40	5	**67**	30	3	**33**
	% (0°)	33	30	2	**65**	32	3	**35**
annealing in vacuum	% (80°)	0	4	8	**12**	77	11	**88**
	% (0°)	0	8	15	**23**	68	9	**77**

concentrations obtained for different detection angles (23% for 0° vs 12% for 80°). This means that the vanadium tends to agglomerate at the surface in case of annealing in oxygen, while annealing in vacuum leads to a situation where the vanadium ions avoid the surface. The overall vanadium concentration was less in the layers whose surface STM images are shown in Figure 5.2, which is probably the

reason why the images do not exhibit any clear indication of the presence of vanadium atoms at the surface at all.

Most of the vanadium atoms have a V^{4+} or V^{5+} oxidation state after annealing in oxygen while there is no V^{5+} in the reduced oxide. The concentration ratio $[V^{3+}]/[V^{4+}]$ for the reduced oxide is ~2 for both detection angles. The corresponding concentration ratio for the titanium ions ($[Ti^{3+}]/[Ti^{4+}]$) is 0.13-0.14, which shows that reduction affects the vanadium ions much more than the titanium ions. Table 5.1 also shows that the Ti^{3+} and V^{3+} concentrations in the reduced layer are not too different. Here some percent difference should be not be taken too serious since the error margin for the Ti^{3+} concentrations is surely significant since the Ti^{3+} peaks are just weak shoulders in the Ti 2p structures in Figure 5.9. This indicates that the reduction may occur via the following reaction:

$$Ti^{4+} + V^{4+} + O^{2-} \rightarrow Ti^{3+} + V^{3+} + \tfrac{1}{2} O_{2\,(g)} \qquad \text{Equation (1)}$$

as opposed to the mechanism for a layer without vanadium:

$$2\,Ti^{4+} + O^{2-} \rightarrow 2\,Ti^{3+} + \tfrac{1}{2} O_{2\,(g)} \qquad \text{Equation (2)}$$

The reduction according to equation (1) would produce Ti^{3+} and V^{3+} in equal amounts, in rough agreement with the numbers listed in Table 5.1. We note that the Ti 2p spectra of the reduced mixed oxide layer in Figure 5.8 are similar to spectra measured for a regular TiO_2(110) (1 × 2) surface,[59,107,111] consistent with similar degrees of reduction.

It was found that the fourth atomic ionization energies are 46.71 eV for vanadium ($V^{3+} \rightarrow V^{4+}$) and 43.08 eV for titanium ($Ti^{3+} \rightarrow Ti^{4+}$).[112,113] The higher ionization energy of vanadium is a hint that the reduction of vanadium in TiO_2 might cost less energy than the reduction of Ti which would lead to an enhanced reducibility of TiO_2 with admixed vanadium, as experimentally observed. Since vanadium ions occupy the same lattice sites as titanium ions according to a recent photoelectron diffraction study, this simple picture may be somewhat reasonable.[114] In addition VO_2 (rutile structure) has a bulk oxygen vacancy formation energy of 3.53 eV,[115] which is lower than the corresponding value (≥ 4.35 eV) for TiO_2.[116] This is a further indication that a reduction process involving vanadium ions is energetically preferred.

Besides, the formation energies of BOVs at the (110) surfaces of regular and V-doped TiO_2 have also been calculated with DFT slab calculations.[65] In their model a vanadium atom replaces a 5-fold coordinated surface Ti atom. According to their

results, the energy to remove a certain bridging oxygen atom from the neighborhood of a 5-fold coordinated V atom is 3.37 eV, which is lower than the energy of 3.72 eV for pure TiO_2(110). While this model is not strictly applicable to the current situation, since the vanadium atoms prefer to stay below the very surface in the case of a reduced mixed oxide, it is nevertheless another indication that the introduction of vanadium into TiO_2 may result in an increased reducibility. The observation that vanadium prefers a location below the surface is in accord with the results of a calculation by Asaduzzaman and Krueger who found that vanadium atom prefer substitutional sub-surface sites over surface sites.[117]

5.4 Summary of chapter 5

In this chapter surface structures and chemical activities of the Ti + V mixed oxides were carefully discussed. All evidences show that V doping has a heavy impact on the properties of TiO_2(110). The presence of vanadium ions increases the reducibility of the layers which leads to a high density of reduction related features at the surface. When a small amount of vanadium (e.g. 2%) is introduced into a layer, a high density of BOVs is produced by annealing at 800 K for some minutes. When more vanadium ($\geq$ 8%) is dissolved in the layer, annealing at 800 K produces a (1 × 2) reconstruction with cross-links as known for heavily reduced TiO_2(110). From the reactivity tests with methanol as the probe molecule, a large amount of formaldehyde was produced from the surface with 2% vanadium, while the (1 × 2) related rod-like surface structures appear to be largely inactive. The reactivity tests also prove the increased reducibility by the vanadium doping. The origin of this special effect of vanadium was elucidated by checking the oxidation states of vanadium and titanium in the mixed oxide exposed to reducing and oxidizing conditions. It was shown that the reducibility of the vanadium ions in the thin film is higher than that of the titanium ions, and thus the energy for the removal of oxygen from the vicinity of vanadium atoms in the TiO_2(110) layer is smaller than that in the pure TiO_2(110) layer without vanadium.

Chapter 6

Ti + V mixed oxide layers under oxidizing conditions

This chapter discusses the effect of vanadium doping of TiO_2(110) under oxidizing conditions. Oxidization of the Ti + V mixed oxide layers induces complex structures at the surface: several oxidation states of vanadium coexist; different types of clusters are formed; new channels of methanol oxidation at the surface are found. Based on STM of the surface structures, LEED data and methanol TPD spectra, cluster models and reaction mechanisms are discussed.

6.1 Optimization of the oxidation condition

Surfaces with complex structures might be expected for the oxidized Ti + V mixed oxide layers. On the one hand, doping with V increases the reducibility of TiO_2(110) and induces defects such as BOVs and even a (1 × 2) surface reconstruction may be formed under reducing conditions; on the other hand, it has been known that oxidation of TiO_2(110) without vanadium induces surface features like oxygen adatoms, TiO_2 clusters and rosette-like rough structures (see section 2.1). When Ti + V mixed oxide layers are exposed to oxidizing conditions, new features might be induced at the surface. In order to simplify the investigation of such a complex surface, the oxidizing conditions were carefully chosen and optimized so that new features related to vanadium were easier to be identified. Three parameters were considered: the applied O_2 partial pressure, the annealing temperature, and the oxygen pressure during cool down.

The oxygen partial pressure applied during the preparation of the oxidized layers plays a crucial role and influences heavily the surface structures. Figure 6.1(a) shows STM images of an oxidized TiO_2 layer with 1% V that was annealed at 800 K for 20

min in O_2 with a partial pressure of about 1×10^{-5} mbar. Large terraces were formed with small protrusions and rods along [$1\bar{1}0$]. From an enlarged image of the same surface in Figure 6.1(b), the rods have a length of 5~10 nm cross-linked with short rods along [0 0 1], which resembles the rosette-like structure that was observed on the oxidized surface of a bulk TiO_2 crystal (Figure 4.9(b)). The surface roughness disappeared after annealed the sample in vacuum at 900 K for 20 min, as shown in Figure 6.1(c) and (d). It was found that no such rough surface was observed when the partial pressure of O_2 during the preparation of the mixed oxide samples was only 1×10^{-6} mbar.

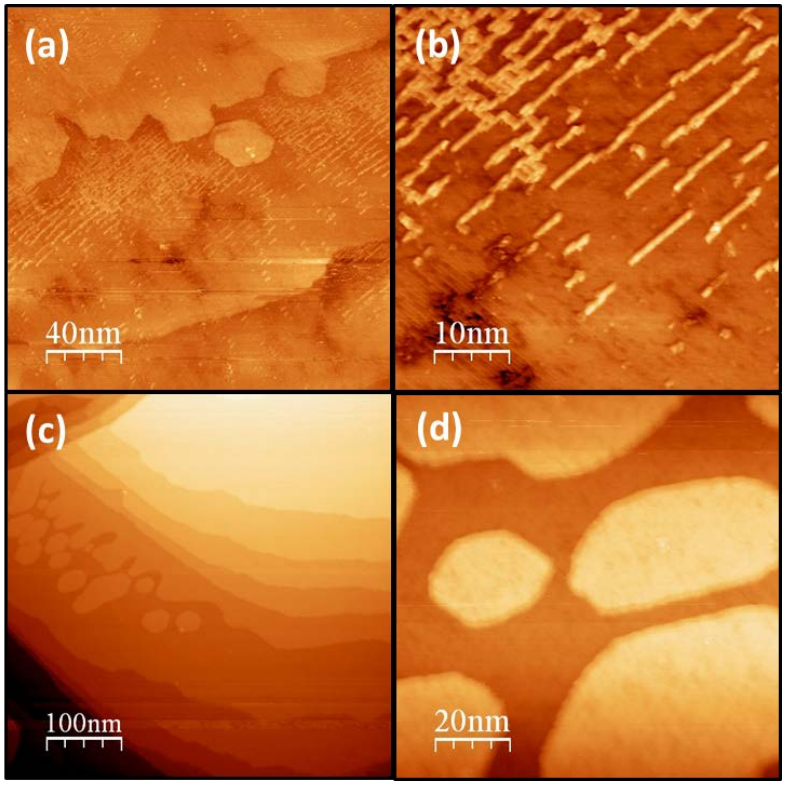

Figure 6.1 STM images of a TiO_2 layer doped with 1% V. (a) The layer was annealed at 800 K for 20 min in O_2 (1×10^{-5} mbar). (b) An enlarged STM image of the same sample. (c) The oxidized layer was then annealed at 900 K for 20 min in vacuum. (d) An enlarged STM image of the same sample.

The applied annealing temperature is another important parameter that influences the surface structure. It has already been shown (see section 4.3) that for the oxidized TiO_2 thin film, only oxygen adatoms were observed at the surface when the thin film was annealed at 600 K in oxygen, while TiO_2 clusters together with oxygen adatoms

were found when the annealing temperature was increased to 800 K. To simplify the analysis of the oxidized Ti + V mixed oxide layers, an annealing temperature of 600 K was chosen so that the formation of TiO_2 clusters were mostly avoided.

It also matters whether the sample is cooled in vacuum or in O_2 which also influence the surface structure. It was found that O_2 was released from the surface when the oxidized layers were heated (see Figure 6.10 in the section about reactivity). The release of O_2 started from ~460 K and continued till 800 K upon heating. To prevent the surface from getting reduced after the annealing in O_2, an oxidizing atmosphere was maintained until 420 K during the cool down procedure.

To sum up briefly, the oxidized layers were prepared by annealing at 600 K in 1×10^{-6} mbar of O_2 followed by cooling in O_2 with the same partial pressure until 420 K. At this temperature the oxygen supply was switched off and the sample was cooled down to room temperature in vacuum. These procedures guarantees surface structures with low complexity, so that an identification of new features appearing at the oxidized surface is possible. The samples used for the analysis of the structure and reactivity in the following sections were thus prepared under these optimized conditions.

6.2 Surface structure of the oxidized layers

In chapter 5 it has been shown that annealing of the Ti + V mixed oxide in vacuum results in a distribution of V below the surface of the thin film. However, annealing of the mixed oxide in oxygen leads to the diffusion of vanadium from the bulk to the surface. Figure 6.2 displays V 2p spectra measured at normal (0°) and grazing angles (60°) for Ti + V mixed oxide thin films with different vanadium concentrations before and after oxidation. The concentrations of vanadium were calculated based on the intensities of the V 2p and the Ti 2p peaks (not shown). They are listed in Table 6.1. All vanadium concentrations after oxidation are higher than before oxidation, and the concentrations at grazing angle (60°) are higher than the values at normal angle (0°), which indicates that vanadium atoms prefer surface sites of the oxidized layers. Three different oxidation states (V^{3+}, V^{4+} and V^{5+}) were considered in the peak fitting procedure with binding energies similar to literature values.[76,107,108,109] At low V concentrations, the V atoms are mainly in a V^{4+} or V^{3+} state, while at a high concentration of 14.1%, V^{5+} emerges.

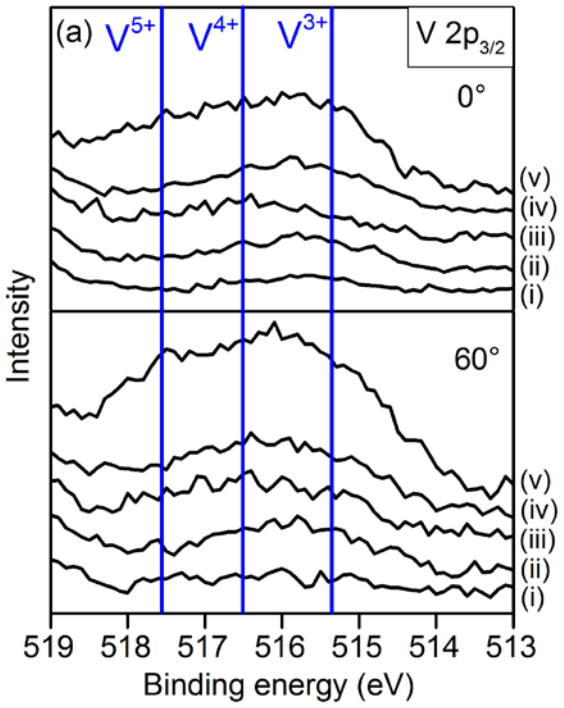

Figure 6.2 XPS spectra of the V 2p core levels of oxidized Ti+V mixed oxides at detection angles of 0°(normal) and 60°(grazing) with respect to the surface normal. The corresponding vanadium concentrations are listed in table6.1.

Table 6.1 V concentrations of five different Ti + V mixed oxide layers before and after oxidation. The reduced films were prepared by annealing the samples in vacuum at 800 K for 10 min. The oxidized films were prepared by annealing the reduced films at 600 K in 1×10^{-6} mbar of O_2 for 10 min followed by cooling in O_2 with the same partial pressure until 420 K.

	detection angle	sample i	sample ii	sample iii	sample iv	sample v
reduced	0°	0.8%	1.5%	2.3%	3.5%	7.9%
oxidized	0°	1.0%	2.6%	3.7%	4.3%	10.8%
	60°	1.4%	3.1%	4.8%	5.8%	14.1%

In the following surface structures observed in STM images will be discussed. The identification of the structures will be mainly based on a comparison of the geometries of features in the STM images to those of known species at the TiO_2(110) surface. A list of the known species and their geometries is given in Table 6.2.

Table 6.2 The geometries of several typical species at the TiO_2(110) surface.

species	appearance	site	height
Bridging oxygen vacancy	Bright spot	Between Ti rows	0.3 Å
Hydroxyl group	Bright spot	Between Ti rows	0.6 Å
Oxygen adatom	Bright spot	Above Ti rows	0.6 Å
TiO_2 cluster	Bright spot	Between Ti rows	2.2 Å
TiO_2 rosette-structure	Rosette-like	On the terraces	3.2 Å
Ti_2O_3 rod	rod along [001]	On the terraces	3.2 Å 4 Å
TiO_2 (1 × 2) cross-links	(1 × 2) structure	Terraces	3.2 Å

With 1% vanadium

Figure 6.3 compares the surface structures of a TiO_2 layer with 1% V before and after oxidation. The reduced layer was annealed at 800 K in vacuum for 10 min. STM images of identical areas on this surface were recorded with different tunneling parameters and are shown in Figure 6.3(a) and (b). Many bright spots (BOVs, 15%) between the bright rows (Ti rows) are observed, together with some bright spots (3 Å high) on the Ti Tows and short (1 × 2) rods along [001]. The STM images do not change significantly when different bias voltages are applied.

However, the STM images of oxidized surfaces depend notably on the STM bias voltage. Figure 6.3(c) and (d) display STM images of the sample after oxidation which was conducted by annealing at 600 K in O_2 (1×10^{-6} mbar). In both images identical areas are marked with dashed rectangles. For tunneling parameters of 2 V, 0.1 nA bright spots between the rows are still observed in Figure 6.3(c), but their density is lower (~5%) than that observed for the reduced sample. When a higher bias voltage of 2.5 V is applied, several new features become visible. As shown in Figure 6.3(d), the bright spots between the rows get brighter, while another type of spots with less brightness appeared between the rows. Such features are usually assigned to hydroxyl groups (brighter) and bridging oxygen vacancies (less bright) for TiO_2(110) without vanadium. Even though the sample was oxidized, it is not surprising that there are still BOVs at the surface since doping with vanadium increases the reducibility of the thin film. In the present case, the reduction of the thin film proceeds simultaneously with the oxidation by oxygen, which results in a partially oxidized (or partially reduced) surface. The presence of hydroxyl groups was also expected due to the presence of residual water in the gas phase which

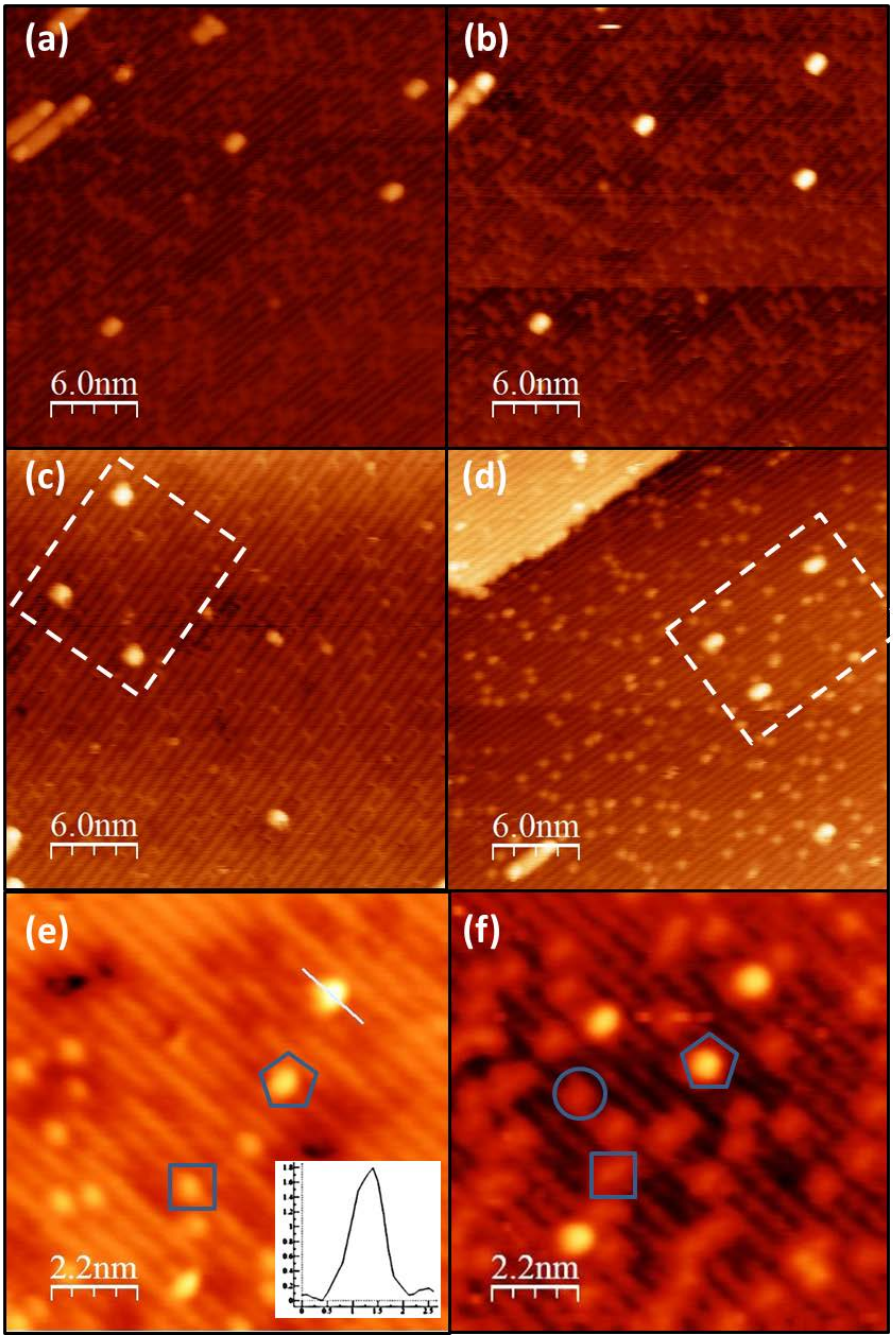

Figure 6.3 Comparison of STM images of reduced and oxidized TiO_2 layers with 1% V recorded with different tunneling parameters: a reduced layer annealed at 800 K in vacuum and recorded with 2 V, 0.1 nA (a) and 2.5 V, 0.1 nA (b); an oxidized layer annealed at 600 K in O_2 (1×10^{-6} mbar) and recorded with 2 V, 0.1 nA (c) and 2.5 V, 0.1 nA (d); another oxidized layer annealed at 600 K in O_2 (1×10^{-6} mbar) and recorded with 1.5 V, 0.1 nA (e) and 2.5 V, 0.1 nA (f).

decomposes at the surface. Beside these two features between the Ti rows, an additional feature on the Ti rows was observed. The bright spots on the Ti rows have a height of 0.7 Å which is similar to the appearance of oxygen adatoms observed on oxidized TiO_2 thin films without vanadium doping. Such adatoms can be trapped by BOVs but due to the dynamic nature of the concurrent oxidation/reduction processes it is conceivable that a certain concentration of oxygen adatoms is stabilized at the surface despite the presence of BOVs

Oxygen adatoms on the Ti rows were also observed in another measurement. It was found that oxgen adatoms became visible in STM images when voltages of either 1.5 V or 2.5 V were applied (squares mark oxygen adatoms in Figure 6.3(e) and (f)), while the hydroxyl groups (see circle in Figure 6.3(f)) did not show up for a bias voltage of 1.5 V. In addition, a new feature was observed (marked by pentagons in Figure 6.3): bright spots of 1.8 Å height on the Ti rows. This type of feature was seen in images with different bias voltages and does not match any of the species listed in Table 6.2. It is probably due to a vanadium-related aggregate. This assumption is supported by STM images of layers with a higher vanadium concentration.

With 3% vanadium

Figure 6.4(a) and (b) show STM images of an oxidized TiO_2 layer with 3% V. Although the images were recorded with the same tunneling parameters (2.5 V, 0.1 nA), depression spots were observed on the terrace in the middle part of image (a) while bright spots show up in the same area in image (b). By carefully overlapping image (b) on image (a), the bright spots and the depression spots were found to be located at the same sites on the Ti rows and were thus assigned to the same species. The depression spots are not a common feature and are usually induced by a change of the tip state. It is inferred that a change of the tip apex happened during the scanning of image (a), since bright spots on the Ti rows were also found in the upper part of the image.

The density of the bright spots is about 5% per unit cell, and the height profile along the line shown in (c) gives a height of 1.8 Å. These features are likely vanadium-related structures, as discussed before for the layer with 1% of vanadium. Due to the higher vanadium concentration they appear with a somewhat higher concentraion in Figure 6.4. In addition, in image (c) a bright short rod with height of 3 Å is observed. This is probably a feature similar to the spots in Figure 6.3 (a)-(d), and may be assigned to a short version of the "Ti_2O_3 rods" found on (1 × 2) reconstructed surfaces.[110]

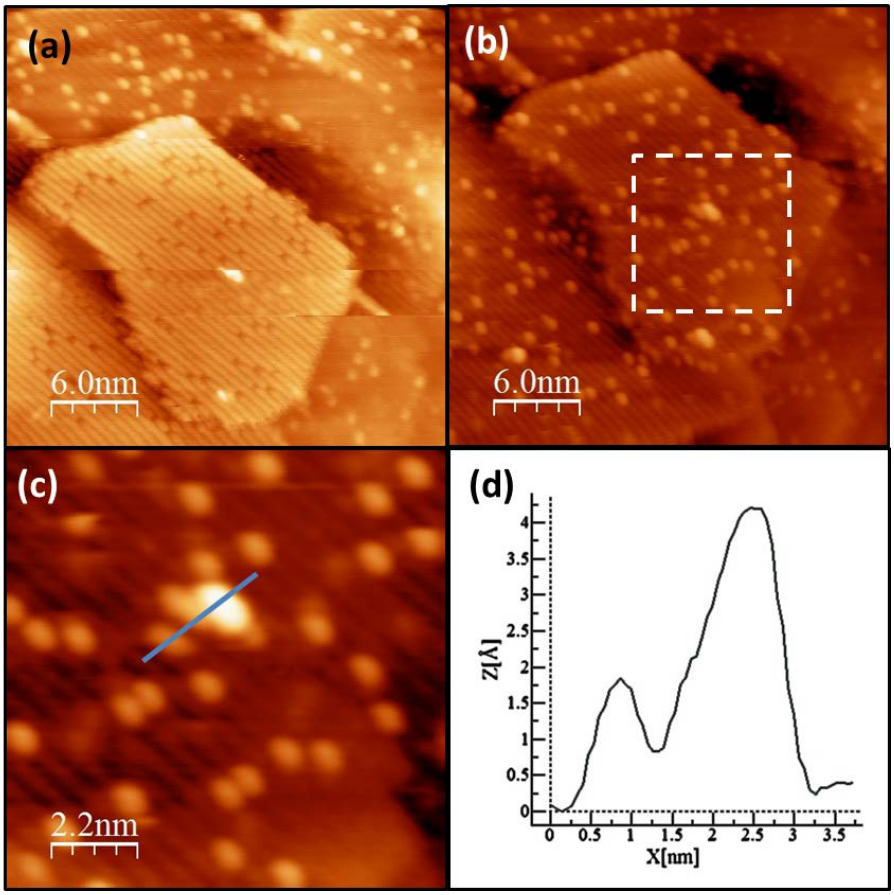

Figure 6.4 (a) STM image (2.5 V, 0.1 nA) of an oxidized TiO_2 layer with 3% V. (b) image of the same area with the same tunneling parameters. The different appearances of (a) and (b) may be due to a change of the tip state. (c) An enlarged image of the scanning area marked by the dashed square in (b). (d) Height profile measured along the line in image (c).

With 6% vanadium

The surface structure of the oxidized thin film with 6% V is compared to the surface structure before oxidation in Figure 6.5. On the surface of the reduced layer annealed at 800 K in vacuum, "Ti_2O_3 rods" appear on the (1 × 1) terraces due to the reducing effect of the vanadium. The "Ti_2O_3 rods" are still observed after oxidation, see panels (b), (c), and the height profile in (d).

The enlarged image in Figure 6.5(c) shows that vanadia clusters (bright spots on the Ti rows; one is marked by a pentagon) are still observed at the (1 × 1) terrace. Additionally some aggregates on the "Ti_2O_3 rods" are observed. Such features on (1 × 2) rods are not observed for reduced TiO_2(110) without doping and therefore they are assigned to clusters containing vanadium. This means that oxidation of the layer

induces vanadia clusters not only on the Ti rows at the (1 × 1) terrace but also on the (1 × 2) "Ti_2O_3 rods".

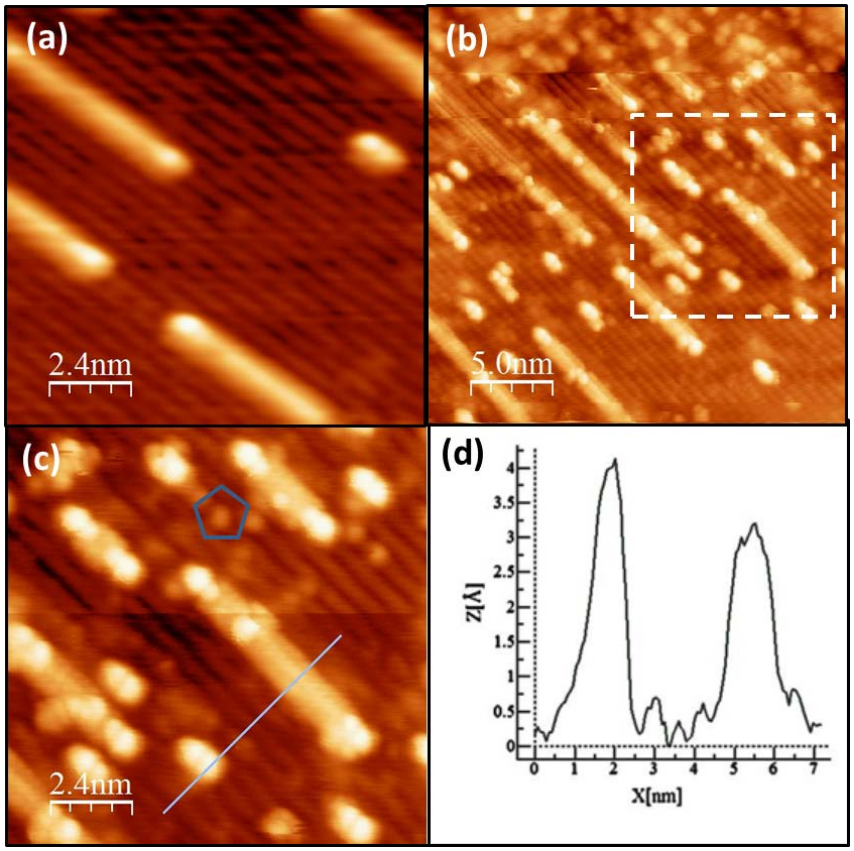

Figure 6.5 STM images of a TiO_2 layer with 6% V before and after oxidation: (a) reduced layer annealed at 800 K in vacuum (2.0 V, 0.1 nA); (b) oxidized layer prepared at 600 K in O_2 (1×10^{-6} mbar) (2.5 V, 0.1 nA). An enlarged image of the oxidized layer is shown in (c). (d) Height profile measured along the line in image (c).

With 14% vanadium

Figure 6.6(a) displays a STM image of an oxidized layer with 14% vanadium. Large terraces are seen together with some bright spots. More structural information is found in image (b) which has a higher magnification. Although the surface appears very rough, the (1 × 2) structure with cross-links is still visible. Many bright protrusions are visible forming an extra layer of clusters. For the oxidized layer with 6% vanadium (Figure 6.5) it was shown that vanadia clusters were induced on the (1 × 2) "Ti_2O_3 rods". The extra layer of clusters on the (1 × 2) surface is probably

composed of vanadia clusters as well. This inference is supported by an analysis of XPS spectra of the layer before and after oxidation. Figure 6.7 shows that the concentration of vanadium increases by about 33% upon oxidation and a new oxidation state of +5 for vanadium appears. To obtain the images in Figure 6.6, a higher bias voltage of +3.5 V with a lower tunneling current of 0.03 nA had to be used (usually 2.5 V 0.1 nA for an oxidized layer with a lower vanadium concentration). This may be due to the presence of V^{5+} related aggregates at the surface since these may have a significant gap in the electronic density of states.

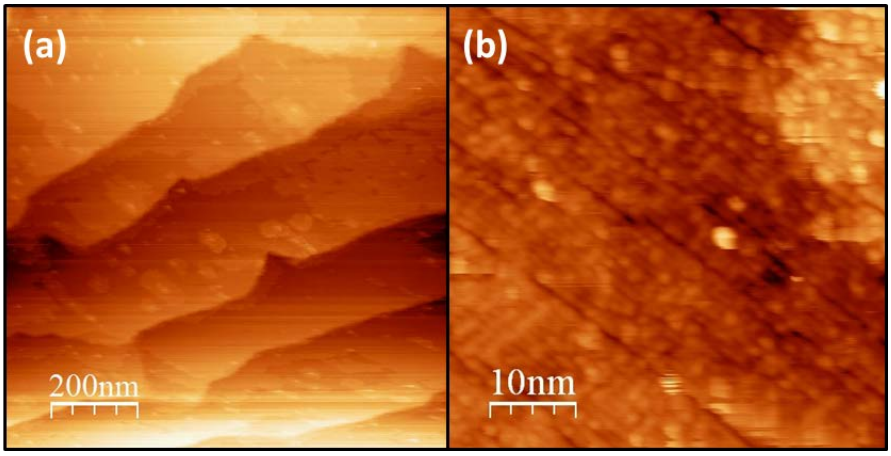

Figure 6.6 STM images of an oxidized TiO_2 layer with 14% V (3.5 V, 0.03 nA): (a) large area of 1000 nm × 1000 nm and (b) small area of 50 nm × 50 nm.

An analysis of the LEED pattern revealed more structural information about this oxidized layer with 14% V. In the pattern in Figure 6.8(a) sharp (1 × 2) spots are visible which is consistent with the (1 × 2) surface reconstruction. Additional spots probably related to the vanadia overlayer (marked by arrows) are observed as well. Schematic LEED patterns of TiO_2 (110) (1 × 2) and V_2O_5(001) produced with software "LEEDpat"[118] are shown in Figure 6.8(b). White spots are for TiO_2(110) (1 × 2) and blue spots are for V_2O_5(001). In the [001] direction, the distance between the V_2O_5 spots and the TiO_2 spots in the simulation fits well to the distance in the observed pattern, while it does not fit well in the other direction, which might mean that the surface could at least partially be covered with extended structure having structure features also found in V_2O_5. The manifold of spots may be related to double diffraction or even Moiré formation.

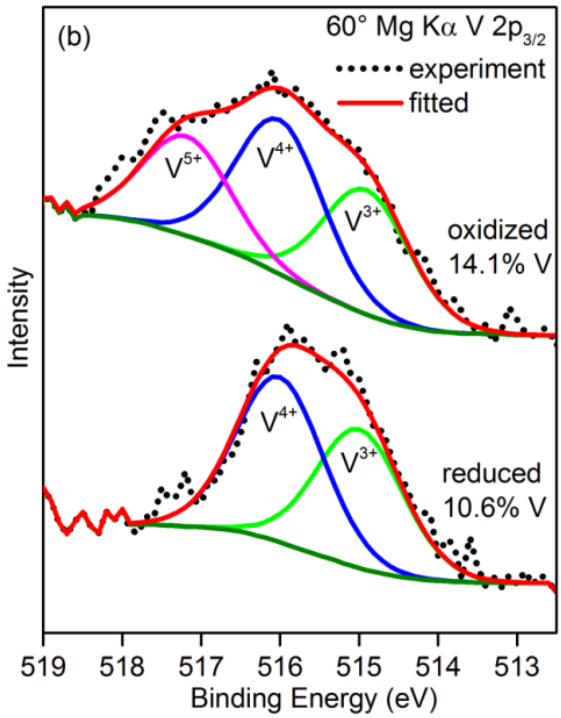

Figure 6.7 XPS spectra (60°) of the V $2p^{3/2}$ level of a TiO_2 layer with 14% V before and after oxidation. Two (lower panel) or three (upper panel) oxidation states of vanadium were identified by peak fitting.

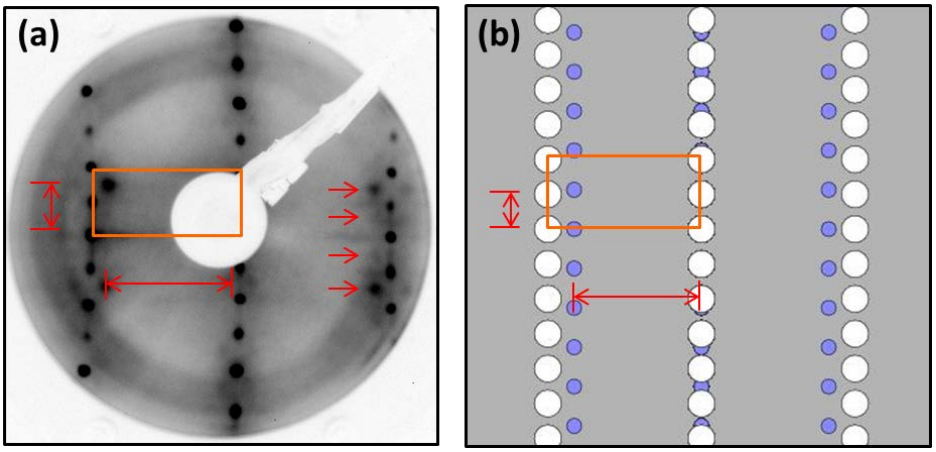

Figure 6.8 (a) LEED pattern of an oxidized TiO_2 layer with 14% V. (b) schematic LEED pattern produced with the software "LEEDpat", showing the LEED pattern of TiO_2 (1 × 2) overlapped with that of V_2O_5(001).

6.3 Reactivity of the oxidized layers

In order to check the reactivity of the samples, TPD tests using methanol as the probe molecule were conducted. In the experiments the samples were prepared by annealing the Ti + V mixed oxide in 10^{-6} mbar of oxygen (isotope ^{18}O) at 600 K, while ^{16}O is contained in methanol ($CH_3{}^{16}OH$). Masses 33 and 31 were selected to identify the desorption of CH_3OH which may contain ^{16}O or ^{18}O. Similarly masses 32, 34, and 36 were selected to check the desorption of oxygen. Since a chamber background of $C^{18}O$ cannot be completely eliminated, mass 29 instead of mass 30 was selected for formaldehyde.

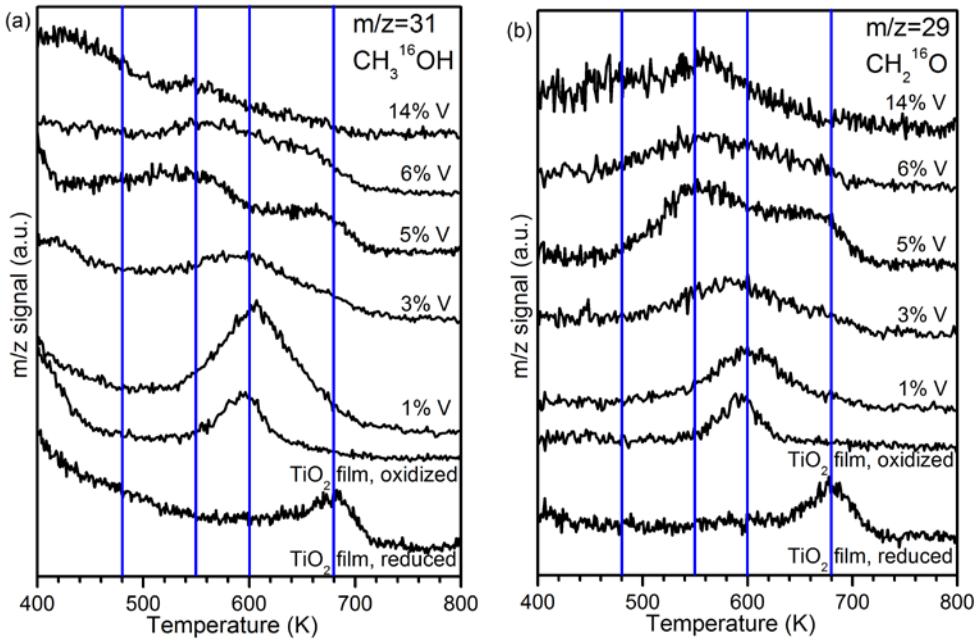

Figure 6.9 (a) Methanol (m/z=31) and (b) formaldehyde (m/z=29) TPD spectra of oxidized Ti + V thin films with various V concentrations (1%, 3%, 5%, 6%, and 14%). Spectra from pure TiO_2 thin film layers exposed to oxidized and reduced conditions are also shown for comparison.

Figure 6.9 displays methanol (m/z 31) and formaldehyde (m/z 29) desorption spectra of methanol on Ti + V mixed oxides with V concentrations from 1% to 14%. The contribution of methanol to the m/z 29 signal was subtracted prior to plotting. The main products of the reaction of methanol at the oxidized Ti + V thin film surfaces are methanol and formaldehyde. The desorption spectra depend on the

vanadium content in the films. The spectra of m/z 33 for $CH_3{}^{18}OH$ were also recorded. However, no signal was detected, which means methanol containing the isotope ^{18}O was not produced.

For the mixed oxide layer with 1% V, intensive peaks of methanol and formaldehyde in the range of 500 K to 700 K are observed. Each of the peaks is composed of a main peak at 600 K and a shoulder at ~680 K. At 600 K a peak is observed for an oxidized layer without vanadium and reduced TiO_2(110) without vanadium produces a peak at 680 K. Therefore it is reasonable to assume that the two peaks composing the whole wide feature originate from reactions similar to those on oxidized and reduced TiO_2 thin films without vanadium. Analysis of Figure 6.3 has shown that the mixed oxide layer with 1% V has a mixed oxidized/reduced surface where BOVs and oxygen adatoms coexist. BOVs are the sites for the methanol reaction at 680 K, and oxygen adatoms are responsible for the reaction at 600 K. Those reaction paths together dominate the reaction of methanol on films with 1% V.

For the mixed oxide layer with 3% V, broad peaks from 500 K to 700 K are still observed for methanol and formaldehyde. However a new peak at 550 K is identified in the spectra while the peak centered at ~600 K is much smaller. The peak at 550 K becomes more prominent when the concentration of vanadium in the thin film is increased to 5%. As discussed before, vanadium-related features appear on the (1 × 1) terraces at such vanadium concentrations and therefore it is quite probably that the peak at 550 K is due to these features. The higher intensity of the 550 K peak in the spectrum of the film with 5% V may be assigned to the higher concentration of the V-related features.

For the oxidized thin films with 5%, 6% and 14% of vanadium, another peak at around 480 K appears in the methanol and formaldehyde desorption spectra. Its intensity increases with increasing vanadium concentration. For such concentrations of vanadium in the layers, (1 × 2) rods with vanadia clusters on them appear on the oxidized surfaces. The peak at 480 K is probably related to these vanadia clusters.

While no methanol with ^{18}O was produced, oxygen gas ($^{18}O_2$, m/z 36) desorption was detected during TPD of the oxidized layers. As shown in Figure 6.10, no oxygen desorbs from the reduced surface (spectrum c), while oxygen desorbs from the oxidized surfaces between 500 K and 800 K. The spectra of the oxidized Ti + V thin films shows more complex oxygen signals with higher intensities than the spectrum of vanadium for pure TiO_2(110). Also, there are several sharp peak in the spectra of the layers containing vanadium while the spectrum of regular TiO_2(110) exhibits just

abroad structure. At the surface of the pure TiO_2 thin film, oxygen adatoms are a main feature and their combination upon heating accounts for the oxygen desorption. On the other hand, several structural features appear at the oxidized surfaces. Oxygen desorption from such surfaces is probably not only due to the adatoms but will also contain contributions from the decomposition of vanadia clusters. A relevant point is that oxygen evolution starts at lower temperatures for the mixed oxides, which is probably attributed to their increased reducibility.

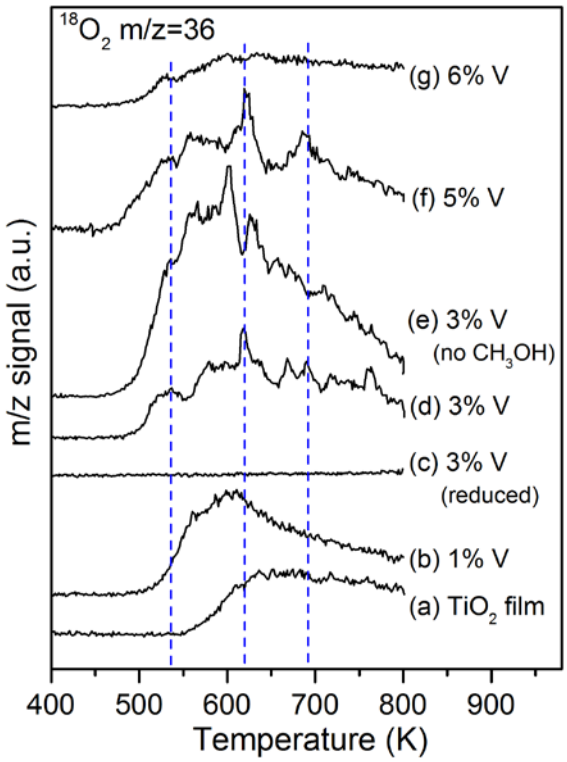

Figure 6.10 Oxygen TPD spectra ($^{18}O_2$, m/z 36) of oxidized Ti + V mixed oxides with various V concentrations. Spectra from an oxidized TiO_2 thin film (a) and a reduced mixed oxide film with 3% V (c) are also shown for comparison. Most of the spectra were recorded in the context of the methanol desorption experiments and therefore in the case of all spectra except (e), the surfaces were dosed with methanol prior to TPD. Spectrum (e) shows that the oxygen desorption is not due to the presence of methanol, but it is possible that the fine structure of the spectra is affected by it.

The release of oxygen from the decomposition of vanadia has been reported for both bulk crystals and thin films. Su and Schlögl tested the thermal decomposition of a bulky V_2O_5 crystal and found a transformation from V_2O_5 at around 473 K via VO_2

to V_2O_3, a stable state at 873 K. [119] The temperature range for the transformation is close to the temperature of the onset of O_2 desorption observed here.[119] Sturm et al. studied the thermal stability of a well-ordered V_2O_5(001) thin films on Au (111) and found also the desorption of oxygen.[120] Sharp peaks were observed by them, even though at a temperature (~873 K) higher than the observed peak temperatures (600 K, 700 K) in the present experiments. [120] The decomposition temperature may depend on the structure of vanadia and the material of support. In this case vanadia is mainly in the form of clusters supported by TiO_2 thin films. Also, V_2O_5 is observed mainly for higher V concentrations in the layers so that for layers with a smaller V concentration the decomposition of features with vanadium in the lower oxidation states must be relevant.

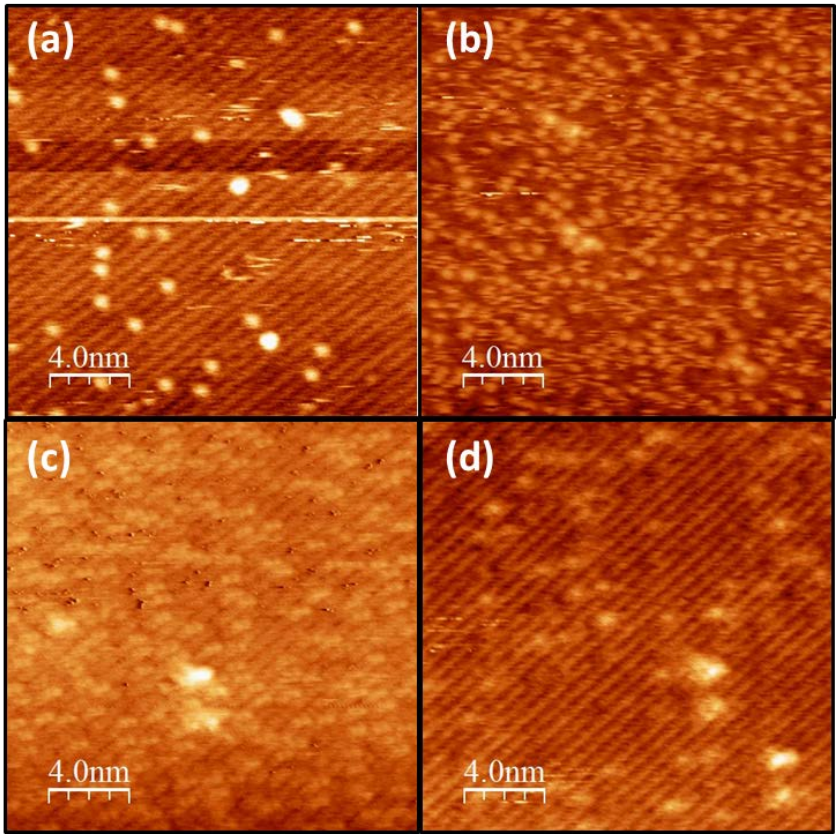

Figure 6.11 STM images of an oxidized TiO_2 thin film with 1% vanadium (a), and after 0.5 L methanol adsorption at 300 K (b) followed by flashing to 340 K (c) and 400 K (d) sequentially. (Tunneling parameters: 3.5 V, 0.1 nA for image (a); 2 V, 0.1 nA for image (b) (c) and (d)).

The reaction sites of methanol at the oxidized surfaces were further studied by direct imaging of the surface after methanol adsorption. Figure 6.11 compares STM images of the oxidized surface of the mixed oxide layer with 1% vanadium before and after adsorption of 0.5 L methanol. In Figure 6.11(a) oxygen adatoms and several vanadia clusters are observed at the oxidized surface as identified from the bright spots on the Ti rows. After dosing methanol to the surface at 300 K, many spots due to methoxy/hydroxyl groups are distributed densely on the Ti rows (Figure 6.11(b)), due to the dissociation of methanol at the 5-fold Ti sites at the surface. According to the TPD spectra of methanol, those methoxy/hydroxyl groups recombine and desorb upon heating to 400 K. Figure 6.11(c) and (d) indeed show that less bright spots on Ti rows are observed after flashing the sample to 340 K. When the sample is heated to 400 K, only 5% bright spots are left at the surface. The remaining spots are supposed to be the dissociated groups on the oxygen adatoms and vanadia clusters, where reaction takes place at higher temperature.

6.4 Discussion of the reaction mechanism

The reactivity tests of the oxidized layers have shown that at a very low V concentration (1%) CH_2O desorbs at 600 K. When vanadia clusters accumulate at the surface at vanadium concentrations above 3%, a new desorption channel appears at 550 K. Even higher vanadium contents lead to a peak at an even lower desorption temperature of 480 K. The results of these TPD tests are similar to results of previous studies of vanadia on TiO_2(110). Wang and Madix reported a decreasing CH_2O desorption temperature from 642 K to 551 K to 517 K with increasing vanadia coverage from 0.3 ML to 0.6 ML to 1 ML respectively.[78] Wong et al. found that the CH_2O desorption temperature is a function of the oxidation state of the vanadium cations.[79] A temperature of 615 K was claimed to be related to clusters containing predominantly V^{3+}, while clusters containing V^{5+} should be responsible for desorption at 485 K.[79] However these two papers did not report surface structure information.

Reactivity experiments combined with structure analysis were performed by Metiu and others.[83,121,122] They found that post-oxidized VO aggregates on TiO_2 produce the most formaldehyde at about 600 K. With the help of STM experiments and DFT calculations, they suggested that VO_3 monomer clusters were responsible for the reactivity. In the present case, desorption of formaldehyde at 600 K was also observed for the sample with low V concentration (1%). However in the STM images discussed here the vanadia clusters are located above the Ti rows, while in

Metiu et al.'s experiments the VO_3 aggregates were found to be located in the upper threefold hollow sites. Therefore the observed vanadia clusters discussed here are probably of another type than the VO_3 monomer clusters. The different results are probably to be attributed to the different preparation procedures. In their case, vanadia clusters were deposited onto TiO_2(110) at room temperature using a home-built apparatus that produces mass-selected clusters. In the case discussed here vanadia clusters were produced by the oxidation of vanadium atoms from subsurface areas of the reduced Ti + V mixed oxide layer. Not only the preparation of the clusters, but also the support of the clusters is different. In here-discussed case the vanadia clusters were supported by reduced TiO_2(110) layers with admixed vanadium, which may influence the cluster formation as well.

The morphology of vanadia clusters with coverages of sub-monolayers on TiO_2(110) was also investigated by Agnoli et al.[80,82] They found vanadia clusters on top of the fivefold-coordinated Ti rows of the substrate at low coverage[80,82], which is the same location as in the present case. Based on photoemission, photoelectron diffraction experiments, and DFT calculations, the clusters were identified as tetramer V_4O_6 nanoclusters, which are composed of 2 units of V_2O_3 (Figure 6.12(a)), resembling the structure of Ti_2O_3 rods at the TiO_2 surface.[82] In view of the similar appearance and the identical adsorption sites, such V_4O_6 clusters would be a suitable model for the vanadia cluster at low vanadium concentrations in the present case.

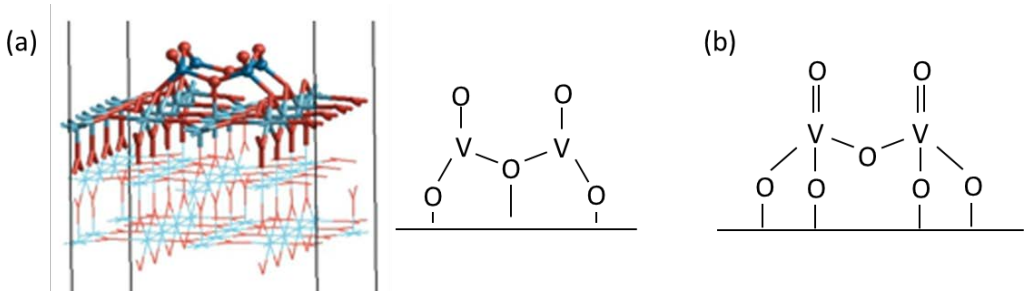

Figure 6.12 (a) Model of a V_4O_6 nanocluster which is composed of 2 units of V_2O_3 (Adapted with permission from ref [82]. Copyright 2013 American Chemical Society.) (b) model of a V_2O_5 cluster (Adapted with permission from ref 1. Copyright 2012 Elsevier.)

For oxidized layers with a higher vanadium content, V^{5+} was identified with XPS. Beck et al. proposed a model of dimeric vanadyl V_2O_5 supported on TiO_2 (Figure

6.12(b)), and based on this model they suggested a Mars–van Krevelen mechanism for the partial oxidation reaction of ethanol towards aldehyde.[1,123] This type of cluster and a similar mechanism of methanol partial oxidation may also be applied in the here-discussed case.

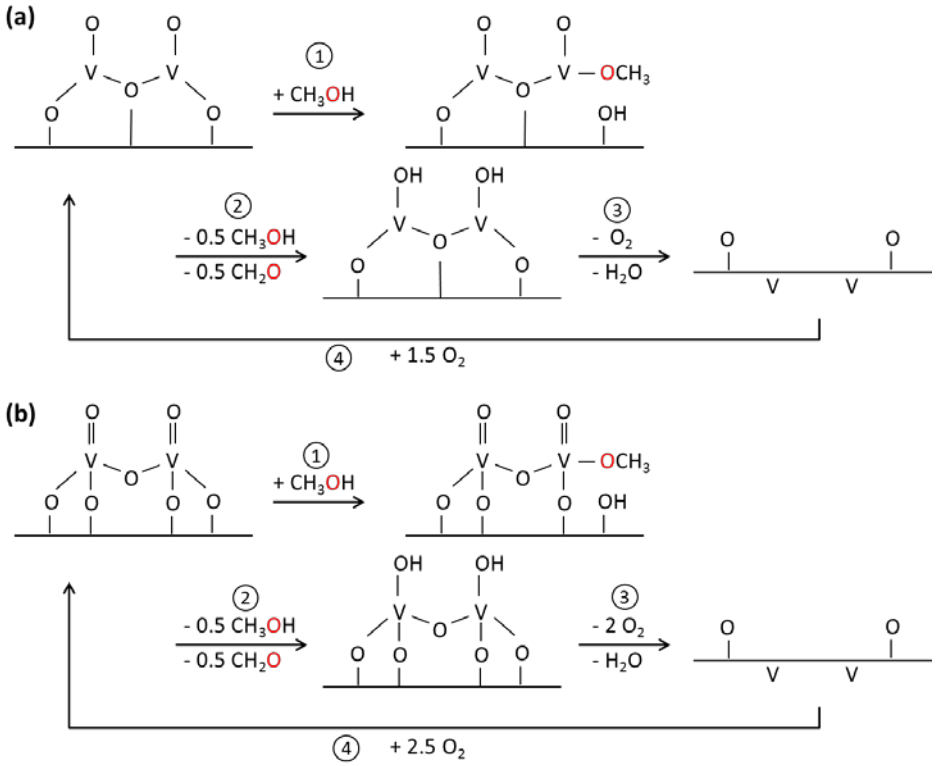

Figure 6.13 Mechanistic models of methanol partial oxidation by (a) $(V_2O_3)_2$ vanadia clusters and (b) V_2O_5 vanadia clusters. Oxygen in black color is ^{18}O while red oxygen is ^{16}O. The long horizontal line represents the $TiO_2(110)$ surface. The catalytic steps are labeled with ①②③ and ④. The models are adapted from ref 1.

Based on the cluster models (V_4O_6 and V_2O_5) and the observed TPD results, reaction mechanisms of methanol oxidation are proposed as shown in Figure 6.13. Four main processes involved and explained as following:

1. Methanol dissociates into methoxy groups that bind to vanadium sites and hydrogen binding to surface oxygen.
2. When the sample is heated to 550 K (for V_4O_6 clusters) or 480 K (for V_2O_5 clusters), a disproportionation reaction occurs between methoxyl groups forming methanol and formaldehyde.

3. Meanwhile upon heating, oxygen gas from the decomposition of clusters and water from the reaction of hydroxyls with the surface desorb, leading to a reduced surface with vanadium atoms possibly diffusing below the surface. There is no experimentally clear relationship between step 2 and step 3.
4. Under oxidizing conditions, vanadium atoms may be trapped at the surface by oxidation which leads to vanadium oxide clusters. Thus a catalytic cycle involving the reduction and oxidation of the catalyst according to Mars–van Krevelen mechanism may form.

The suggested reaction mechanisms (Mars–van Krevelen mechanism[123]) adapted from ref [1] fit well to the results of the TPD experiments. The models indicate that both methanol and formaldehyde are produced upon the adsorption of methanol at the surface. Oxygen is released from the decomposition of vanadia clusters. No oxygen from methanol participates in the release of oxygen. The reaction temperatures for the two cluster models are probably different, which is in agreement with the experimental results. Reduction and oxidation of the clusters form a catalytic cycle, which was reflected by the repeatable TPD experiments.

6.5 Summary of chapter 6

In this chapter, the surface structure and reactivity of the oxidized sufaces were characterized. At low vanadium concentration, vanadia clusters are observed above the Ti rows at the surface. This type of cluster triggers a new reaction channel for the partial oxidation of methanol towards formaldehyde at 550 K, besides the reaction at 600 K on pure TiO_2(110). At higher vanadium concentration, vanadia clusters with an oxidation state of V^{5+} were found to cover the (1 × 2) surface. In this case formaldehyde desorbs at 480 K. Together with the desorption of methanol and formaldehyde, oxygen is released from the thermal decomposition of the vanadia clusters. Mechanistic models derived from the Mars–van Krevelen mechanism are suggested based on the observed structures and reactivities of the oxidized Ti + V thin films.

Chapter 7

Conclusions and outlook

Vanadium oxide powder samples supported on titania have been shown to efficiently catalyze the partial oxidation of alcohols towards aldehydes.[1] The presented work addresses the surface properties of vanadia-titania mixed oxide layers prepared on a rutile (110) single crystal. The surface structure and the reactivity of mixed oxides with various vanadium concentrations was systematically studied using the surface science techniques XPS, STM, LEED, and TPD.

Ti + V mixed oxide layers were prepared using a well-developed recipe: Ti and V were deposited (simultaneously or sequentially) in an oxygen atmosphere on a TiO_2(110) single crystal substrate with an interlayer of Ti + Ta mixed oxide that prevents the diffusion of vanadium from the layers into the substrate at high temperature. As a first step, pure TiO_2(110) thin films without vanadium were studied to provide a basis for further analysis. Ti cation exchange between the overlayer and the rutile substrate was found to be prevented by the Ti + Ta mixed oxide interlayer. Thus, fully oxidized or strongly reduced TiO_2(110) layers could be grown on the substrate without changing the state of the substrate to a comparable extent. The chemical and structural properties of TiO_2(110) layers prepared this way are essentially identical to those of a single crystal surface.

Experiments with Ti + V mixed oxide layers reduced by annealing in vacuum revealed a heavy impact of vanadium doping onto the properties of the layers. Vanadium ions reside below the surface as concluded from STM results and the distribution of vanadium measured with angle-resolved XPS. The presence of sub-surface vanadium ions increases the reducibility of the layers: even a small concentration of vanadium induces a high density of bridging oxygen vacancies at the surface after mild annealing; higher vanadium concentrations induce the formation of a (1×2) reconstructed surface as known for heavily reduced TiO_2(110). Reactivity tests with methanol as a test molecule support the conclusion that the layers are heavily reduced and that the vanadium atoms are below the surface since

the TPD did not exhibit any indication of a direct vanadium-methanol interaction. The increased reducibility is a consequence of the fact that the energy for the removal of oxygen from the vicinity of vanadium ions is smaller than the energy for the removal of oxygen from the vicinity of titanium atoms in undoped TiO_2(110).

Oxidation of the Ti + V mixed oxide layers leads to interesting processes. On the one hand, vanadium doping causes a reduction of the TiO_2(110) layers; on the other hand, annealing in oxygen leads to an oxidation of the layers which drives vanadium to the surface. Thus several features coexist at this partially oxidized surface: bridging oxygen vacancies, oxygen adatoms, and vanadia clusters of at least two types. In methanol TPD data, formaldehyde desorption maxima at 680 K and 600 K related to bridging oxygen vacancies and oxygen adatoms as also observed for undoped TiO_2(110) are seen. In addition, partial oxidation of methanol towards formaldehyde is also found at lower temperatures of 550 K and 480 K. The reaction at 550 K takes place on vanadia clusters located above the Ti rows on the oxidized surface. The reaction at 480 K is related to vanadia clusters on the (1 × 2) surface. At high vanadium concentrations, such vanadia clusters, which contain V^{5+} according to XPS, densely cover the (1 × 2) surface. The methanol partial oxidation reaction catalyzed by these vanadia clusters occurs according to the well-known Mars–van Krevelen mechanism, where oxygen from the vanadia clusters participates in the oxidation of reactants.

In summary, the surface structure of Ti + V mixed oxide thin layers and the partial oxidation of methanol thereon were systematically characterized. Analysis of the experimental results unveils an increased reducibility caused by the vanadium ions. If the layers are exposed to reducing conditions the vanadium ions nearly exclusively stay below the surface while oxidation induces the formation of vanadia clusters at the surface. The latter are responsible for two reaction channels in the partial oxidation of methanol which are at lower temperature than the commonly observed channels for TiO_2(110) without vanadium. Those findings provide a deeper understanding of how dopants influence the properties of host oxides and shed lights on the catalytic process of alcohols on mixed oxides.

List of Figures

List of Tables

Bibliography

(1) Beck, B.; Harth, M.; Hamilton, N. G.; Carrero, C.; Uhlrich, J. J.; Trunschke, A.; Shaikhutdinov, S.; Schubert, H.; Freund, H.-J.; Schlögl, R.; et al. Partial Oxidation of Ethanol on Vanadia Catalysts on Supporting Oxides with Different Redox Properties Compared to Propane. *J. Catal.* **2012**, *296*, 120–131.

(2) Wachs, I. E. Recent Conceptual Advances in the Catalysis Science of Mixed Metal Oxide Catalytic Materials. *Catal. Today* **2005**, *100*, 79–94.

(3) Dinse, A.; Frank, B.; Hess, C.; Habel, D.; Schomäcker, R. Oxidative Dehydrogenation of Propane over Low-Loaded Vanadia Catalysts: Impact of the Support Material on Kinetics and Selectivity. *J. Mol. Catal. A Chem.* **2008**, *289*, 28–37.

(4) Ertl, G.; Knözinger, H.; Schüth, F.; Weitkamp, J. *Handbook of Heterogeneous Catalysis*; Wiley-VCH Verlag GmbH: Weinheim, Germany, 2008.

(5) Hagen, J. *Industrial Catalysis: A Practical Approach*, Second edi.; Wiley-VCH Verlag GmbH: Weinheim, Germany, 2006.

(6) Cui, Y.; Shao, X.; Baldofski, M.; Sauer, J.; Nilius, N.; Freund, H.-J. Adsorption, Activation, and Dissociation of Oxygen on Doped Oxides. *Angew. Chem. Int. Ed.* **2013**, *52*, 11385–11387.

(7) Freund, H.-J.; Kuhlenbeck, H.; Staemmler, V. Oxide Surfaces. *Reports Prog. Phys.* **1996**, *59*, 283–347.

(8) Freund, H.-J.; Pacchioni, G. Oxide Ultra-Thin Films on Metals: New Materials for the Design of Supported Metal Catalysts. *Chem. Soc. Rev.* **2008**, *37*, 2224–2242.

(9) Kuhlenbeck, H.; Shaikhutdinov, S.; Freund, H.-J. Well-Ordered Transition Metal Oxide Layers in Model Catalysis--a Series of Case Studies. *Chem. Rev.* **2013**, *113*, 3986–4034.

(10) Campbell, C. T. Ultrathin Metal Films and Particles on Oxide Surfaces: Structural, Electronic and Chemisorptive Properties. *Surf. Sci. Rep.* **1997**, *27*, 1–111.

(11) Nilius, N.; Freund, H.-J. Activating Nonreducible Oxides via Doping. *Acc. Chem. Res.* **2015**, *48*, 1532–1539.

(12) Wachs, I. E. Catalysis Science of Supported Vanadium Oxide Catalysts. *Dalton*

Trans. **2013**, *42*, 11762–11769.

(13) Atrei, A.; Bardi, U.; Rovida, G. Structure and Composition of the Titanium Oxide Layers Formed by Low-Pressure Oxidation of the $Ni_{94}Ti_6$(110) Surface. *Surf. Sci.* **1997**, *391*, 216–225.

(14) Lai, X.; Guo, Q.; Min, B. K.; Goodman, D. W. Synthesis and Characterization of Titania Films on Mo(110). *Surf. Sci.* **2001**, *487*, 1–8.

(15) Papageorgiou, A. C.; Pang, C. L.; Chen, Q.; Thornton, G. Low-Dimensional, Reduced Phases of Ultrathin TiO_2. *ACS Nano* **2007**, *1*, 409–414.

(16) Atrei, A.; Cortigiani, B.; Ferrari, A. M. Epitaxial Growth of TiO_2 Films with the Rutile (110) Structure on Ag(100). *J. Phys.: Condens. Matter* **2012**, *24*, 445005–445013.

(17) McCavish, N. D.; Bennett, R. A. Ultra-Thin Film Growth of Titanium Dioxide on W(100). *Surf. Sci.* **2003**, *546*, 47–56.

(18) Pang, C. L.; Grinter, D. C.; Matharu, J.; Thornton, G. A Scanning Tunneling Microscopy Study of Ultrathin Film Rutile TiO_2(110) Supported on W(100)-O(2×1). *J. Phys. Chem. C* **2013**, *117*, 25622–25627.

(19) Primorac, E. Doctoral Dissertation, Humboldt-Universität zu Berlin, 2017.

(20) Munuera, G.; Fernandez, A.; Soria, J.; Conesa, J.; Sanz, J. Mechanism of Hydrogen Gas-Sensing at Low Temperatures Using Rh/TiO_2 System. *Sens. Actuators* **1989**, *18*, 337–348.

(21) Johansson, L. Static SIMS Studies of Coated TiO_2 Pigments. *Surf. Interface Anal.* **1993**, *20*, 304–308.

(22) Sathiyanarayanan, S.; Azim, S. S.; Venkatachari, G. Corrosion Protection of Magnesium ZM 21 Alloy with Polyaniline-TiO_2 Composite Containing Coatings. *Prog. Org. Coat.* **2007**, *59*, 291–296.

(23) Yan, M. F.; Rhodes, W. W. Preparation and Properties of TiO_2 Varistors. *Appl. Phys. Lett.* **1982**, *40*, 536–537.

(24) Pandey, R. N.; Babu, K. S. C.; Srivastava, O. N. High Conversion Efficiency Photoelectrochemical Solar Cells. *Prog. Surf. Sci.* **1996**, *52*, 125–192.

(25) Hoffmann, M. R.; Martin, S. T.; Choi, W.; Bahnemann, D. W. Environmental Applications of Semiconductor Photocatalysis. *Chem. Rev.* **1995**, *95*, 69–96.

(26) Fujishima, A.; Zhang, X.; Tryk, D. A. TiO_2 Photocatalysis and Related Surface Phenomena. *Surf. Sci. Rep.* **2008**, *63*, 515–582.

(27) Diebold, U. The Surface Science of Titanium Dioxide. *Surf. Sci. Rep.* **2003**, *48*, 53–229.

(28) Pang, C. L.; Lindsay, R.; Thornton, G. Structure of Clean and Adsorbate-Covered Single-Crystal Rutile TiO_2 Surfaces. *Chem. Rev.* **2013**, *113*, 3887–3948.

(29) Dohnálek, Z.; Lyubinetsky, I.; Rousseau, R. Thermally-Driven Processes on

Rutile TiO_2(110)-(1×1): A Direct View at the Atomic Scale. *Prog. Surf. Sci.* **2010**, *85*, 161–205.

(30) Pang, C. L.; Lindsay, R.; Thornton, G. Chemical Reactions on Rutile TiO_2(110). *Chem. Soc. Rev.* **2008**, *37*, 2328–2353.

(31) Li, M.; Hebenstreit, W.; Diebold, U.; Tyryshkin, A. M.; Bowman, M. K.; Dunham, G. G.; Henderson, M. A. The Influence of the Bulk Reduction State on the Surface Structure and Morphology of Rutile TiO_2(110) Single Crystals. *J. Phys. Chem. B* **2000**, *104*, 4944–4950.

(32) Lu, G.; Linsebigler, A.; Yates, J. T. Ti^{3+} Defect Sites on TiO_2(110): Production and Chemical Detection of Active Sites. *J. Phys. Chem.* **1994**, *98*, 11733–11738.

(33) Bowker, M. The Surface Structure of Titania and the Effect of Reduction. *Curr. Opin. Solid State Mater. Sci.* **2006**, *10*, 153–162.

(34) Wendt, S.; Schaub, R.; Matthiesen, J.; Vestergaard, E. K.; Wahlström, E.; Rasmussen, M. D.; Thostrup, P.; Molina, L. M.; Lægsgaard, E.; Stensgaard, I.; et al. Oxygen Vacancies on TiO_2(110) and Their Interaction with H_2O and O_2: A Combined High-Resolution STM and DFT Study. *Surf. Sci.* **2005**, *598*, 226–245.

(35) Onishi, H.; Iwasawa, Y. Reconstruction of TiO_2(110) Surface: STM Study with Atomic-Scale Resolution. *Surf. Sci.* **1994**, *313*, L783–L789.

(36) Bennett, R. a; Stone, P.; Price, N. J.; Bowker, M. Two (1×2) Reconstructions of TiO_2(110): Surface Rearrangement and Reactivity Studied Using Elevated Temperature Scanning Tunneling Microscopy. *Phys. Rev. Lett.* **1999**, *82*, 3831–3834.

(37) Møller, P. J.; Wu, M. C. Surface Geometrical Structure and Incommensurate Growth: Ultrathin Cu Films on TiO_2(110). *Surf. Sci.* **1989**, *224*, 265–276.

(38) Pang, C.; Haycock, S.; Raza, H.; Murray, P.; Thornton, G.; Gulseren, O.; James, R.; Bullett, D. Added Row Model of TiO_2(110) 1×2. *Phys. Rev. B* **1998**, *58*, 1586–1589.

(39) Asari, E.; Souda, R. Atomic Structure of TiO_2(110)-p(1×2) and p(1×3) Surfaces Studied by Impact Collision Ion-Scattering Spectroscopy. *Phys. Rev. B* **1999**, *60*, 719–722.

(40) Blanco-Rey, M.; Abad, J.; Rogero, C.; Méndez, J.; López, M. F.; Román, E.; Martín-Gago, J. a.; De Andrés, P. L. LEED-IV Study of the Rutile TiO_2(110) -1×2 Surface with a Ti-Interstitial Added-Row Reconstruction. *Phys. Rev. B - Condens. Matter Mater. Phys.* **2007**, *75*, 10–13.

(41) Ng, K.-O.; Vanderbilt, D. Structure and Apparent Topography of TiO_2(110) Surfaces. *Phys. Rev. B* **1997**, *56*, 10544–10548.

(42) Li, M.; Hebenstreit, W.; Diebold, U.; Henderson, M. a.; Jennison, D. R. Oxygen-Induced Restructuring of Rutile TiO_2(110): Formation Mechanism, Atomic Models, and Influence on Surface Chemistry. *Faraday Discuss.* **1999**,

114, 245–258.

(43) Henderson, M. A. Mechanism for the Bulk-Assisted Reoxidation of Ion Sputtered TiO_2 Surfaces: Diffusion of Oxygen to the Surface or Titanium to the Bulk? *Surf. Sci.* **1995**, *343*, L1156–L1160.

(44) Onishi, H.; Iwasawa, Y. Dynamic Visualization of a Metal-Oxide-Surface/Gas-Phase Reaction: Time-Resolved Observation by Scanning Tunneling Microscopy at 800 K. *Phys. Rev. Lett.* **1996**, *76*, 791–794.

(45) Yingge, D.; Dohnálek, Z.; Lyubinetsky, I. Transient Mobility of Oxygen Adatoms upon O_2 Dissociation on Reduced TiO_2(110). *J. Phys. Chem. C* **2008**, *112*, 2649–2653.

(46) Wendt, S.; Sprunger, P. T.; Lira, E.; Madsen, G. K. H.; Li, Z.; Hansen, J. Ø.; Matthiesen, J.; Blekinge-Rasmussen, A.; Laegsgaard, E.; Hammer, B.; et al. The Role of Interstitial Sites in the Ti3d Defect State in the Band Gap of Titania. *Science* **2008**, *320*, 1755–1759.

(47) Du, Y.; Deskins, N. A.; Zhang, Z.; Dohnalek, Z.; Dupuis, M.; Lyubinetsky, I. Formation of O Adatom Pairs and Charge Transfer upon O_2 Dissociation on Reduced TiO_2(110). *Phys. Chem. Chem. Phys.* **2010**, *12*, 6337–6344.

(48) Henderson, M. A.; Otero-Tapia, S.; Castro, M. E. The Chemistry of Methanol on the TiO_2(110) Surface: The Influence of Vacancies and Coadsorbed Species. *Faraday Discuss.* **1999**, *114*, 313–329.

(49) Zhang, Z.; Bondarchuk, O.; White, J. M.; Kay, B. D.; Dohnálek, Z. Imaging Adsorbate O-H Bond Cleavage: Methanol on TiO_2(110). *J. Am. Chem. Soc.* **2006**, *128*, 4198–4199.

(50) Sanchez de Armas, R.; Oviedo, J.; Miguel, M. A. S.; Sanz, J. F. Methanol Adsorption and Dissociation on TiO_2(110) from First Principles Calculations. *J. Phys. Chem. C* **2007**, *111*, 10023–10028.

(51) Zhang, Z.; Bondarchuk, O.; Kay, B. D.; White, J. M.; Dohnálek, Z. Direct Visualization of 2-Butanol Adsorption and Dissociation on TiO_2(110). *J. Phys. Chem. C* **2007**, *111*, 3021–3027.

(52) Gamble, L.; Jung, L. S.; Campbell, C. T. Decomposition and Protonation of Surface Ethoxys on TiO_2(110). *Surf. Sci.* **1996**, *348*, 1–16.

(53) Kim, Y. K.; Kay, B. D.; White, J. M.; Dohnálek, Z. Alcohol Chemistry on Rutile TiO_2(110): The Influence of Alkyl Substituents on Reactivity and Selectivity. *J. Phys. Chem. C* **2007**, *111*, 18236–18242.

(54) Zhao, J.; Yang, J.; Petek, H. Theoretical Study of the Molecular and Electronic Structure of Methanol on a TiO_2(110) Surface. *Phys. Rev. B* **2009**, *80*, 235416.

(55) Bates, S.; Gillan, M.; Kresse, G. Adsorption of Methanol on TiO_2(110): A First-Principles Investigation. *J. Phys. Chem. B* **1998**, *2*, 2017–2026.

(56) Henderson, M. A. A Surface Science Perspective on TiO_2 Photocatalysis. *Surf. Sci. Rep.* **2011**, *66*, 185–297.

(57) Zamora, M.; López, T.; Gómez, R.; Asomoza, M.; Melendrez, R. Oligomerization of Acetone over Titania-Doped Catalysts (Li, Na, K and Cs): Effect of the Alkaline Metal in Activity and Selectivity. *Catal. Today* **2005**, *107-108*, 289–293.

(58) Isomura, N.; Wu, X.; Watanabe, Y. Atomic-Resolution Imaging of Size-Selected Platinum Clusters on TiO_2(110) Surfaces. *J. Chem. Phys.* **2009**, *131*, 164707–164710.

(59) Abad, J.; Rogero, C.; Méndez, J.; López, M. F.; Martín-Gago, J. A.; Román, E. Ultra-Thin Si Overlayers on the TiO_2(110)-(1×2) Surface: Growth Mode and Electronic Properties. *Surf. Sci.* **2006**, *600*, 2696–2704.

(60) Karslıoğlu, O.; Song, X.; Kuhlenbeck, H.; Freund, H.-J. Mo+TiO_2(110) Mixed Oxide Layer: Structure and Reactivity. *Top. Catal.* **2013**, *56*, 1389–1403.

(61) Matthey, D.; Wang, J. G.; Wendt, S.; Matthiesen, J.; Schaub, R.; Lægsgaard, E.; Hammer, B.; Besenbacher, F. Enhanced Bonding of Gold Nanoparticles on Oxidized TiO_2(110). *Science* **2007**, *315*, 1692–1696.

(62) Batzill, M.; Morales, E. H.; Diebold, U. Influence of Nitrogen Doping on the Defect Formation and Surface Properties of TiO_2 Rutile and Anatase. *Phys. Rev. Lett.* **2006**, *96*, 026103–026106.

(63) Bechstein, R.; Kitta, M.; Schütte, J.; Kühnle, A.; Onishi, H. Evidence for Vacancy Creation by Chromium Doping of Rutile Titanium Dioxide (110). *J. Phys. Chem. C* **2009**, *113*, 3277–3280.

(64) Chrétien, S.; Metiu, H. Density Functional Study of the CO Oxidation on a Doped Rutile TiO_2(110): Effect of Ionic Au in Catalysis. *Catal. Letters* **2006**, *107*, 143–147.

(65) Kim, H. Y.; Lee, H. M.; Pala, R. G. S.; Shapovalov, V.; Metiu, H. CO Oxidation by Rutile TiO_2(110) Doped with V, W, Cr, Mo, and Mn. *J. Phys. Chem. C* **2008**, *112*, 12398–12408.

(66) Bartholomew, C. H.; Farrauto, R. J.; Wiley, C. J. Part One : Introduction and Fundamentals. *Fundam. Ind. Catal. Process.* **2006**, 2006.

(67) Artiglia, L.; Agnoli, S.; Granozzi, G. Vanadium Oxide Nanostructures on Another Oxide: The Viewpoint from Model Catalysts Studies. *Coord. Chem. Rev.* **2015**, *301-302*, 106–122.

(68) Bañares, M. A.; Martínez-Huerta, M. V.; Gao, X.; Fierro, J. L. G.; Wachs, I. E. Dynamic Behavior of Supported Vanadia Catalysts in the Selective Oxidation of Ethane. In Situ Raman, UV-Vis DRS and Reactivity Studies. *Catal. Today* **2000**, *61*, 295–301.

(69) Zhao, C.; Wachs, I. E. An Operando Raman, IR, TPSR Spectroscopic Investiagtion of the Selective Oxidation of Propylene to Acrolein over Supported Vanadia Catalysts. *2007 AIChE Annu. Meet.* **2007**, 11363–11372.

(70) Weckhuysen, B. M.; Keller, D. E. Chemistry, Spectroscopy and the Role of

Supported Vanadium Oxides in Heterogeneous Catalysis. *Catal. Today* **2003**, *78*, 25–46.

(71) Kim, T.; Wachs, I. E. CH_3OH Oxidation over Well-Defined Supported V_2O_5/Al_2O_3 Catalysts: Influence of Vanadium Oxide Loading and Surface Vanadium-Oxygen Functionalities. *J. Catal.* **2008**, *255*, 197–205.

(72) Baron, M.; Abbott, H.; Bondarchuk, O.; Stacchiola, D.; Uh, A.; Shaikhutdinov, S.; Freund, H. J.; Popa, C.; Ganduglia-Pirovano, M. V. Resolving the Atomic Structure of Vanadia Monolayer Catalysts: Monomers, Trimers, and Oligomers on Ceria. *Angew. Chem. Int. Ed.* **2009**, *48*, 8006–8009.

(73) Biener, J.; Bäumer, M.; Wang, J.; Madix, R. J. Electronic Structure and Growth of Vanadium on TiO_2(110). *Surf. Sci.* **2000**, *450*, 12–26.

(74) Agnoli, S.; Castellarin-Cudia, C.; Sambi, M.; Surnev, S.; Ramsey, M. G.; Granozzi, G.; Netzer, F. P. Vanadium on TiO_2(110): Adsorption Site and Sub-Surface Migration. *Surf. Sci.* **2003**, *546*, 117–126.

(75) Biener, J.; Bäumer, M.; Madix, R. J. A Synchrotron Study of the Deposition of Vanadia on TiO_2(110). *Surf. Sci.* **1999**, *432*, 178–188.

(76) Price, N. J.; Reitz, J. B.; Madix, R. J.; Solomon, E. I. A Synchrotron XPS Study of the Vanadia–titania System as a Model for Monolayer Oxide Catalysts. *J. Electron. Spectros. Relat. Phenom.* **1999**, *98-99*, 257–266.

(77) Wang, Q.; Madix, R. J. Preparation and Reactions of V_2O_5 Supported on TiO_2(110). *Surf. Sci. Lett.* **2001**, *474*, L213–L216.

(78) Wang, Q.; Madix, R. J. Partial Oxidation of Methanol to Formaldehyde on a Model Supported Monolayer Vanadia Catalyst: Vanadia on TiO_2(110). *Surf. Sci.* **2002**, *496*, 51–63.

(79) Wong, G. S.; Concepcion, M. R.; Vohs, J. M. Reactivity of Monolayer V_2O_5 Films on TiO_2(110) Produced via the Oxidation of Vapor-Deposited Vanadium. *Surf. Sci.* **2003**, *526*, 211–218.

(80) Agnoli, S.; Sambi, M.; Granozzi, G.; Castellarin-Cudia, C.; Surnev, S.; Ramsey, M.; Netzer, F. P. The Growth of Ultrathin Films of Vanadium Oxide on TiO_2(110). *Surf. Sci.* **2004**, *562*, 150–156.

(81) Kim, H. Y.; Lee, H. M.; Metiu, H. Oxidative Dehydrogenation of Methanol to Formaldehyde by a Vanadium Oxide Cluster Supported on Rutile TiO_2(110): Which Oxygen Is Involved? *J. Phys. Chem. C* **2010**, *114*, 13736–13738.

(82) Artiglia, L.; Agnoli, S.; Vittadini, A.; Verdini, A.; Cossaro, A.; Floreano, L. Atomic Structure and Special Reactivity Toward Methanol Oxidation of Vanadia Nanoclusters on TiO_2(110). *J. Am. Chem. Soc.* **2013**, *135*, 17331–17338.

(83) Price, S. P.; Tong, X.; Ridge, C.; Neilson, H. L.; Buffon, J. W.; Robins, J.; Metiu, H.; Bowers, M. T.; Buratto, S. K. Catalytic Oxidation of Methanol to Formaldehyde by Mass-Selected Vanadium Oxide Clusters Supported on a TiO_2(110) Surface. *J. Phys. Chem. A* **2014**, *2*, 8309–8313.

(84) Artiglia, L.; Agnoli, S.; Savio, L.; Pal, J.; Celasco, E.; Rocca, M.; Bondino, F.; Magnano, E.; Castellarin-cudia, C.; Netzer, F. P.; et al. From Vanadia Nanoclusters to Ultrathin Films on TiO_2(110): Evolution of the Yield and Selectivity in the Ethanol Oxidation Reaction. *ACS Catal.* **2014**, *4*, 3715–3723.

(85) Feulner, P.; Menzel, D. Simple Ways to Improve "Flash desorption" Measurements from Single Crystal Surfaces. *J. Vac. Sci. Technol.* **1980**, *17*, 662–663.

(86) Scofield, J. H. Hartree-Slater Subshell Photoionization Cross-Sections at 1254 and 1487 eV. *J. Electron. Spectros. Relat. Phenom.* **1976**, *8*, 129–137.

(87) Tanuma, S.; Powell, C. J.; Penn, D. R. Calculations of Electron Inelastic Mean Free Paths. *Surf. Interface Anal.* **1993**, *21*, 165–176.

(88) Ratner, B.; Castner, D. *Surface Analysis– The Principal Techniques*; 2009.

(89) Niemantsverdriet, J. W. *Spectroscopy in Catalysis*, Third Edit.; Wiley-VCH Verlag GmbH & Co. KGaA: Weinheim, Germany, 2007.

(90) Osman Karslıoğlu. Structural and Chemical Characterizations of Mo-Ti Mixed Oxide Layers, Humboldt-Universität zu Berlin, 2013.

(91) Redhead, P. A. Thermal Desorption of Gases. *Vacuum* **1962**, *12*, 203–211.

(92) Chan, C. M.; Weinberg, W. H. An Analysis of Thermal Desorption Mass Spectra. I. *Appl. Surf. Sci.* **1978**, *1*, 360.

(93) Habenschaden, E.; Küppers, J. Evaluation of Flash Desorption Spectra. *Surf. Sci.* **1984**, *138*.

(94) Yim, C. M.; Pang, C. L.; Thornton, G. Oxygen Vacancy Origin of the Surface Band-Gap State of TiO_2(110). *Phys. Rev. Lett.* **2010**, *104*, 2–5.

(95) Wendt, S.; Sprunger, P. T.; Lira, E.; Madsen, G. K. H.; Li, Z.; Hansen, J. Ø.; Matthiesen, J.; Blekinge-Rasmussen, A.; Laegsgaard, E.; Hammer, B.; et al. The Role of Interstitial Sites in the Ti3d Defect State in the Band Gap of Titania. *Science* **2008**, *320*, 1755–1759.

(96) Di Valentin, C.; Pacchioni, G.; Selloni, A. Reduced and N-Type Doped TiO_2: Nature of Ti^{3+} Species. *J. Phys. Chem. C* **2009**, *113*, 20543–20552.

(97) Song, X.; Primorac, E.; Kuhlenbeck, H.; Freund, H.-J. Decoupling a Thin Well-Ordered TiO_2(110) Layer from a TiO_2(110) Substrate with a Ti + Ta Mixed Oxide Interlayer. *J. Phys. Chem. C* **2016**, *120*, 8185–8190.

(98) Li, Z.; Smith, R. S.; Kay, B. D.; Dohnálek, Z. Determination of Absolute Coverages for Small Aliphatic Alcohols on TiO_2(110). *J. Phys. Chem. C* **2011**, *115*, 22534–22539.

(99) Kim, K. S.; Barteau, M. A.; Farneth, W. E. Adsorption and Decomposition of Aliphatic Alcohols on Titania. *Langmuir* **1988**, *4*, 533–543.

(100) Farfan-Arribas, E.; Madix, R. J. Different Binding Sites for Methanol Dehydrogenation and Deoxygenation on Stoichiometric and Defective

TiO_2(110) Surfaces. *Surf. Sci.* **2003**, *544*, 241–260.

(101) Lang, X.; Wen, B.; Zhou, C.; Ren, Z.; Liu, L.-M. First-Principles Study of Methanol Oxidation into Methyl Formate on Rutile TiO_2(110). *J. Phys. Chem. C* **2014**, *118*, 19859–19868.

(102) Onishi, H.; Iwasawa, Y. Atom-Resolved Observation of Na Ensembles Activating CO2 Adsorption on a TiO_2(110)-(1×1) Surface as the Genesis of Basic Sites. *Catal. Letters* **1996**, *38*, 89–94.

(103) Bowker, M.; Bennett, R. A. The Role of Ti^{3+} Interstitials in TiO_2(110) Reduction and Oxidation. *J. Phys.: Condens. Matter* **2009**, *21*, 474224–474232.

(104) Yim, C. M.; Pang, C. L.; Thornton, G. Probing the Local Electronic Structure of the Cross-Linked (1×2) Reconstruction of Rutile TiO_2(110). *Surf. Sci.* **2016**, *650*, 71–75.

(105) Cui, X.; Wang, Z.; Tan, S.; Wang, B.; Yang, J.; Hou, J. G. Identifying Hydroxyls on the TiO_2(110)-1×1 Surface with Scanning Tunneling Microscopy. *J. Phys. Chem. C* **2009**, *113*, 13204–13208.

(106) Zhou, C.; Ren, Z.; Tan, S.; Ma, Z.; Mao, X.; Dai, D.; Fan, H.; Yang, X.; LaRue, J.; Cooper, R.; et al. Site-Specific Photocatalytic Splitting of Methanol on TiO_2(110). *Chem. Sci.* **2010**, *1*, 575–580.

(107) Göpel, W.; Anderson, J. A.; Frankel, D.; Jaehnig, M.; Phillips, K.; Schäfer, J. A.; Rocker, G. Surface Defects of TiO_2(110): A Combined XPS, XAES and ELS Study. *Surf. Sci.* **1984**, *139*, 333–346.

(108) Diebold, U.; Madey, T. E. TiO_2 by XPS. *Surf. Sci. Spectra* **1996**, *4*, 227–231.

(109) Silversmit, G.; Depla, D.; Poelman, H.; Marin, G. B.; Gryse, R. De. Determination of the V2p XPS Binding Energies for Different Vanadium Oxidation States (V^{5+} to V^{0+}). *J. Electron. Spectros. Relat. Phenom.* **2004**, *135*, 167–175.

(110) Song, X.; Primorac, E.; Kuhlenbeck, H.; Freund, H. J. Effect of Vanadium Admixing on the Surface Structure of TiO_2(110) under Non-Oxidizing Conditions. *Surf. Sci.* **2016**, *653*, 181–186.

(111) Wang, L.-Q.; Baer, D. R.; Engelhard, M. H. Creation of Variable Concentrations of Defects on TiO_2(110) Using Low-Density Electron Beams. *Surf. Sci.* **1994**, *320*, 295–306.

(112) James, A. M.; Lord, M. P. *Macmillan's Chemical and Physical Data*; Macmillan Press: Basingstoke, UK, 1992.

(113) Huheey, J. E.; Keiter, E. A.; Harper, R. K. *Inorganic Chemistry: Principles of Structure and Reactivity*; Harper Collins: New York, USA, 1993.

(114) Duncan, D. A.; Kreikemeyer-Lorenzo, D.; Primorac, E.; Karslioğlu, O.; Naschitzki, M.; Unterberger, W.; Kuhlenbeck, H.; Woodruff, D. P. V-Doped TiO_2(110): Quantitative Structure Determination Using Energy Scanned Photoelectron Diffraction. *Surf. Sci.* **2014**, *630*, 64–70.

(115) Mellan, T. A.; Grau-Crespo, R. Density Functional Theory Study of Rutile VO_2 Surfaces. *J. Chem. Phys.* **2012**, *137*, 154706.

(116) Pabisiak, T.; Kiejna, A. Energetics of Oxygen Vacancies at Rutile TiO_2(110) Surface. *Solid State Commun.* **2007**, *144*, 324–328.

(117) Asaduzzaman, A. M.; Krüger, P. Adsorption and Cluster Growth of Vanadium on TiO_2(110) Studied by Density Functional Theory. *J. Phys. Chem. C* **2008**, *112*, 4622–4625.

(118) Hermann, K.; Hove, M. A. Van. Http://www.fhi-berlin.mpg.de/KHsoftware/LEEDpat/.

(119) Su, D. S.; Schlögl, R. Thermal Decomposition of Divanadium Pentoxide V_2O_5: Towards a Nanocrystalline V_2O_3 Phase. *Catal. Letters* **2002**, *83*, 115–119.

(120) Sturm, J. M.; Guimond, S.; Göbke, D.; Romanyshyn, Y.; Naschitzki, M.; Kuhlenbeck, H.; Freund, H.-J. Well-Ordered V_2O_5(001) Thin Films on Au (111): Growth and Thermal Stability. *J. Phys. Chem.* **2008**, *5*, 11835–11846.

(121) Shapovalov, V.; Metiu, H. VO_x (X= 1-4) Submonolayers Supported on Rutile TiO_2(110) and CeO_2(111) Surfaces: The Structure, the Charge of the Atoms, the XPS Spectrum, and the Equilibrium Composition in the Presence of Oxygen. *J. Phys. Chem. C* **2007**, *111*, 14179–14188.

(122) Price, S. P.; Tong, X.; Ridge, C.; Shapovalov, V.; Hu, Z.; Kemper, P.; Metiu, H.; Bowers, M. T.; Buratto, S. K. STM Characterization of Size-Selected V_1, V_2, VO, and VO_2 Clusters on a TiO_2(110)-(1×1) Surface at Room Temperature. *Surf. Sci.* **2011**, *605*, 972–976.

(123) Mars, P.; van Krevelen, D. W. Oxidations Carried out by Means of Vanadium Oxide Catalysts. *Chem. Eng. Sci.* **1954**, *3*, 41–59.

Appendix A – Abstract

Heterogeneous catalysts of vanadium oxides supported on titania powder exhibit a high yield of aldehyde from the partial oxidation of alcohols. Understanding the reaction mechanism of this catalytic process in detail requires a detailed characterization of the surface structure and the interaction of the alcohols with the catalyst, which is challenging for complex systems like the vanadia-titania system. Well-defined oxide layers prepared on single crystals modeling the real catalysts offer an approach to investigate the surface properties of such systems. Vanadia-titania mixed oxides were prepared on a rutile (110) single crystal according to a recipe developed by our research group. Oxidized as well as reduced mixed oxides were investigated with surface science techniques like XPS, STM, LEED, and TPD.

Doping with vanadium has a heavy impact on the surface properties of TiO_2(110). Vanadium ions were found to be located below the surface in reduced layers. Their presence increases the reducibility of the layers as is evident from a high density of reduction related features at the surface. Oxidation of the mixed oxide layers induces the diffusion of vanadium to the surface where it forms vanadia clusters: at low vanadium concentration, vanadia clusters were observed above the Ti rows at the surface; at higher vanadium concentration, vanadia clusters containing V^{5+} were found to cover the reduced TiO_2(110) (1 × 2) surface. A study of the oxidation states of Ti and V before and after oxidation revealed that the increased reducibility of the layers is related to the vanadium ions that are reduced more easily than the titanium ions. The energy for the removal of oxygen from the vicinity of vanadium atoms in the TiO_2(110) layer is smaller than that for the removal of oxygen from TiO_2(110) without vanadium.

In the reactivity tests using methanol as a prototype molecule, the oxidized layers exhibit several reaction channels for the partial oxidation of methanol towards formaldehyde. The channel leading to formaldehyde desorption at about 680 K is related to bridging oxygen vacancies at the surface, while oxygen adatoms are involved in the reaction leading to desorption at 600 K. Vanadia clusters of two different types at the oxidized surface trigger another two reaction channels at lower temperatures, 550 K and 480 K. It is shown that the reaction in both channels proceeds according to the well-known Mars–van Krevelen mechanism.

Appendix B – Zusammenfassung

Heterogene Vanadiumoxid-Katalysatoren auf pulverförmigen Titaniaträgern erzielen hohe Aldehyd-Ausbeuten für die partielle Oxidation von Alkoholen. Um den Reaktionsmechanismus dieses katalytischen Prozesses zu verstehen, ist eine eingehende Charakterisierung der Oberfläche und der Wechselwirkung des Alkohols mit dem Katalysator notwendig, was jedoch für hochkomplexe Systeme wie Vanadia-Titania eine Herausforderung darstellt. Wohldefinierte Oxidschichten, die auf Einkristallen hergestellt sind, können als Modell für den realen Katalysator dienen und die Oberflächenanalyse hierdurch ermöglichen. Vanadia-Titania-Mischoxide wurden auf einer Rutil(110)-Einkristalloberfläche nach einer in unserer Gruppe entwickelten Methode präpariert. Oxidierte und reduzierte Mischoxide wurden mit Oberflächentechniken wie XPS, STM, LEED und TPD untersucht.

Dotierung mit Vanadium beeinflusst die Oberflächeneigenschaften von TiO_2(110) erheblich. Vanadiumionen wurden in reduzierten Schichten unter der Oberfläche lokalisiert. Ihre Anwesenheit erhöht die Reduzierbarkeit der Schichten, was sich in einer hohen Dichte von charakteristischen Oberflächenmerkmalen zeigt. Oxidation der Mischoxidschichten induziert die Diffusion von Vanadium zur Oberfläche, wo sich Vanadiacluster bilden: bei niedriger Vanadiumkonzentration wurden Vanadiacluster auf Ti-Reihen an der Oberfläche beobachtet: bei höherer Vanadiumkonzentration wurden Vanadiacluster mit V^{5+}-Spezies gefunden, welche die reduzierte TiO_2(110) (1 × 2)-Oberfläche bedecken. Eine Untersuchung der Oxidationszustände von Ti und V vor und nach der Oxidation zeigte, dass die erhöhte Reduzierbarkeit der Schichten mit den Vanadiumionen zusammenhängt, welche sich leichter reduzieren lassen als die Titanionen. Die Energie für die Entfernung von Sauerstoff aus der Nachbarschaft von Vanadiumatomen in der TiO_2(110)-Lage ist geringer als die Energie für die Sauerstoffentfernung aus vanadiumfreiem TiO_2(110).

In Reaktivitätsstudien mit Methanol als Sondenmolekül zeigten die oxidierten Schichten mehrere Reaktionskanäle für die partielle Oxidation von Methanol zu Formaldehyd. Ein Mechanismus, bei dem Formaldehyd bei 680 K desorbiert, hängt mit verbrückenden Sauerstofffehlstellen in der Oberfläche zusammen, während hingegen Sauerstoffadsorbate einen Reaktionspfad befördern, bei dem Formaldehyd bei 600 K desorbiert. Zwei unterschiedliche Typen von Vanadiaclustern auf der oxidierten Oberfläche ermöglichen zwei weitere Reaktionskanäle, bei 550 K bzw. 480 K. Es wird gezeigt, dass diese beiden Reaktionsmechanismen nach dem bekannten Mars-van-Krevelen-Mechanismus verlaufen.

Appendix C – Publications

1. **X. Song**, E. Primorac, H. Kuhlenbeck, H.-J. Freund, Effect of vanadium admixing on the surface structure of TiO_2(110) under non-oxidizing conditions, Surface Science, 653, (2016) 181–186.

2. **X. Song**, E. Primorac, H. Kuhlenbeck, H.-J. Freund, Decoupling a thin well-ordered TiO_2(110) layer from a TiO_2(110) substrate with a Ti + Ta mixed oxide interlayer, Journal of Physical Chemistry C, 120, (2016) 8185–8190.

3. O. Karslioglu, **X. Song**, H. Kuhlenbeck, H.J. Freund, Mo+TiO_2(110) mixed oxide layer: structure and reactivity, Topics in Catalysis, 56 (2013) 1389-1403.

4. **X. Song**, H. Kuhlenbeck, H.-J. Freund, Partial oxidation of methanol by vanadia-titania mixed oxide thin films. (in preparation).

Appendix D – Curriculum Vitae

For reasons of data protection, the curriculum vitae is not published in the electronic version.